Method of Moments Analysis of Artificial Media Composed of Dielectric Wire Objects

M.E. Peters and E.H. Newman

The Ohio State University

ElectroScience Laboratory

Department of Electrical Engineering
Columbus, Ohio 43212

Technical Report 721566-3
Contract No. N00014-89-J-1007 P00007
July 1994

Department of the Navy
Office of Naval Research
800 N. Quincy St.
Arlington, VA 22217-5000

NOTICES

When Government drawings, specifications, or other data are used for any purpose other than in connection with a definitely related Government procurement operation, the United States Government thereby incurs no responsibility nor any obligation whatsoever, and the fact that the Government may have formulated, furnished, or in any way supplied the said drawings, specifications, or other data, is not to be regarded by implication or otherwise as in any manner licensing the holder or any other person or corporation, or conveying any rights or permission to manufacture, use, or sell any patented invention that may in any way be related thereto.

50272-101

REPORT DOCUMENTATION PAGE	1. REPORT NO.	2.	3. Recipient's Accession No.

4. Title and Subtitle Method of Moments Analysis of Artificial Media Composed of Dielectric Wire Objects	5. Report Date July 1994 6.
7. Author(s) M.E. Peters and E.H. Newman	8. Performing Org. Rept. No. 721566-3
9. Performing Organisation Name and Address The Ohio State University ElectroScience Laboratory 1320 Kinnear Road Columbus, OH 43212	10. Project/Task/Work Unit No. 11. Contract(C) or Grant(G) No. (C) N00014-89-J-1007 P00007 (G)
12. Sponsoring Organisation Name and Address Department of the Navy, Office of Naval Research 800 N. Quincy St. Arlington, VA 22217-5000	13. Report Type/Period Covered Technical Report 14.

15. Supplementary Notes

16. Abstract (Limit: 200 words)

The problem considered is an integral equation and periodic method of moments (PMM) solution determining the effective permittivity and permeability of an artificial medium. The artificial medium is composed of a 3D periodic array of identical arbitrarily-shaped thin conductive or dielectric wire objects arranged in a homogeneous host medium. In general, the artificial medium is anisotropic, in which case the effective permittivity and permeability tensors are determined. The method is based upon finding the complex wavenumber and the eigenfunction currents and fields, for a plane wave propagating in the artificial medium. Three methods are presented for determining the complex effective constitutive parameters of the artificial medium, all using various results of the PMM solution.

The PMM solution solves for the currents induced in or on the wire objects. Mutual coupling between the wire objects is included in the PMM formulation. This mutual coupling affects the eigenfunction currents in the wire objects, the average eigenfunction fields in the artificial medium, and hence the effective permittivity and permeability tensors for the artificial medium. All fields are expressed as spectral summations of propagating and evanescent plane waves.

Sample results are included to illustrate the method of the PMM solution, and to present some interesting points and characteristics of the periodic artificial media treatable by the solution. It is shown that for a given direction of propagation through the artificial medium, there are in general two distinct modes of plane wave propagation. These plane wave modes of propagation, as well as the eigenfunction currents in the wire objects, can change with the direction of propagation.

17. Document Analysis a. Descriptors

DIELECTRIC
MATERIALS
USER MANUAL
MOMENT METHOD

b. Identifiers/Open-Ended Terms

c. COSATI Field/Group

18. Availability Statement	19. Security Class (This Report)	21. No. of Pages
A. Approved for public release; Distribution is unlimited.	Unclassified	156
	20. Security Class (This Page) Unclassified	22. Price

(See ANSI-Z39.18) *See Instructions on Reverse* OPTIONAL FORM 272 (4-77)
Department of Commerce

Contents

List of Figures

List of Tables

Chapter 1

Introduction

An artificial medium is basically a macroscopic analog of a real medium, and typically consists of a large number of scattering objects distributed (more or less) uniformly in some host or background medium. The scattering objects affect the behavior of electric and magnetic fields inside the artificial medium. For example, a general plane wave in an artificial medium propagates with an *effective* wavenumber different than that of the host material or the scattering objects. As a result, artificial media can be characterized by an effective permittivity and effective permeability. In general, artificial media are anisotropic, and the constitutive parameters are tensor quantities.

When a plane wave propagates through an artificial medium, currents are induced in (or on) the scattering objects. As shown in Figure 1.1, these currents can be viewed as macroscopic current moments, analogous to the microscopic dipole moments induced in the molecules of an actual dielectric [1]. The effect of the macroscopic current moments is to produce a net electric and magnetic current moment per unit volume, and thus the artificial medium has some complex effective permittivity and permeability different from the host medium.

The complex effective constitutive parameters of the artificial medium are a function of frequency, the electrical size, shape, spacing, and orientation of the scattering objects, and the constitutive parameters of both the host medium and the scattering objects. Also, in contrast to real media, the constitutive parameters can be a function of the direction of propagation through the artificial medium. By properly choosing

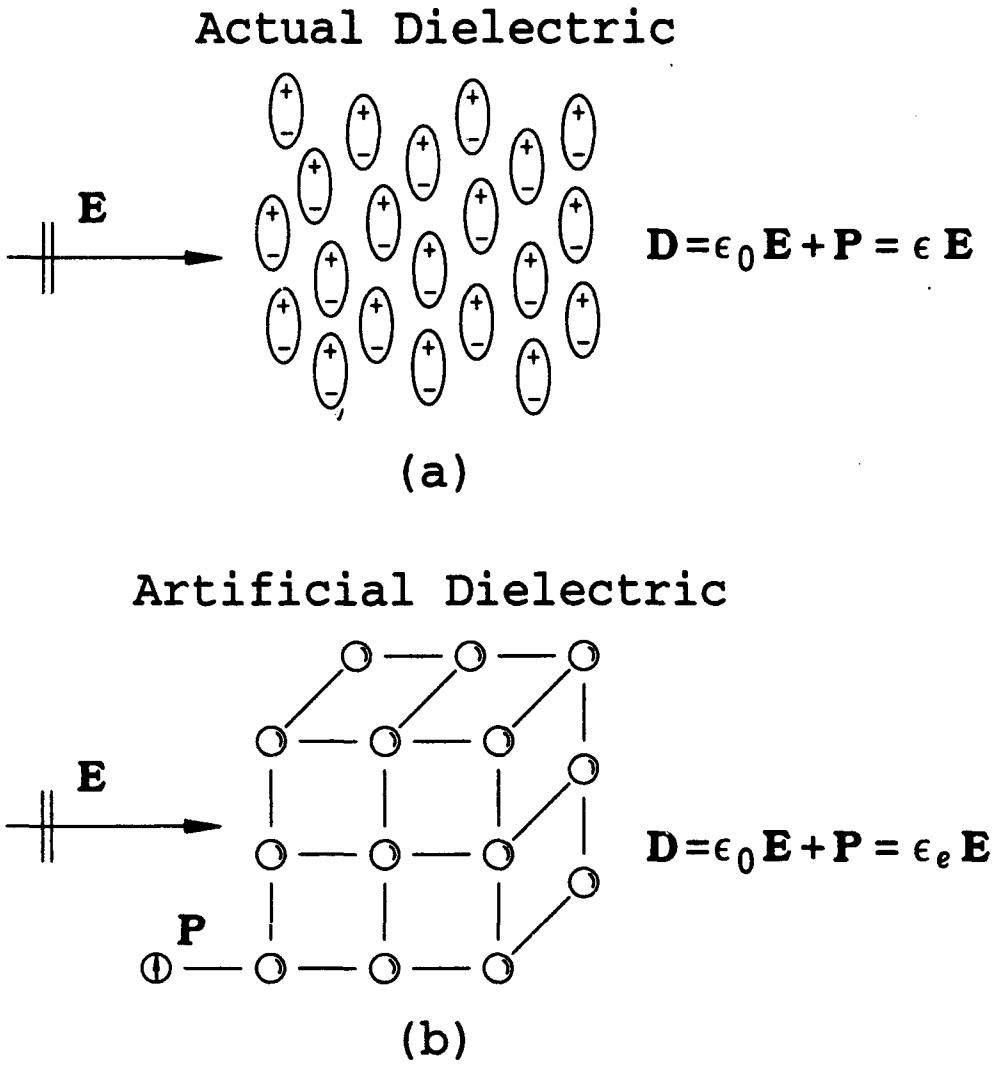

Figure 1.1: The artificial dielectric model.

the geometry and composition, it may be possible to design an artificial medium of desired permittivity, permeability and loss tangent.

This dissertation presents an integral equation and periodic method of moments (PMM) [2, 3, 4] solution to the problem of determining the effective permittivity and permeability of an artificial medium. The artificial medium is composed of a 3D periodic array of identical arbitrarily–shaped thin conductive or dielectric wire objects.

The solution proceeds as follows. First, an integral equation is formulated for a plane wave of unknown wavenumber propagating in an artificial medium of infinite extent in all three dimensions. Next, this integral equation is solved by the PMM, yielding the complex effective wavenumber of the plane wave, the eigenfunction currents in the wire objects, and the eigenfunction fields in the artificial medium. From these quantities, the effective constitutive parameters of the artificial medium are determined.

Three methods are formulated for determining the effective constitutive parameters. The first method determines what constitutive parameters a real medium must have to produce the same effective wavenumber solved for in the PMM solution. It is shown that this method applies only in certain simple geometries. The second and third methods are more general, and are based on the assumption that current and field quantities inside the artificial medium can be viewed in an average sense. The second method enforces the constitutive relationship equations using the current moments and eigenfunction fields averaged over a lattice cell. The third method enforces Maxwell's source–free equations (for a plane wave) applied to the eigenfunction fields averaged over a lattice cell.

The concept of artificial media was first introduced by Kock [5] in 1948 as applied to the design of microwave lenses. The problem was to produce a lightweight material with suitable index of refraction at microwave frequencies. Kock presented analysis of artificial dielectrics consisting of cubic arrays of spheres, discs and metallic strips. His preliminary work did not include interaction between the objects, and thus the objects and spacing must be electrically small with the objects small in terms of the spacing.

Other applications include modeling a plasma as an artificial dielectric by Rotman [6] in the study of radio wave propagation. Bahl and Gupta [7] designed a leaky-wave antenna using the results of Brown [8]. King, Thiel and Park [9] inserted pins in a ground plane to synthesize a given surface reactance. Sihvola [10] modeled mixtures of rain and hail as artificial dielectrics in the analysis of microwave attenuation. A recent application of an artificial dielectric mixture is in the microwave welding of polymers by Wu and Benatar [11], where a lossy dielectric of desired conductivity is produced by the proper mixture of HCl doped polyaniline particles in a polyethylene host.

Arrays of spherical objects have been further treated by Lewin [12] where he accounts for the effects of plane wave scattering by nearby metal spheres, and by Corkum [13] where he uses the Clausius-Massotti equation [1, Sec. 2.8.1] suggested by Kock. Corkum's analysis accounts the permeability of such an array, as well as the permittivity of a dielectric sphere array. Arrays of thin conducting disks have also received considerable treatment. For the magnetic field normal to the disks, Estrin [14] modeled the current on an isolated disk as a magnetic dipole and solved for the permeability in the case where the disks are far enough apart to neglect interaction. Estrin [15] also considered the anisotropic properties of a 3D array of disks in his analysis of oblique incident waves on such a medium. Brown and Jackson [16] include multipole interaction terms to provide a solution accurate for closely packed disks. Further analysis of the metallic strip artificial dielectric, consisting of 2D metallic strips oriented transverse to both the direction of propagation and the electric field, is given by Brown [17] in which he formulates a more accurate theory based on transmission line theory. Also, Kolettis and Collin [18] presented a waveguide modal analysis for general directions of propagation through this strip media. Experimental results for the metallic strip artificial dielectric are presented by Kolettis and Collin [18], and Cohn [19].

Collin [20, Ch. 12] presents an extensive evaluation of artificial dielectrics, and his work serves as a good summary of much of the early work done in the area. He presents a simple static Lorentz solution which, only accounts for dipole interactions

between objects, and thus, the objects must be electrically closely spaced and small in relative to the spacing. To account for larger objects, multipole terms can be included in the expressions for the fields.

The PMM solution presented in this dissertation was first suggested and utilized by Blanchard and Newman [21, 22]. They analyzed a 2D array of dielectric rods and a 3D array of straight perfect electric conducting dipoles. The current work included here is an extension of this preliminary work in several important ways. It analyzes periodic arrays of arbitrary conductive or dielectric wire objects, and allows for lossy materials. Also, methods are formulated to determine the anisotropic properties of artificial media, i.e., the effective permittivity and permeability tensors.

The theory of the given solution to artificial media is presented in Chapter 2. This theory includes the derivation of the integral equation for a plane wave propagating in the artificial medium. The periodic method of moments (PMM) solution to the integral equation is presented, with specialization to the arbitrarily–shaped thin wire objects arranged in the 3D periodic lattice structure. This solution yields the complex wavenumber, as well as the eigenfunction currents and fields, of the plane wave propagating in the artificial media. A discussion of how these quantities are used to determine the effective constitutive parameters of artificial media is included. Finally, expressions for the fields of a 2D planar array and a 3D volume array of current elements are derived. These field expressions provide the basis for the PMM solution and the eigenfunction fields in the artificial medium.

Chapter 3 presents the evaluation of the MM impedance matrix, and involves the computation of several distinct terms. Chapter 4 presents the evaluation of the average eigenfunction electric and magnetic fields of the plane wave. The eigenfunction fields are spoken of in an average sense, i.e., they are averaged over the center lattice cell. Chapter 5 presents results obtained from the solution presented in this dissertation. These results are intended to illustrate the methods and techniques, as well as to present some interesting points about artificial media. Chapter 6 presents the usage of the computer program **ADWIRS**, which was developed in FORTRAN to analyze an artificial medium composed of a 3D periodic array of identical arbitrarily–shaped

thin conductive or dielectric wire objects arranged in a homogeneous host medium. The program **ADWIRS** yields the solution of the plane wave propagating in the artificial dielectric, including the eigenfunction currents and fields, and the electric and magnetic dipole moments.

Many of the mathematical details of the PMM solution are given in appendices for clarity and to improve the readability of this dissertation. Appendix H presents a solution to the problem of determining the effective permittivity of an artificial dielectric composed of a 3D periodic array of small identical dielectric material sp... The theory is similar to that presented in Chapter 2, but it is not as general and complete. However, the implementation of the method is quite different, due to the scattering objects being spheres instead of wire objects. Appendix H is intended to be a self-contained document, with few references to material elsewhere in this dissertation.

Chapter 2

Theory

This chapter presents the integral equation and PMM solution for a plane wave propagating through an artificial medium composed of thin conductive or dielectric wire objects arranged in a periodic lattice. This solution yields the complex wavenumber of the plane wave that can propagate without excitation through the artificial medium, i.e., the eigenfunction solution for the artificial medium. The solution also yields the shape of the *eigenfunction currents* in the scattering objects, from which the *eigenfunction fields* can be determined. Throughout this paper, all fields and currents are assumed to be time harmonic with the $e^{j\omega t}$ time dependence suppressed.

Two methods are presented for determining the effective permittivity and permeability tensors of the artificial medium. The *polarization method* is based on enforcing the constitutive relationship equations in an average sense in the artificial medium, and uses the average eigenfunction currents and fields per unit volume. The *Maxwell's equations method* is based on the assumption that Maxwell's equations for the plane wave are satisfied in an average sense in the artificial medium. This method uses the average eigenfunction fields per unit volume and the complex vector wavenumber of the plane wave.

As shown in Figure 2.1, the geometry of the artificial medium consists of a 3D triple periodic array of wire objects located in a homogeneous and isotropic host medium. The homogeneous host medium has constitutive parameters (μ_0, ϵ_0), wavelength λ_0, wavenumber k_0, and is not necessarily free space and may be lossy. The wire objects (shown as V–dipoles in the Figure 2.1) may be composed of an arbitrary conductive

or dielectric material. The wires have radius a, constitutive parameters (μ_0, ϵ_1), and wavenumber k_1. The complex permittivity of the wire objects, ϵ_1, is given by

$$\epsilon_1 = \epsilon_{1r}\,\epsilon_0 - j\,\frac{\sigma_1}{\omega} = \epsilon_{1r}\,\epsilon_0\,(1 - j\,\tan\delta_1) \tag{2.1}$$

where σ_1 is the conductivity of the wire object (in Ω^{-1}/ meter) and $\tan\delta_1$ is the loss tangent of the wire objects. The wire objects are arranged in a lattice cell structure with spacings d_u, d_v and d_w in the $\hat{\mathbf{u}}, \hat{\mathbf{v}}$ and $\hat{\mathbf{w}}$ directions, respectively. This lattice cell structure need not be rectangular, and its unit vectors are

$$\begin{aligned} \hat{\mathbf{u}} &= \hat{\mathbf{x}}, \\ \hat{\mathbf{v}} &= v_x\hat{\mathbf{x}} + v_y\hat{\mathbf{y}} \qquad \text{and} \\ \hat{\mathbf{w}} &= w_x\hat{\mathbf{x}} + w_y\hat{\mathbf{y}} + w_z\hat{\mathbf{z}}. \end{aligned}$$

The elements are referenced by the index $\mathbf{Q} = (i_u, j_v, k_w)$ where $-\infty \leq (i_u, j_v, k_w) \leq \infty$. The reference or center wire object is centered at the origin and is indexed by $\mathbf{Q} = 0 = (0,0,0)$. Also, let $\Lambda\mathbf{Q} = i_u d_u\hat{\mathbf{u}} + j_v d_v\hat{\mathbf{v}} + k_w d_w\hat{\mathbf{w}}$ be the position vector from the origin to the center of lattice cell $\mathbf{Q}$.

Following the general methods presented by Blanchard and Newman [21, 22], the effective parameters of the artificial medium are determined by first assuming that a plane wave of unknown wavenumber is propagating through the medium. If the plane wave is propagating in the $\hat{\mathbf{u}}_k$ direction, assumed to be known, then it will be of the form

$$e^{-j\mathbf{k}_e\cdot\mathbf{R}}, \tag{2.2}$$

where $\mathbf{k}_e = k_e\,\hat{\mathbf{u}}_k = k_{ex}\hat{\mathbf{x}} + k_{ey}\hat{\mathbf{y}} + k_{ez}\hat{\mathbf{z}}$ is the unknown complex vector wavenumber (or *wave–vector*), and $\mathbf{R} = x\hat{\mathbf{x}} + y\hat{\mathbf{y}} + z\hat{\mathbf{z}}$ is the position vector. For a given direction $\hat{\mathbf{u}}_k$, it is desired to find k_e such that this plane wave satisfies Maxwell's source free equations and all of the boundary conditions in the artificial medium, corresponding to the normal mode of propagation for the artificial medium, i.e., the eigenfunction solution for the artificial medium. Once the wavenumber k_e is known, then the shape of the eigenfunction currents in the material wire objects can be determined. From these eigenfunction currents, the eigenfunction fields can then be found.

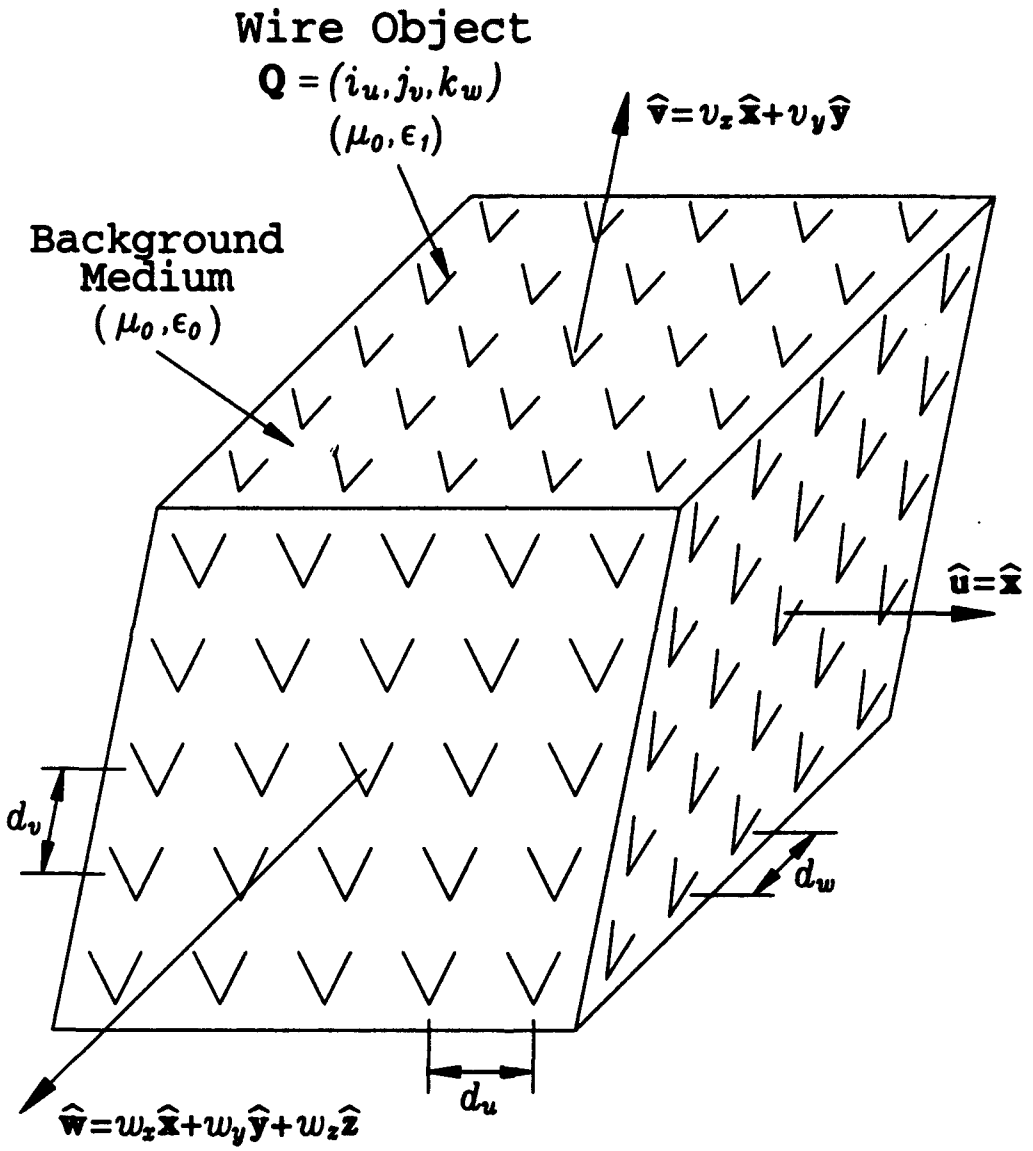

Figure 2.1: The 3D volume lattice geometry.

For plane wave propagation in a given direction through a homogeneous anisotropic medium, it is known that there are two distinct eigenfunction modes of propagation [23, Sec. 4.25], [24, Sec. 14.2.2]. Each mode of propagation corresponds to a distinct complex wavenumber and polarisation of the plane wave. Also, for homogeneous anisotropic media, the nine elements of the permittivity and permeability tensors are independent of the direction of propagation through the medium [23, Ch. 4], [24, Sec. 14.1].

It will be shown that the theory of two distinct modes of plane wave propagation extends to plane wave propagation through artificial media. Thus, for a given direction of propagation $\hat{\mathbf{u}}_k$ through an artificial medium, there are two values of k_e corresponding to the two eigenfunction solutions for the artificial medium. Each value of k_e corresponds to a distinct polarization of the plane wave, and to distinct eigenfunction currents on the wire objects, and hence, to distinct eigenfunction fields in the artificial medium. Also, it will be shown that the permittivity and permeability tensors typically will have only a slight variation on the direction of propagation in an artificial medium. One possible exception is when the eigenfunction current shapes are a strong function of the direction of propagation.

2.1 The Integral Equation

In formulating the integral equation for the artificial medium, as shown in Figure 2.2, the volume equivalence theorem is used to replace the wire objects by the host medium and the equivalent electric volume polarization currents [1, Sec. 7.7]

$$\mathbf{J} = j\omega(\epsilon_1 - \epsilon_0)\mathbf{E}^t, \tag{2.3}$$

where $\mathbf{E}^t$ is the total electric field inside the wire objects. Since the permeabilities of the host medium and the wire objects are identical, there are no magnetic currents in the wire objects. In the limiting case where the wires become perfectly conducting, the volume current J approaches a surface current on the wire surfaces. The current

J exists in (or on) each and every wire object, and is written as

$$\mathbf{J} = \sum_{\mathbf{Q}} \mathbf{J}^{\mathbf{Q}}, \tag{2.4}$$

where $\mathbf{J}^{\mathbf{Q}}$ is the current in wire object Q, and the summation is over all values of Q, i.e., $-\infty \leq (i_u, j_v, k_w) \leq \infty$. Since we seek a solution to Maxwell's source free equations, there are no impressed currents, and thus $\mathbf{E}^{\mathbf{t}}$ is the electric field of J radiating in the homogeneous host medium. Equation (2.3) can be rearranged as the homogeneous equation

$$-\mathbf{E}^{\mathbf{t}} + \frac{\mathbf{J}}{j\omega(\epsilon_1 - \epsilon_0)} = 0 \quad \text{in each wire object Q,} \tag{2.5}$$

and is to be solved for the complex wavenumber k_z, and the current in the center or Q = 0 wire object, by the PMM.

Due to the periodic nature of the array of wire objects, and of the plane wave of Equation (2.2), the current is identical in each wire object except for an amplitude and phase change corresponding to the value of the plane wave at the center of the lattice cell. In other words, the current in wire object Q differs from the current in the center wire object by the complex multiplier

$$C^{\mathbf{Q}} = e^{-j\mathbf{k}_z \cdot \mathbf{A}\mathbf{Q}}. \tag{2.6}$$

As a result, the only unknowns are k_z and the current in the center wire object.

2.2 PMM Solution of the Integral Equation

Equation (2.5) will be solved by the periodic moment method (PMM) [2, 3, 4]. The first step in the PMM solution is to expand the unknown current J as

$$\mathbf{J} = \sum_{\mathbf{Q}} \mathbf{J}^{\mathbf{Q}} \approx \sum_{\mathbf{Q}} C^{\mathbf{Q}} \sum_{n=1}^{N} I_n \mathbf{J}_n^{\mathbf{Q}}, \tag{2.7}$$

where the $\mathbf{J}_n^{\mathbf{Q}}$ are N linearly independent expansion functions for the current in wire object Q, and the I_n are N unknown expansion coefficients, with $n = 1, 2, \ldots, N$.

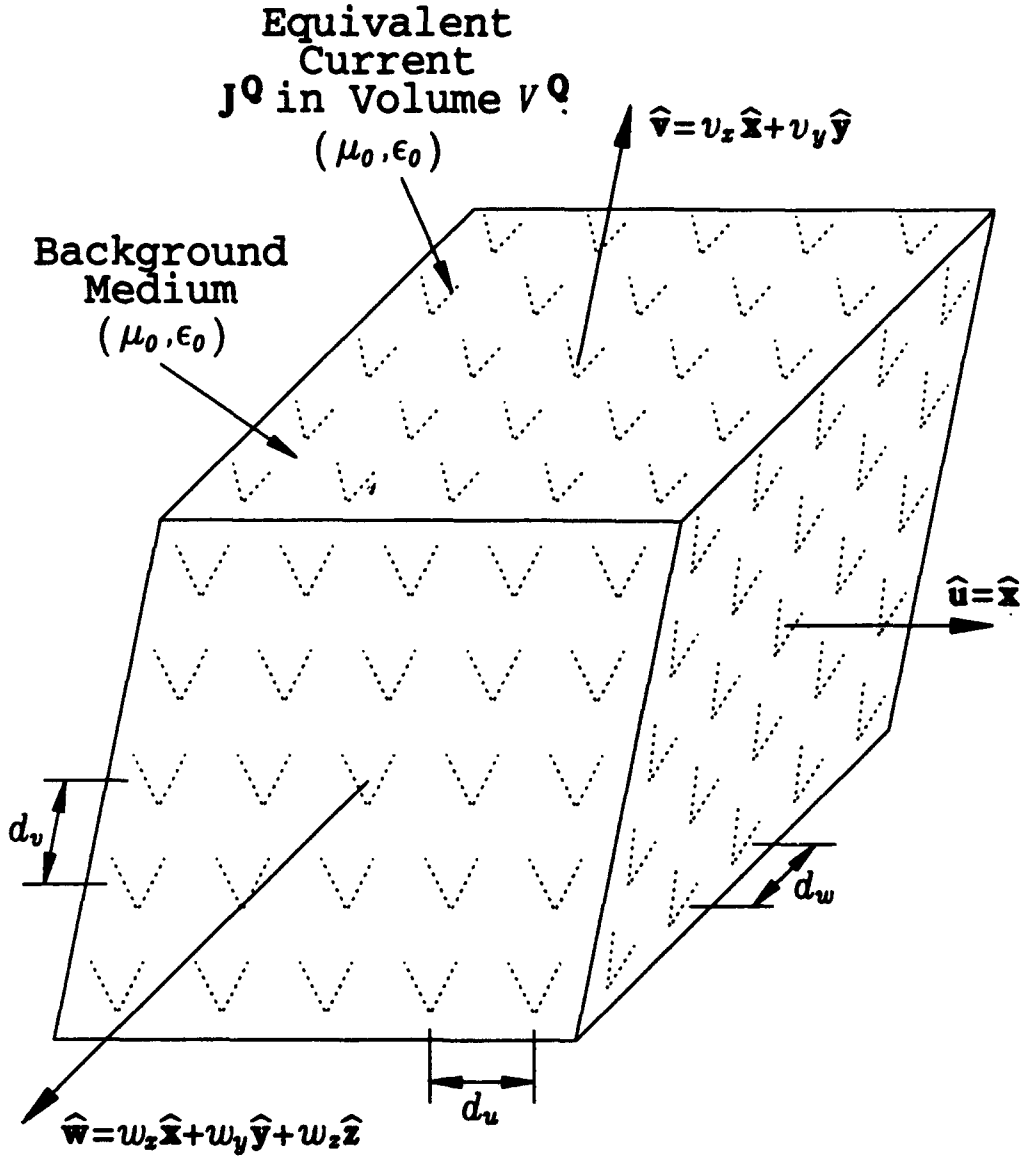

Figure 2.2: The equivalent 3D volume lattice geometry after application of the volume equivalence theorem.

Note that for a given n, all the $\mathbf{J}_n^{\mathbf{Q}}$ are identical in shape, with the only difference being that a given $\mathbf{J}_n^{\mathbf{Q}}$ is defined only on wire object Q, i.e.,

$$\mathbf{J}_n^{\mathbf{0}}(\mathbf{R}) = \mathbf{J}_n^{\mathbf{Q}}(\mathbf{R} - \Lambda\mathbf{Q}). \tag{2.8}$$

Due to the periodic nature of the problem, it is only necessary to enforce Equation (2.5) over V^0, the volume of the center wire object.

Next, define N linearly independent weighting functions in the center wire object, denoted as $\mathbf{W}_m$ with $m = 1, 2, ..., N$. Substituting J of Equation (2.7) into Equation (2.5), and taking the inner product of the result with the N weighting functions, reduces Equation (2.5) to an order N matrix equation which can be written as

$$[Z + \Delta Z]\, I = [Z]\, I = 0. \tag{2.9}$$

Here, $[Z] = [Z + \Delta Z]$ is the order N impedance matrix and I is the length N solution vector containing the I_n expansion coefficients of Equation (2.7). The impedance matrix elements are given by $(m, n = 1, 2, ..., N)$

$$Z_{mn}(k_e) = \sum_{\mathbf{Q}} C^{\mathbf{Q}} Z_{mn}^{\mathbf{Q}} = -\sum_{\mathbf{Q}} C^{\mathbf{Q}} \int_{V_m} \mathbf{E}_n^{\mathbf{Q}} \cdot \mathbf{W}_m \, dv \tag{2.10}$$

$$\Delta Z_{mn} = \frac{1}{j\omega(\epsilon_1 - \epsilon_0)} \int_{V_m} \mathbf{J}_n^{\mathbf{0}} \cdot \mathbf{W}_m \, dv, \tag{2.11}$$

where $\mathbf{E}_n^{\mathbf{Q}}$ is the electric field of $\mathbf{J}_n^{\mathbf{Q}}$, the n^{th} expansion function in wire object Q, radiating in the homogeneous host medium. The integration is over V_m, the volume of weighting function m. The ΔZ_{mn} terms do not depend on k_e, but the Z_{mn} terms do through their dependence upon $C^{\mathbf{Q}}$. Note that the ΔZ_{mn} terms are non–zero only when the expansion functions $\mathbf{J}_n^{\mathbf{Q}}$ are in the center $\mathbf{Q} = \mathbf{0}$ wire object. Also, the ΔZ_{mn} terms vanish when the wires are perfectly conducting, since $|\epsilon_1| \to 0$. The impedance matrix terms, $Z_{mn}(k_e)$ and ΔZ_{mn}, are evaluated in Chapter 3, for the piecewise sinusoidal (PWS) material wire expansion and weighting functions defined in Section 2.2.1.

The homogeneous matrix Equation (2.9) will have a non–trivial solution only if the determinant of the impedance matrix is zero. Thus, k_e is found by solving the

fundamental equation

$$|Z(k_c) + \Delta Z| = |Z| = 0, \tag{2.12}$$

usually on an iterative basis.

2.2.1 The MM Expansion and Weighting Functions for Material Wires

In this section, MM expansion and weighting functions suitable for thin conductive or dielectric wires are defined. The expansion functions used are those employed by Newman [25], which incorporate known behavioral variations of the thin material wires. As shown in Figure 2.3, a *dipole* expansion function n consists of two *monopole* current segments. Monopole nj is oriented along the z_{nj}–axis, with zero current at $z_{nj} = 0$ rising to unity current at $z_{nj} = d_{nj}$. The polarity of the current, on a monopole basis, always flows from the zero current end toward the unity current end. However, dipole expansion function n has polarity such that current flows from the $j = 1$ monopole to the $j = 2$ monopole. Current is continuous, and of value unity, across the terminals of the dipole. The terminals of the dipole is where monopole 1 intersects with monopole 2, i.e., the point $z_{nj} = d_{nj}$. In this manner, expansion function n is written as $(n = 1, 2, ..., N)$

$$\mathbf{J}_n = \mathbf{J}_{n1}(\rho_{n1}, z_{n1}) - \mathbf{J}_{n2}(\rho_{n2}, z_{n2}) \tag{2.13}$$

where, for $j = 1, 2$

$$\mathbf{J}_{nj}(\rho_{nj}, z_{nj}) = \hat{\mathbf{z}}_{nj}\, J^z_{nj}(\rho_{nj}, z_{nj}) + \hat{\boldsymbol{\rho}}_{nj}\, J^\rho_{nj}(\rho_{nj}, z_{nj}) \tag{2.14}$$

with ρ_{nj} and z_{nj} being the local radial and axial coordinates for monopole segment nj.

The expansion function contains an axial and a radial component corresponding to the transverse magnetic (TM) to z fields inside the thin material wire [25]. These components are written as

$$J^z_{nj}(\rho_{nj}, z_{nj}) = C\, J_0(k_\rho\, \rho_{nj})\, F_{nj}(k_z\, z_{nj}) \quad \text{and} \tag{2.15}$$

$$J^{\rho}_{nj}(\rho_{nj}, z_{nj}) = \frac{-C}{k_\rho} J_1(k_\rho \rho_{nj}) F'_{nj}(k_z z_{nj}) \tag{2.16}$$

where C is a normalization constant, J_i is a Bessel function of order i ($i = 0, 1$), the prime $'$ denotes differentiation with respect to z_{nj}, and from the wave equation,

$$k_\rho^2 + k_z^2 = k_1^2.$$

The normalization constant C is chosen such that $J^{\rho}_{nj}(\rho_{nj}, z_{nj})$ has unit terminal current, i.e.,

$$C = \left[\int_0^{2\pi} \int_0^a J_0(k_\rho \rho_{nj})\, \rho_{nj}\, d\rho_{nj}\, d\phi\right]^{-1} = \frac{k_\rho}{2\pi a\, J_1(k_\rho a)}. \tag{2.17}$$

Note that the radial component J^{ρ}_{nj} is dependent upon the axial component J^{z}_{nj}, and thus there is only one unknown current. The function $F_{nj}(k_z z_{nj})$ defines the axial variation of the expansion functions, as explained next.

As shown in Figure 2.3, dipole expansion functions are always zero at the endpoints but rise to unity at the terminals. Since the current vanishes at the endpoints of a perfectly conducting wire, these expansion functions are used for modeling the current on perfectly conducting wire objects. They are also used for modeling the current away from wire endpoints on imperfect conductive or dielectric wires objects. The axial variation of a dipole expansion function consists of two monopole axial variations. Choosing $k_z = k_0$, the monopole axial variation is

$$F_{nj}(k_z z_{nj}) = \begin{cases} \frac{\sin(k_0 z_{nj})}{\sin(k_0 d_{nj})} & \text{if } 0 \le z_{nj} \le d_{nj} \\ \\ 0 & \text{otherwise.} \end{cases} \tag{2.18}$$

For imperfect conductive or dielectric wire objects, or when wire objects physically touch across adjacent cells, the current will not necessarily vanish at the wire object endpoints. To model such a current, *monopole* expansion functions are used. A monopole expansion function consists of only the $j = 1$ current segment. In analogy to Equation (2.13), monopole expansion function n is written as

$$\mathbf{J}_n = \mathbf{J}_{n1}(\rho_{n1}, z_{n1}), \tag{2.19}$$

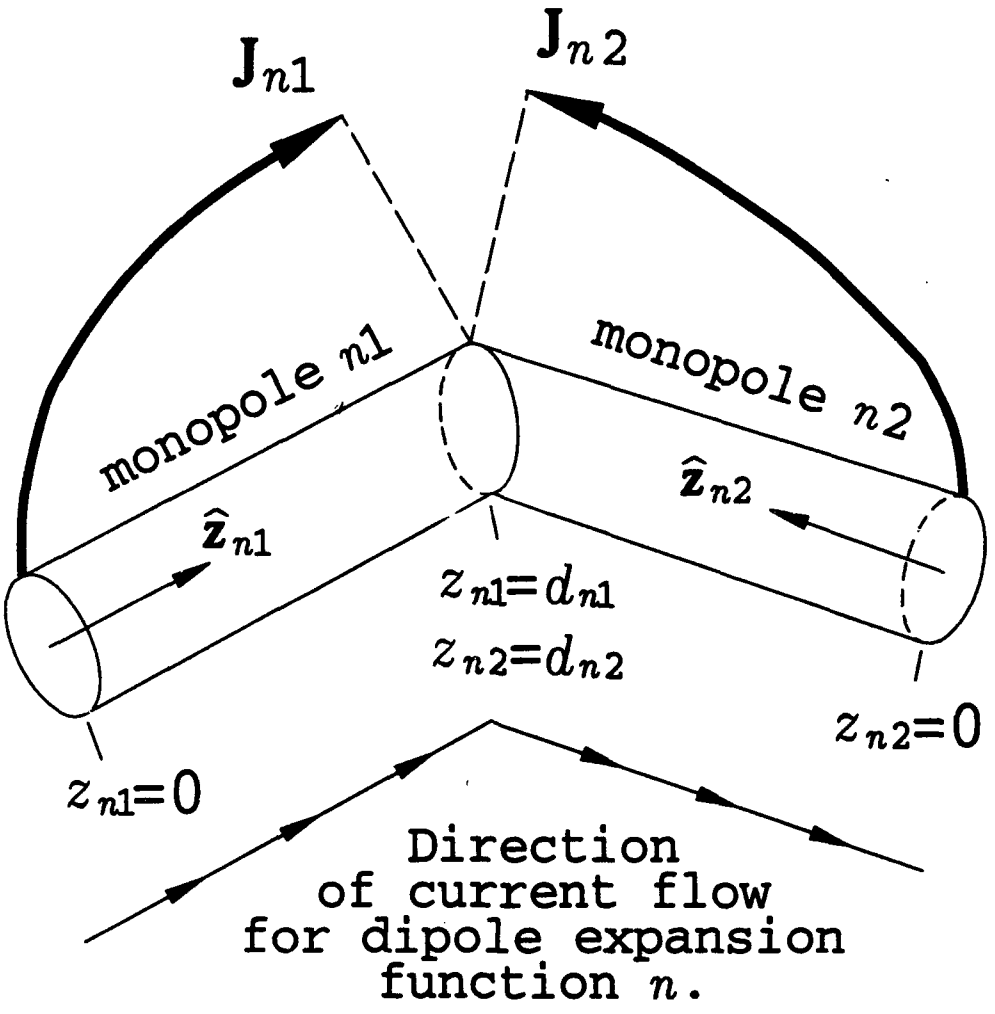

Figure 2.3: A typical dipole MM expansion function.

and the axial and radial variations remain the same as for the dipole expansion functions.

The weighting functions contain only an axial component and have axial variation the same as the expansion functions. However, the radial variation is constant. Therefore, a dipole weighting function is defined as

$$\mathbf{W}_m = \frac{1}{\pi a^2} \left[\hat{\mathbf{z}}_{m1} F_{m1}(k_z z_{m1}) - \hat{\mathbf{z}}_{m2} F_{m2}(k_z z_{m2}) \right] \tag{2.20}$$

and a monopole weighting function is defined as

$$\mathbf{W}_m = \frac{1}{\pi a^2} \hat{\mathbf{z}}_{m1} F_{m1}(k_z z_{m1}) \tag{2.21}$$

for $m = 1, 2, ..., N$.

2.2.2 Evaluation of the Eigenfunction Currents

Assume that a value of k_e has been found such that the fundamental Equation (2.12) is satisfied. Now it is desired to determine the eigenfunction currents in the wire objects. The MM matrix equation for the eigenfunction current in the center wire object can be written as

$$\begin{bmatrix} \mathcal{Z}_{11} & \mathcal{Z}_{12} & \cdots & \mathcal{Z}_{1N} \\ \mathcal{Z}_{21} & \mathcal{Z}_{22} & \cdots & \mathcal{Z}_{2N} \\ \vdots & \vdots & \ddots & \vdots \\ \mathcal{Z}_{N1} & \mathcal{Z}_{N2} & \cdots & \mathcal{Z}_{NN} \end{bmatrix} \begin{bmatrix} I_1 \\ I_2 \\ \vdots \\ I_N \end{bmatrix} = \begin{bmatrix} 0 \\ 0 \\ \vdots \\ 0 \end{bmatrix}. \tag{2.22}$$

Recall that the determinant of the impedance matrix is zero, and thus this system of equations cannot be solved for the current coefficients I in the usual manner. However, the eigenfunction currents can be determined, to within a constant, by setting an arbitrary non-zero element of I to unity, and then reducing Equation (2.22) to an order $N-1$ system of equations for the remaining $N-1$ current coefficients. For example, setting the last coefficient $I_N = 1$, Equation (2.22) reduces to

$$\begin{bmatrix} \mathcal{Z}_{11} & \mathcal{Z}_{12} & \cdots & \mathcal{Z}_{1,N-1} \\ \mathcal{Z}_{21} & \mathcal{Z}_{22} & \cdots & \mathcal{Z}_{2,N-1} \\ \vdots & \vdots & \ddots & \vdots \\ \mathcal{Z}_{N-1,1} & \mathcal{Z}_{N-1,2} & \cdots & \mathcal{Z}_{N-1,N-1} \end{bmatrix} \begin{bmatrix} I_1 \\ I_2 \\ \vdots \\ I_{N-1} \end{bmatrix} = \begin{bmatrix} -\mathcal{Z}_{1N} \\ -\mathcal{Z}_{1N} \\ \vdots \\ -\mathcal{Z}_{N-1,N} \end{bmatrix}, \tag{2.23}$$

which can be solved using standard techniques. This method yields the eigenfunction currents on the wire objects to within a constant.

2.3 Determination of the Effective Constitutive Parameters

This section discusses the determination of the effective permittivity and permeability tensors, denoted by $(\bar{\epsilon}_e, \bar{\mu}_e)$, for an anisotropic artificial medium. A discussion of the roots k_e to Equation (2.12) is included, and different approaches to evaluating $(\bar{\epsilon}_e, \bar{\mu}_e)$ are presented.

Much of the theory contained in this section follows from anisotropic media theory as applied to crystal optics [23, Ch. 4], [24, Ch. 14]. This theory seems to apply to the macroscopic model of artificial media, provided the arbitrary material wire objects are not too electrically large or spaced too far apart and the eigenfunction current shape is not a strong function of the direction of propagation.

2.3.1 Discussion of the Roots k_e and Polarization

The first step in determining the equivalent permittivity and permeability of the artificial medium is to determine the roots, k_e, to Equation (2.12). For a given direction of propagation through an anisotropic artificial medium composed of arbitrary scattering objects, there are two fundamental roots, k_e, to Equation (2.12) [23, Sec. 4.25], [24, Sec. 14.2.2]. Each root corresponds to a distinct polarization of the plane wave in the artificial medium, and its corresponding eigenfunction currents and fields.

For special geometries, the roots may be repeated roots or degenerate to the host medium wavenumber $k_e = k_0$. For example, repeated roots (two roots with the same numerical value for k_e) will occur for propagation normal to a symmetric wire cross with equal length vertical and horizontal members. One root corresponds to vertical polarization, and the other root corresponds to horizontal polarization. If the scattering object is of 2D or of 3D extent, the two roots will be different from the host medium wavenumber. If the scattering object is of 1D extent (i.e. a linear dipole), then there will be one root $k_e = k_0$, corresponding to a plane wave with polarization

perpendicular to the dipole, and one root $k_e \neq k_0$, corresponding to polarization parallel to the dipole.

In a real homogeneous anisotropic medium the elements of the tensor constitutive parameters are independent of the direction of propagation [23, Ch. 4], [24, Sec. 14.1]. However, in an artificial medium, these elements may depend on the direction of propagation. If the material wire objects are not too electrically large or spaced too far apart, and the eigenfunction current shape is not strongly dependent on the direction of propagation, then any direction–dependent variation of the tensor constitutive parameter elements should be small or negligible. However, if the eigenfunction current shape is a strong function of the direction of propagation, then the tensor constitutive parameter elements may also vary with the direction of propagation.

Note that in developing Equation (2.12), the polarization of the plane wave was not specified. Thus, when a root of Equation (2.12) is found, the polarization is unknown. To find the polarization one can first compute the corresponding eigenfunction currents using Equation (2.23), and then the eigenfunction electric and magnetic fields, as presented in Chapter 4. The polarization of the electric field is taken as the polarization corresponding to the chosen value of k_e. Once the eigenfunction fields are known, the characteristic impedance of the artificial medium, denoted η_e, can be evaluated as the ratio of the electric to magnetic eigenfunction fields tangential to the assumed direction of propagation. If the host medium and the scattering objects are lossless, then k_e and η_e will be positive real numbers. However, if either the host medium or the scattering objects have loss, then k_e will be a complex number in the fourth quadrant, and η_e will be a complex number in the sector $\pm 45°$ of the positive real axis [26, Sec. 2-3].

Since the scattering objects in an artificial medium are typically electrically small, one is usually interested in the eigenfunction modes with the smallest k_e. However, it is important to note that larger roots, with larger k_e, may exist. One manner in which higher order roots do exist is through the periodic nature of the complex multiplier $C^{\mathbf{Q}}$ of Equation (2.6). For example, in a problem where propagation is in the $\hat{\mathbf{u}}_k = \hat{\mathbf{z}}$

direction, $C^{\mathbf{Q}}$ simplifies to

$$C^{\mathbf{Q}} = e^{-jk_x(k_w d_w w_x)}. \tag{2.24}$$

Recall that $C^{\mathbf{Q}}$ is the only term in the fundamental root Equation (2.12) that depends on k_x. Let $k_x = k_{x0}$ be the smallest root to Equation (2.12), where $\mathrm{Re}(k_{x0}) > 0$. It can be seen by inspection of Equation (2.24) that if k_{x0} is a root, then so will be values of k_x where

$$k_x = k_{x0} \pm \frac{2p\pi}{d_w w_x} \quad \text{for } p = 1, 2, 3, \ldots \tag{2.25}$$

Thus, for some geometries, there exists a periodic occurrence of roots to Equation (2.12). However, for the material presented here, the lowest order root is the only root of interest, i.e., $k_x = k_{x0}$ is assumed. It should be noted that higher order roots *may exist* that correspond to higher order modal eigenfunction solutions in the artificial medium, however, no such roots have been found to this date.

2.3.2 Polarization Method

Consider the determination of the dyadic effective permittivity and permeability $(\bar{\epsilon}_e, \bar{\mu}_e)$ for an anisotropic artificial medium. It is assumed that for a given geometry, the two roots k_x, their corresponding eigenfunction currents $\mathbf{J}^0$ on the center element, and their eigenfunction fields averaged over the volume of the center cell $(\mathbf{E}^0, \mathbf{H}^0)$, have all been determined. In the limit as $k_x \to k_0$, the eigenfunction currents vanish and the eigenfunction fields become identical to a plane wave in the host medium.

The electric and magnetic dipole moment per unit volume in the center cell can now be computed as [20, Ch. 12.5]

$$\mathbf{P}^0 = \frac{1}{j\omega\Delta v} \int_{V^0} \mathbf{J}^0 \, dv = \epsilon_0 \bar{\chi}^e \cdot \mathbf{E}^0 \tag{2.26}$$

$$\mathbf{M}^0 = \frac{1}{2\Delta v} \int_{V^0} \mathbf{R} \times \mathbf{J}^0 \, dv = \bar{\chi}^m \cdot \mathbf{H}^0 \tag{2.27}$$

where V^0 represents the region of the center cell of volume Δv, and $\bar{\chi}^e$ and $\bar{\chi}^m$ are the dimensionless symmetric [23, Sec. 4.24], [24, Sec. 14.1] effective electric and magnetic susceptibility tensors, respectively, for the artificial medium. Equation

(2.27) shows that even perfectly conducting or pure dielectric scattering objects can have a magnetic moment, and thus an effective permeability different from the host medium. Assuming that the usual constitutive relationships, which are valid point by point in a real medium, hold in an average sense in an artificial medium, the average electric and magnetic flux densities in the center cell are given by

$$\mathbf{D}^0 = \epsilon_0 \mathbf{E}^0 + \mathbf{P}^0 = \epsilon_0 \mathbf{E}^0 + \epsilon_0 \bar{\chi}^e \cdot \mathbf{E}^0 = \bar{\epsilon}_e \cdot \mathbf{E}^0 \tag{2.28}$$

$$\mathbf{B}^0 = \mu_0(\mathbf{H}^0 + \mathbf{M}^0) = \mu_0(\mathbf{H}^0 + \bar{\chi}^m \cdot \mathbf{H}^0) = \bar{\mu}_e \cdot \mathbf{H}^0. \tag{2.29}$$

From Equations (2.28) and (2.29), the dyadic effective permittivity and permeability are given by

$$\bar{\epsilon}_e = (\bar{I} + \bar{\chi}^e)\epsilon_0 \tag{2.30}$$

$$\bar{\mu}_e = (\bar{I} + \bar{\chi}^m)\mu_0 \tag{2.31}$$

where $\bar{I}$ is the unit dyad.

Explicitly showing Equation (2.26) relating the effective electric susceptibility to the average electric field and the electric dipole moment per unit volume in the center cell,

$$\epsilon_0 \begin{bmatrix} \chi^e_{xx} & \chi^e_{xy} & \chi^e_{xz} \\ \chi^e_{yx} & \chi^e_{yy} & \chi^e_{yz} \\ \chi^e_{zx} & \chi^e_{zy} & \chi^e_{zz} \end{bmatrix} \begin{bmatrix} E^0_x \\ E^0_y \\ E^0_z \end{bmatrix} = \begin{bmatrix} P^0_x \\ P^0_y \\ P^0_z \end{bmatrix}. \tag{2.32}$$

Equation (2.32) is equivalent to three equations in the nine components of $\bar{\chi}^e$, and is the result of one of the two roots of Equation (2.12). The other root will produce a dyadic equation, similar to Equation (2.32) with the same $\bar{\chi}^e$, but with different $\mathbf{E}^0$ and $\mathbf{P}^0$. The two dyadic equations, along with the condition that $\bar{\chi}^e$ is symmetric, can now be solved for the nine components of $\bar{\chi}^e$. Once $\bar{\chi}^e$ is known, then $\bar{\epsilon}_e$ is determined simply from Equation (2.30). The determination of $\bar{\mu}_e$ is parallel to that presented for $\bar{\epsilon}_e$, but uses the dyadic Equation (2.27).

2.3.3 Maxwell's Equations Method

Another method of determining the tensor constitutive parameters of the artificial medium follows directly from Maxwell's equations. For this method, it is assumed

that Maxwell's equations apply to the average fields in the center cell of the artificial medium. Applying the well-known source-free Maxwell's equations to the plane wave fields of the form assumed in Equation (2.2), it is obtained that [27, Sec. 2.3]

$$\nabla \times \mathbf{H} = -j\omega\mathbf{D} \qquad \Longrightarrow \qquad \mathbf{k}_e \times \mathbf{H}^0 = -\omega\mathbf{D}^0 = -\omega\bar{\epsilon}_e \cdot \mathbf{E}^0 \tag{2.33}$$

$$\nabla \times \mathbf{E} = j\omega\mathbf{B} \qquad \Longrightarrow \qquad \mathbf{k}_e \times \mathbf{E}^0 = \omega\mathbf{B}^0 = \omega\bar{\mu}_e \cdot \mathbf{H}^0 \tag{2.34}$$

$$\nabla \cdot \mathbf{D} = 0 \qquad \Longrightarrow \qquad \mathbf{k}_e \cdot \mathbf{D}^0 = 0, \tag{2.35}$$

$$\nabla \cdot \mathbf{B} = 0 \qquad \Longrightarrow \qquad \mathbf{k}_e \cdot \mathbf{B}^0 = 0 \tag{2.36}$$

where the tensor constitutive relationships of Equations (2.28) and (2.29) have been used.

Explicitly showing Equation (2.33) relating the effective wave-vector and permittivity tensor to the average electric and magnetic fields per unit volume in the center cell,

$$\begin{bmatrix} k_{ey}H_z^0 - k_{ez}H_y^0 \\ k_{ez}H_x^0 - k_{ex}H_z^0 \\ k_{ex}H_y^0 - k_{ey}H_x^0 \end{bmatrix} = -\omega \begin{bmatrix} \epsilon_{xx}^e & \epsilon_{xy}^e & \epsilon_{xz}^e \\ \epsilon_{yx}^e & \epsilon_{yy}^e & \epsilon_{yz}^e \\ \epsilon_{zx}^e & \epsilon_{zy}^e & \epsilon_{zz}^e \end{bmatrix} \begin{bmatrix} E_x^0 \\ E_y^0 \\ E_z^0 \end{bmatrix}. \tag{2.37}$$

Equation (2.37) is equivalent to three equations in the nine components of $\bar{\epsilon}_e$, and is the result of one of the two roots of Equation (2.12). The other root will produce a dyadic equation, similar to Equation (2.37) with the same $\bar{\epsilon}_e$, but with different $\mathbf{k}_e$ and ($\mathbf{E}^0$,$\mathbf{H}^0$). The two dyadic equations, along with the condition that $\bar{\epsilon}_e$ is symmetric, can now be solved for the nine components of $\bar{\epsilon}_e$. The determination of $\bar{\mu}_e$ is parallel to that presented for $\bar{\epsilon}_e$, but uses the dyadic Equation (2.34).

2.3.4 Uniaxial Artificial Media

For certain simple anisotropic media, termed uniaxial media, the off diagonal components of $\bar{\chi}^e$ (and $\bar{\chi}^m$) are negligible, and the diagonal components are related to $\mathbf{E}^0$ and $\mathbf{P}^0$ by

$$\chi_{ii}^e = \frac{P_i^0}{\epsilon_0 E_i^0} \qquad i = x, y, z. \tag{2.38}$$

Equation (2.38) can be used to find the ii component of $\bar{\chi}^e$ provided that E_i^0 is non zero. If for a given direction of propagation and root, $E_i^0 \neq 0$ for $i = x, y, z$, then

Equation (2.38) can be used to find all three diagonal components of $\bar{\chi}^e$. If for a given direction of propagation and root $E_i^0 = 0$, then $P_i^0 = 0$, and Equation (2.38) is indeterminate. In this case χ_{ii}^e can be determined from the other root, or by a different direction of propagation.

Consider propagation along of one of the three principle axes in a uniaxial media. The two roots will correspond to polarisations in the directions of the two principle axes transverse to the direction of propagation. For this special case, the effective permittivity and permeability can be determined from the root k_e and characteristic impedance η_e. It is assumed that k_e and η_e have been determined for a given frequency, polarisation and direction of propagation along one of the principle axes. Since k_e and η_e are related to μ_e and ϵ_e by

$$k_e \mp \omega\sqrt{\mu_e \epsilon_e} \quad \text{and} \quad \eta_e = \sqrt{\frac{\mu_e}{\epsilon_e}}, \tag{2.39}$$

then

$$\epsilon_e = \frac{k_e}{\omega \eta_e} \quad \text{and} \quad \mu_e = \frac{\eta_e k_e}{\omega}. \tag{2.40}$$

If the magnetic moment of the scattering objects is negligible, then $\mu_e = \mu_0$, and ϵ_e is given by

$$\epsilon_e = \frac{k_e^2}{\omega^2 \mu_0}. \tag{2.41}$$

The advantage of using Equation (2.41) for pure artificial dielectrics (i.e., $\mu_e = \mu_0$) is that one need not compute η_e.

2.4 Fields of a 2D Planar Array of Current Elements

This section evaluates the exact electric and magnetic fields of a 2D planar array of linear current elements. The theory included here has been presented before [28, 29, 30], however, it is repeated here since it is of great importance in implementing the PMM solution, and to employ notation specific to the artificial dielectric geometry.

Figure 2.4 shows a 2D planar array of infinitesimal current elements arranged on a parallelogram grid. The host medium is homogeneous and isotropic with constitutive

parameters (μ_0, ϵ_0). Note that the host medium is not necessarily free space, and in general is a lossy medium. The unit vectors of the grid are $\hat{\mathbf{u}} = \hat{\mathbf{x}}$ and $\hat{\mathbf{v}} = v_x\hat{\mathbf{x}} + v_y\hat{\mathbf{y}}$, and the spacings of the grid are d_u in the $\hat{\mathbf{u}}$ direction and d_v in the $\hat{\mathbf{v}}$ direction. The elements are referenced by the indices (i_u, j_v) for $-\infty \leq (i_u, j_v) \leq \infty$ and element (i_u, j_v) is located at $\mathbf{R}_{ij} = i_u\, d_u\, \hat{\mathbf{u}} + j_v\, d_v\, \hat{\mathbf{v}}$. All elements are polarized in the arbitrary direction $\hat{\mathbf{a}}$, which may have a component out of the xy plane (or the uv plane.) Corresponding to the value of the plane wave with wave-vector $\mathbf{k_e}$ propagating across the array, the incremental current moment on element (i_u, j_v) is

$$\hat{\mathbf{a}}\, I\, dl'\, e^{-j\mathbf{k_e}\cdot\mathbf{R}_{ij}} = \hat{\mathbf{a}}\, I\, dl'\, e^{-j(i_u\, d_i + j_v\, d_j)} \qquad \text{where}$$

$$\begin{aligned} \mathbf{k_e} &= k_{ex}\,\hat{\mathbf{x}} + k_{ey}\,\hat{\mathbf{y}} + k_{ez}\,\hat{\mathbf{z}}, \\ d_i &= d_u\, k_{ex}, \qquad\qquad \text{and} \\ d_j &= d_v(k_{ex}\, v_x + k_{ey}\, v_y). \end{aligned}$$

The entire array produces some incremental electric vector potential $d\mathbf{A}$, which is the the summation of each individual element's contribution. If the field point is at $\mathbf{R} = x\hat{\mathbf{x}} + y\hat{\mathbf{y}} + z\hat{\mathbf{z}}$, then the contribution of element (i_u, j_v) to $d\mathbf{A}$ is

$$d\mathbf{A}_{ij} = \hat{\mathbf{a}}\,\frac{\mu_0}{4\pi}\, I\, dl'\, e^{-j(i_u\, d_i + j_v\, d_j)}\,\frac{e^{-jk_0|\mathbf{R}-\mathbf{R}_{ij}|}}{|\mathbf{R}-\mathbf{R}_{ij}|}. \tag{2.42}$$

Summing the contributions of every element in the array, it is obtained that

$$d\mathbf{A} = \sum_{j_v}\sum_{i_u} d\mathbf{A}_{ij} = \hat{\mathbf{a}}\,\frac{\mu_0}{4\pi}\, I\, dl' \sum_{j_v} e^{-j(j_v\, d_j)} \sum_{i_u} e^{-j(i_u\, d_i)}\,\frac{e^{-jk_0|\mathbf{R}-\mathbf{R}_{ij}|}}{|\mathbf{R}-\mathbf{R}_{ij}|}. \tag{2.43}$$

In Equation (2.43) it is implicit that the summations are over $-\infty \leq (i_u, j_v) \leq \infty$.

The inner summation of Equation (2.43) can be rewritten as

$$\sum_{i_u} e^{-j(i_u\, d_i)}\,\frac{e^{-jk_0|\mathbf{R}-\mathbf{R}_{ij}|}}{|\mathbf{R}-\mathbf{R}_{ij}|} = \sum_{i_u} e^{-j(i_u\, d_i)}\,\frac{e^{-jk_0\sqrt{(x'-i_u\, d_u)^2 + a^2}}}{\sqrt{(x'-i_u\, d_u)^2 + a^2}} \tag{2.44}$$

where $x' = x - j_v\, v_x\, d_v$ and $a^2 = (y - j_v\, v_y\, d_v)^2 + z^2$. Next, the Poisson sum formula [31]

$$\sum_m e^{jm\omega_0 t}\, F(m\omega_0) = \frac{2\pi}{\omega_0}\sum_n f\left(t + n\frac{2\pi}{\omega_0}\right) \tag{2.45}$$

along with the Fourier transform pair

$$F(\omega) = \frac{e^{-jk_0\sqrt{a^2 + (\omega-\omega_1)^2}}}{\sqrt{a^2 + (\omega-\omega_1)^2}} \Longleftrightarrow f(t) = \frac{e^{j\omega_1 t}}{2j} H_0^{(2)}\left(a\sqrt{k_0^2 - t^2}\right), \tag{2.46}$$

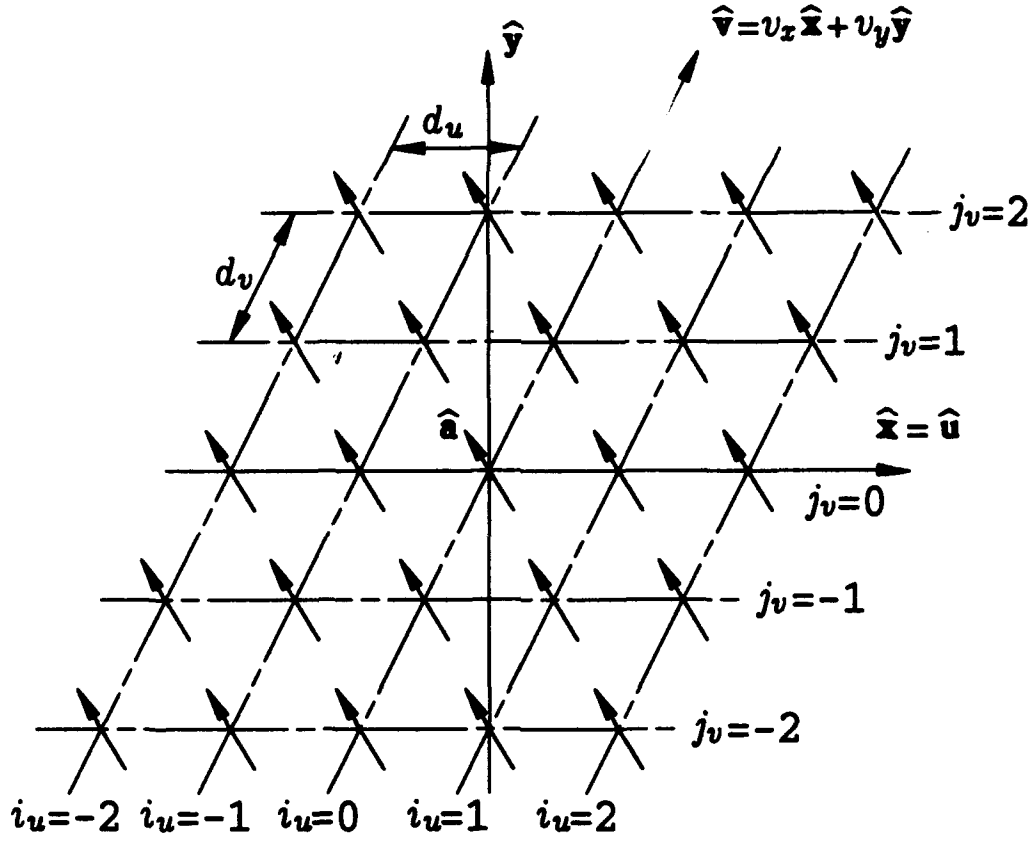

Figure 2.4: A 2D planar array of infinitesimal current elements.

where $H_0^{(2)}(\cdot)$ is the second type Hankel function of order zero, is applied to Equation (2.44). With the variables of transformation defined as

$$\begin{aligned} m &\rightarrow i_u \\ n &\rightarrow n_u \\ \omega_0 &\rightarrow d_u \\ \omega_1 &\rightarrow x' \\ t &\rightarrow -k_{sx} \end{aligned}$$

it is obtained that

$$\sum_{i_u} e^{-j(i_u d_i)} \frac{e^{-jk_0|\mathbf{R}-\mathbf{R}_{ij}|}}{|\mathbf{R}-\mathbf{R}_{ij}|} = \frac{\pi}{jd_u} \sum_{n_u} e^{-jz(k_{sz}+n_u \frac{2\pi}{d_u})} e^{j(j_v v_x d_v)(k_{sx}+n_u \frac{2\pi}{d_u})} \times$$

$$\times H_0^{(2)} \left[a\sqrt{k_0^2 - \left(k_{sx} + n_u \frac{2\pi}{d_u}\right)^2} \right]. \tag{2.47}$$

All the summation indices of Equations (2.45) and (2.47) are of the range $-\infty \leq (m, n, n_u) \leq \infty$

The electric vector potential can be now be written as

$$d\mathbf{A} = \hat{\mathbf{a}} \frac{\mu_0 I dl'}{4jd_u} \sum_{n_u} e^{-jk_0 z(\frac{k_{sx}}{k_0} + n_u \frac{2\pi}{k_0 d_u})} \times$$

$$\times \sum_{j_v} e^{-jk_0[(j_v d_v)(\frac{k_{sy}}{k_0} v_y - n_u v_x \frac{2\pi}{k_0 d_u})]} H_0^{(2)} \left[k_0 r_p \sqrt{(y - j_v v_y d_v)^2 + z^2} \right], \tag{2.48}$$

where $r_p = \sqrt{1 - \left(\frac{k_{sx}}{k_0} + n_u \frac{2\pi}{k_0 d_u}\right)^2}$. The Poisson sum formula of Equation (2.45) is applied a second time using the Fourier transform pair

$$F(\omega) = H_0^{(2)} \left(k_0 r_p \sqrt{z^2 + (\omega - \omega_2)^2} \right) \Longleftrightarrow f(t) = \frac{e^{j\omega_2 t}}{\pi} \frac{e^{-jz\sqrt{(k_0 r_p)^2 - t^2}}}{\sqrt{(k_0 r_p)^2 - t^2}} \tag{2.49}$$

and the transformation variables defined as

$$\begin{aligned} m &\rightarrow j_v \\ n &\rightarrow n_v \\ \omega_0 &\rightarrow v_y d_v \\ \omega_2 &\rightarrow y \\ t &\rightarrow -k_0 \left(\frac{k_{sy}}{k_0} - n_u \frac{v_x}{v_y} \frac{2\pi}{k_0 d_u} \right). \end{aligned}$$

Carrying out this process on the inner summation of Equation (2.48), it is obtained that

$$d\mathbf{A} = \hat{\mathbf{a}}\frac{\mu_0 I dl'}{2jk_0 d_u v_y d_v}\sum_{n_u} e^{-jk_0 x(\frac{k_{sx}}{k_0}+n_u\frac{2\pi}{k_0 d_u})}\sum_{n_v} e^{-jk_0 y(\frac{k_{sy}}{k_0}-n_u\frac{v_x}{v_y}\frac{2\pi}{k_0 d_u}+n_v\frac{2\pi}{k_0 v_y d_v})}\times$$

$$\times\frac{e^{-jk_0 z\sqrt{1-(\frac{k_{sx}}{k_0}+n_u\frac{2\pi}{k_0 d_u})^2-(\frac{k_{sy}}{k_0}-n_u\frac{v_x}{v_y}\frac{2\pi}{k_0 d_u}+n_v\frac{2\pi}{k_0 v_y d_v})^2}}}{\sqrt{1-(\frac{k_{sx}}{k_0}+n_u\frac{2\pi}{k_0 d_u})^2-(\frac{k_{sy}}{k_0}-n_u\frac{v_x}{v_y}\frac{2\pi}{k_0 d_u}+n_v\frac{2\pi}{k_0 v_y d_v})^2}}. \qquad (2.50)$$

It is worthwhile to write Equation (2.50) in the compact form

$$d\mathbf{A} = \hat{\mathbf{a}}\frac{\mu_0 I dl'}{2jk_0 d_u v_y d_v}\sum_{n_u}\sum_{n_v}\frac{e^{-jk_0\mathbf{R}\cdot\hat{\mathbf{r}}_\pm}}{r_z} \quad \text{for} \quad z\begin{cases} >0 \\ <0 \end{cases} \quad \text{where} \qquad (2.51)$$

$$\begin{aligned}
\mathbf{R} &= x\hat{\mathbf{x}} + y\hat{\mathbf{y}} + z\hat{\mathbf{z}}, \\
\hat{\mathbf{r}}_\pm &= r_x\hat{\mathbf{x}} + r_y\hat{\mathbf{y}} \pm r_z\hat{\mathbf{z}}, \\
r_x &= \frac{k_{sx}}{k_0} + n_u\frac{2\pi}{k_0 d_u} \\
r_y &= \frac{k_{sy}}{k_0} - n_u\frac{v_x}{v_y}\frac{2\pi}{k_0 d_u} + n_v\frac{2\pi}{k_0 v_y d_v}, \qquad \text{and} \\
r_z &= \sqrt{1-r_x^2-r_y^2} \qquad \text{such that } \mathrm{Im}(r_z)\le 0.
\end{aligned}$$

In this form, the electric field of the 2D array of infinitesimal current elements is expressed as a double *spectral* summation of plane waves propagating in the spectral direction $\hat{\mathbf{r}}_+$ for positive z and $\hat{\mathbf{r}}_-$ for negative z. Note that in the square root defining r_z, the root is chosen such that the spectral plane wave either propagates or decays exponentially as it moves away from the xy plane. In general, for a lossless host medium ($\mathrm{Im}(k_0) = 0$) there will be a finite number of propagating waves and an infinite number of decaying evanescent waves.

The incremental magnetic field is found simply as

$$d\mathbf{H} = \frac{1}{\mu_0}\nabla\times d\mathbf{A} = \frac{I dl'}{2d_u v_y d_v}\sum_{n_u}\sum_{n_v}\frac{e^{-jk_0\mathbf{R}\cdot\hat{\mathbf{r}}_\pm}}{r_z}\hat{\mathbf{a}}\times\hat{\mathbf{r}}_\pm, \qquad (2.52)$$

and the incremental electric field is found as

$$d\mathbf{E} = \frac{1}{j\omega\epsilon_0}\nabla\times d\mathbf{H} = \frac{I dl'\eta_0}{2d_u v_y d_v}\sum_{n_u}\sum_{n_v}\frac{e^{-jk_0\mathbf{R}\cdot\hat{\mathbf{r}}_\pm}}{r_z}\mathbf{e}_\pm \quad \cdot \text{ where,} \qquad (2.53)$$

$$\mathbf{e}_\pm = (\hat{\mathbf{a}}\times\hat{\mathbf{r}}_\pm)\times\hat{\mathbf{r}}_\pm = (\hat{\mathbf{r}}_\pm\cdot\hat{\mathbf{a}})\hat{\mathbf{r}}_\pm - \hat{\mathbf{a}}. \qquad (2.54)$$

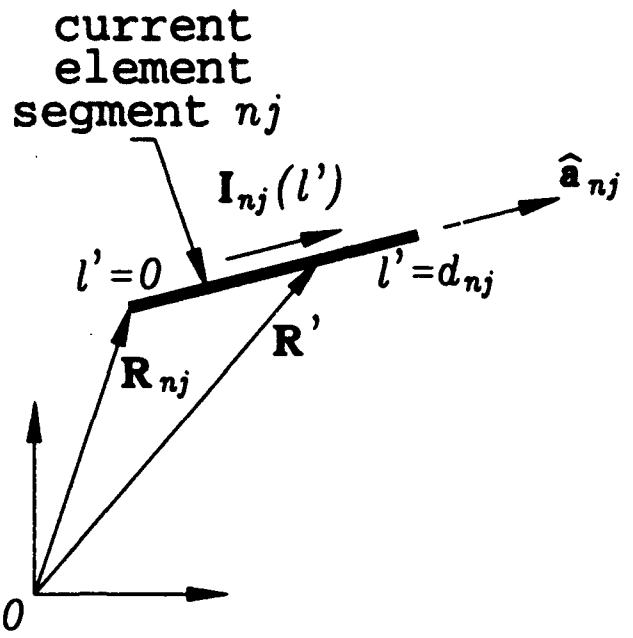

Figure 2.5: Vector relationship for the center $\mathbf{Q} = 0$ current segment nj.

If the reference point moves from the origin to $\mathbf{R}'$, the resulting field is the same as if the reference point stays at the origin, and the field point moves to $\mathbf{R} - \mathbf{R}'$. In this manner, $d\mathbf{E}$ becomes

$$d\mathbf{E} = \frac{I dl' \eta_0}{2 d_u v_y d_v} \sum_{n_u} \sum_{n_v} \frac{e^{-jk_0 \mathbf{R} \cdot \hat{\mathbf{r}}_\pm}}{r_z} \mathbf{e}_\pm \, e^{+jk_0 \mathbf{R}' \cdot \hat{\mathbf{r}}_\pm}. \tag{2.55}$$

The total electric field of a linear current element nj, denoted as $F_{nj}(l')$, is now determined by integrating Equation (2.55) along the length of the current element. Typically, a current element nj will be monopole j ($j = 1$ or 2) of expansion function n. Note that in Equation (2.55) the only variation on the source point $\mathbf{R}'$ is in the last exponential term. As shown in Figure 2.5, if current element nj is straight, the source point $\mathbf{R}'$ can be written as

$$\mathbf{R}' = \mathbf{R}_{nj} + \hat{\mathbf{a}}_{nj} l' \qquad \text{for } 0 \le l' \le d_{nj} \tag{2.56}$$

where $\mathbf{R}_{nj}$ is the position vector from the origin to the reference end of current element nj, and d_{nj} is the length of segment nj.

Figure 2.6 shows that there are three possible distinct regions that the field point $\mathbf{R}$ can be within. The field in Region (I) consists only of left–going waves, so the $\hat{\mathbf{r}}_-$

spectral vector is chosen and the integration is over the entire range of the current element. Similarly, the field in Region (III) consists only of right–going waves, so $\hat{\mathbf{r}}_+$ is chosen and the integration is over the entire current element. In this manner, the electric field in Region (I) can be written as

$$\mathbf{E}_{nj}^{(\mathrm{I})}(\mathbf{R}) = \frac{\eta_0}{2d_u v_y d_v} \sum_{n_u} \sum_{n_v} \frac{e^{-jk_0(\mathbf{R}-\mathbf{R}_{nj})\cdot\hat{\mathbf{r}}_-}}{r_z} \mathbf{e}_{nj-} P^e_{nj-}(0, d_{nj}) \tag{2.57}$$

and the electric field in Region (III) can be written as

$$\mathbf{E}_{nj}^{(\mathrm{III})}(\mathbf{R}) = \frac{\eta_0}{2d_u v_y d_v} \sum_{n_u} \sum_{n_v} \frac{e^{-jk_0(\mathbf{R}-\mathbf{R}_{nj})\cdot\hat{\mathbf{r}}_+}}{r_z} \mathbf{e}_{nj+} P^e_{nj+}(0, d_{nj}). \tag{2.58}$$

The function $P^e_{nj\pm}(a,b)$ is termed the nj^{th} *source pattern factor* and is defined as

$$P^e_{nj\pm}(a,b) = \int_a^b F_{nj}(l')\, e^{+jk_0 l'(\hat{\mathbf{a}}_{nj}\cdot\hat{\mathbf{r}}_\pm)}\, dl' \tag{2.59}$$

where $F_{nj}(l')$ is the current distribution along the length of current segment nj. The source pattern factor is evaluated in greater detail in Appendix A. In Region (II) the electric field at point R consists of left–going waves from that section of the current element denoted by nj_- and right–going waves from that section of the current element denoted by nj_+. Thus, the field at point R in Region (II) is the sum obtained by choosing the $\hat{\mathbf{r}}_-$ spectral vector and integrating Equation (2.55) over nj_- plus choosing the $\hat{\mathbf{r}}_+$ spectral vector and integrating Equation (2.55) over nj_+. Therefore, the electric field in Region (II) can be written as

$$\mathbf{E}_{nj}^{(\mathrm{II})}(\mathbf{R}) = \frac{\eta_0}{2d_u v_y d_v} \sum_{n_u} \sum_{n_v} \left[\frac{e^{-jk_0(\mathbf{R}-\mathbf{R}_{nj})\cdot\hat{\mathbf{r}}_+}}{r_z} \mathbf{e}_{nj+} P^e_{nj+}(a_{nj+}, b_{nj+}) + \right.$$

$$\left. + \frac{e^{-jk_0(\mathbf{R}-\mathbf{R}_{nj})\cdot\hat{\mathbf{r}}_-}}{r_z} \mathbf{e}_{nj-} P^e_{nj-}(a_{nj-}, b_{nj-}) \right]. \tag{2.60}$$

The limits of integration are from a_{nj+} to b_{nj+} for evaluating the P^e_{nj+} integral and from a_{nj-} to b_{nj-} for evaluating the P^e_{nj-} integral. These limits depend upon the specific wire segment geometry, and are given in Section A.1.

Note that if the current element is in a plane parallel to the xy plane, then Region (II) vanishes and there are only two regions. In this case, Equations (2.57) and (2.58) can be used to determine the electric field everywhere.

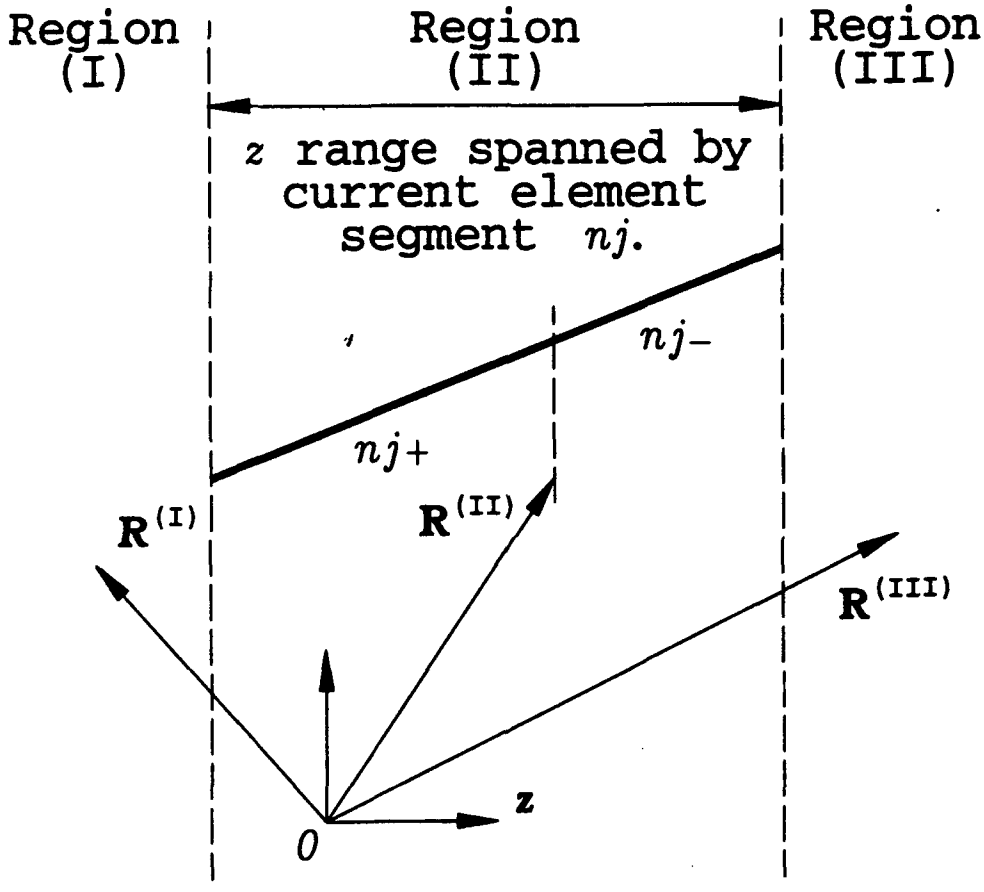

Figure 2.6: The three regions that the field point can be within.

In a similar manner, the magnetic fields in the three distinct regions are:

$$\mathbf{H}_{nj}^{(\mathrm{I})}(\mathbf{R}) = \frac{1}{2d_u v_y d_v} \sum_{n_u} \sum_{n_v} \frac{e^{-jk_0(\mathbf{R}-\mathbf{R}_{nj})\cdot\hat{\mathbf{r}}_-}}{r_z} (\hat{\mathbf{a}}_{nj} \times \hat{\mathbf{r}}_-)\, P^s_{nj-}(0, d_{nj}) \tag{2.61}$$

$$\mathbf{H}_{nj}^{(\mathrm{III})}(\mathbf{R}) = \frac{1}{2d_u v_y d_v} \sum_{n_u} \sum_{n_v} \frac{e^{-jk_0(\mathbf{R}-\mathbf{R}_{nj})\cdot\hat{\mathbf{r}}_+}}{r_z} (\hat{\mathbf{a}}_{nj} \times \hat{\mathbf{r}}_+)\, P^s_{nj+}(0, d_{nj}) \tag{2.62}$$

$$\mathbf{H}_{nj}^{(\mathrm{II})}(\mathbf{R}) = \frac{1}{2d_u v_y d_v} \sum_{n_u} \sum_{n_v} \left[\frac{e^{-jk_0(\mathbf{R}-\mathbf{R}_{nj})\cdot\hat{\mathbf{r}}_+}}{r_z} (\hat{\mathbf{a}}_{nj} \times \hat{\mathbf{r}}_+)\, P^s_{nj+}(a_{nj+}, b_{nj+}) + \right.$$
$$\left. + \frac{e^{-jk_0(\mathbf{R}-\mathbf{R}_{nj})\cdot\hat{\mathbf{r}}_-}}{r_z} (\hat{\mathbf{a}}_{nj} \times \hat{\mathbf{r}}_-)\, P^s_{nj-}(a_{nj-}, b_{nj-}) \right]. \tag{2.63}$$

It should be noted that the fields evaluated in this section are for a single current element nj. This is adequate for evaluating the fields from a monopole expansion function. However, a dipole expansion function is composed of two current segments, and the procedure of this section must be repeated for each section. As shown in Figure 2.5 and in Equation (2.56), the vector $\mathbf{R}_{nj}$ always points from the origin to the zero current endpoint of current segment nj, and the unit vector $\hat{\mathbf{a}}_{nj}$ points from the zero current endpoint to the unity current endpoint.

2.5 Fields of a 3D Volume Array of Current Elements

This section uses the results of Section 2.4 to evaluate the exact electric and magnetic fields of a 3D volume array of linear current elements [32, Ch. 2]. As shown in Figure 2.7, the 3D volume array consists of an infinite parallel stacking of the 2D planar array of elements in the host medium (μ_0, ϵ_0). The 2D layers are referenced by the index k_w for $-\infty \leq k_w \leq \infty$, and are spaced a distance of d_w in the unit direction $\hat{\mathbf{w}} = w_x\hat{\mathbf{x}} + w_y\hat{\mathbf{y}} + w_z\hat{\mathbf{z}}$. Therefore, the vector from the reference point on the $k_w = 0$ plane (the origin) to the equivalent point on any $k_w \neq 0$ plane can be skew to the xy plane, and is given as $k_w d_w \hat{\mathbf{w}}$. The current elements on each plane will be weighted by the plane wave propagating through the volume array. The current weighting corresponding to the plane wave's variation in the $\hat{\mathbf{u}}$ and $\hat{\mathbf{v}}$ directions have already been included in the analysis of Section 2.4. The current weighting corresponding to

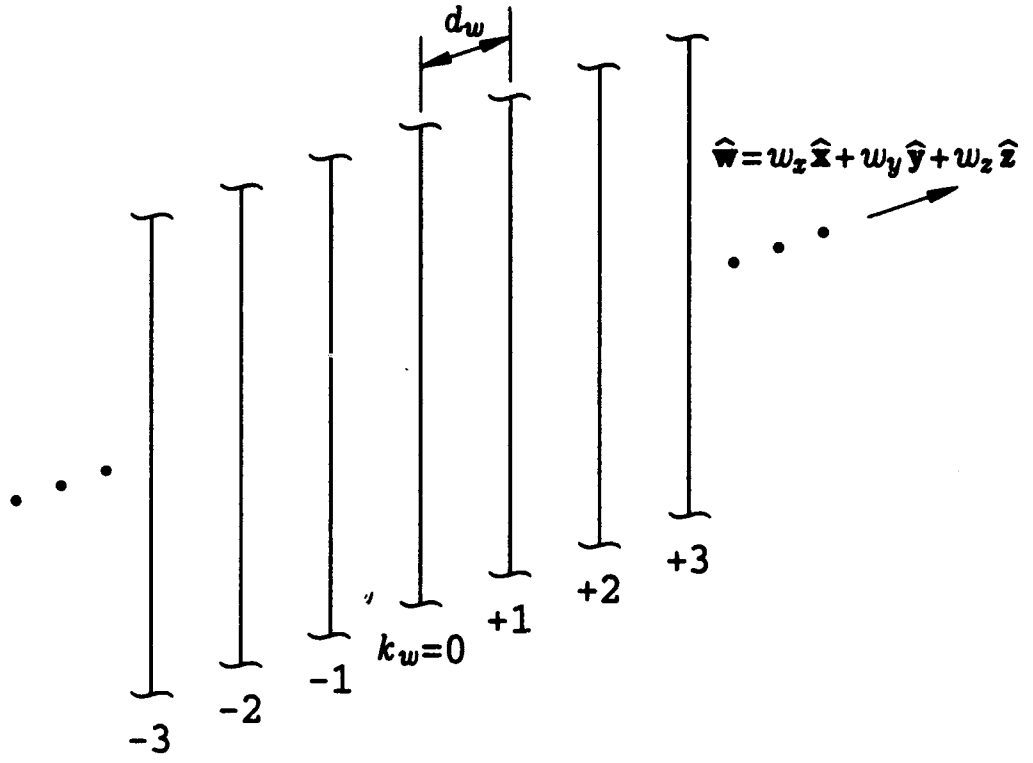

Figure 2.7: A 3D volume array of made of stacked 2D planar arrays.

the plane wave's variation in the $\hat{\mathbf{w}}$ direction is

$$C(k_w) = e^{-j\,k_w\,d_w\,(\mathbf{k_e}\cdot\hat{\mathbf{w}})} = e^{-j(k_w\,d_k)} \qquad \text{where}$$

$$d_k = d_w(k_{ex}\,w_x + k_{ey}\,w_y + k_{ez}\,w_z).$$

Primarily of interest are the fields in the center lattice cell about the origin. These fields are the sum of all the 2D planar element fields for all planes $-\infty \leq k_w \leq \infty$. The fields of the $k_w = 0$ planar array were determined in Section 2.4. The fields of the planes referenced by $k_w = +1, +2, +3, \cdots, +\infty$ consist of only left–going waves in the center lattice cell. Thus, $\mathbf{E}^{(\mathrm{I})}_{nj}(\mathbf{R})$ and $\mathbf{H}^{(\mathrm{I})}_{nj}(\mathbf{R})$ of Equations (2.57) and (2.61) must be weighted by $C(k_w)$ and summed over positive k_w. Similarly, the fields of the $k_w = -1, -2, -3, \cdots, -\infty$ planes consist of only right–going waves in the center

lattice cell. Thus, $\mathbf{E}_{nj}^{(\mathrm{III})}(\mathbf{R})$ and $\mathbf{H}_{nj}^{(\mathrm{III})}(\mathbf{R})$ of Equations (2.58) and (2.62) must be weighted by $C(k_w)$ and summed over negative k_w. It should be noted here that the z range spanned by elements in adjacent k_w planes do not overlap. (See Figure 2.6.) This requirement insures that there are no Region (II) type fields from planes where $k_w \neq 0$. For both positive and negative k_w, to account for the shift in position to the plane indexed by k_w, the vector $\mathbf{R}_{nj}$ (of the field equations for Regions (I) and (III)) must be replaced by $\mathbf{R}_{nj} + k_w d_w \hat{\mathbf{w}}$.

In this manner, the total electric field in the center lattice cell, due to the 3D volume array of all the nj^{th} current elements, can be written as

$$\mathbf{E}_{nj}^{\mathrm{TOT}}(\mathbf{R}) = \mathbf{E}_{nj}(k_w = 0, \mathbf{R}) +$$

$$+ \sum_{k_w=+1}^{+\infty} C(k_w)\,\mathbf{E}_{nj}^{(\mathrm{I})}(k_w, \mathbf{R}) + \sum_{k_w=-1}^{-\infty} C(k_w)\,\mathbf{E}_{nj}^{(\mathrm{III})}(k_w, \mathbf{R}). \tag{2.64}$$

The electric field $\mathbf{E}_{nj}^{(\mathrm{I})}(k_w, \mathbf{R})$ can be written as

$$\mathbf{E}_{nj}^{(\mathrm{I})}(k_w, \mathbf{R}) = \frac{\eta_0}{2d_u v_y d_v} \sum_{n_u} \sum_{n_v} \frac{e^{-jk_0[\mathbf{R}-(\mathbf{R}_{nj}+k_w d_w \hat{\mathbf{w}})]\cdot\hat{\mathbf{r}}_-}}{r_z}\, \mathbf{e}_{nj-}\, P_{nj-}^{s}(0, d_{nj}). \tag{2.65}$$

Inserting $\mathbf{E}_{nj}^{(\mathrm{I})}(k_w, \mathbf{R})$ into the first summation of Equation (2.64) and rearranging the summation order, it is obtained that

$$\sum_{k_w=+1}^{+\infty} C(k_w)\,\mathbf{E}_{nj}^{(\mathrm{I})}(k_w, \mathbf{R})$$

$$= \frac{\eta_0}{2d_u v_y d_v} \sum_{n_u} \sum_{n_v} \left(\sum_{k_w=+1}^{+\infty} e^{-j(k_w \beta_-)} \right) \frac{e^{-jk_0[\mathbf{R}-\mathbf{R}_{nj}]\cdot\hat{\mathbf{r}}_-}}{r_z}\, \mathbf{e}_{nj-}\, P_{nj-}^{s}(0, d_{nj}). \tag{2.66}$$

Similarly, the second summation of Equation (2.64) becomes

$$\sum_{k_w=-1}^{-\infty} C(k_w)\,\mathbf{E}_{nj}^{(\mathrm{III})}(k_w, \mathbf{R})$$

$$= \frac{\eta_0}{2d_u v_y d_v} \sum_{n_u} \sum_{n_v} \left(\sum_{k_w=-1}^{-\infty} e^{-j(k_w \beta_+)} \right) \frac{e^{-jk_0[\mathbf{R}-\mathbf{R}_{nj}]\cdot\hat{\mathbf{r}}_+}}{r_z}\, \mathbf{e}_{nj+}\, P_{nj+}^{s}(0, d_{nj}). \tag{2.67}$$

For Equations (2.66) and (2.67), $\beta_\pm = d_k - k_0 d_w(\hat{\mathbf{w}} \cdot \hat{\mathbf{r}}_\pm) = d_w[\mathbf{k_e} - k_0 \hat{\mathbf{r}}_\pm] \cdot \hat{\mathbf{w}}$.

The innermost summation on k_w can be evaluated in closed form by making use of the summation identity

$$\sum_{k=1}^{\infty} e^{-j\beta k} = \frac{e^{-j\beta}}{1 - e^{-j\beta}}$$

where β is a complex number. The summation on k_w in Equation (2.66) is a straightforward application of this identity. However, the summation on k_w in Equation (2.67) requires a change in the summation index of $k_w \rightarrow -k'_w$, such that the summation is over positive k'_w. The results are

$$\sum_{k_w=+1}^{+\infty} e^{-jk_w\beta_-} = \frac{e^{-j\beta_-}}{1 - e^{-j\beta_-}} \qquad \text{and} \qquad \sum_{k_w=-1}^{-\infty} e^{-jk_w\beta_+} = \frac{e^{j\beta_+}}{1 - e^{j\beta_+}}. \tag{2.68}$$

Combining these results, the total electric field in the center lattice cell can be written as

$$\mathbf{E}_{nj}^{\mathrm{TOT}}(\mathbf{R}) = \mathbf{E}_{nj}(k_w = 0, \mathbf{R}) +$$

$$+ \frac{\eta_0}{2d_u v_y d_v} \sum_{n_u} \sum_{n_v} \left[\left(\frac{e^{-j\beta_-}}{1 - e^{-j\beta_-}} \right) \frac{e^{-jk_0[\mathbf{R} - \mathbf{R}_{nj}]\cdot\hat{\mathbf{r}}_-}}{r_z} \mathbf{e}_{nj-} P^e_{nj-}(0, d_{nj}) + \right.$$

$$\left. + \left(\frac{e^{j\beta_+}}{1 - e^{j\beta_+}} \right) \frac{e^{-jk_0[\mathbf{R} - \mathbf{R}_{nj}]\cdot\hat{\mathbf{r}}_+}}{r_z} \mathbf{e}_{nj+} P^e_{nj+}(0, d_{nj}) \right]. \tag{2.69}$$

Performing a very similar operation on the magnetic field, the total magnetic field in the center lattice cell can be written as

$$\mathbf{H}_{nj}^{\mathrm{TOT}}(\mathbf{R}) = \mathbf{H}_{nj}(k_w = 0, \mathbf{R}) +$$

$$+ \frac{1}{2d_u v_y d_v} \sum_{n_u} \sum_{n_v} \left[\left(\frac{e^{-j\beta_-}}{1 - e^{-j\beta_-}} \right) \frac{e^{-jk_0[\mathbf{R} - \mathbf{R}_{nj}]\cdot\hat{\mathbf{r}}_-}}{r_z} (\hat{\mathbf{a}}_{nj} \times \hat{\mathbf{r}}_-) P^e_{nj-}(0, d_{nj}) + \right.$$

$$\left. + \left(\frac{e^{j\beta_+}}{1 - e^{j\beta_+}} \right) \frac{e^{-jk_0[\mathbf{R} - \mathbf{R}_{nj}]\cdot\hat{\mathbf{r}}_+}}{r_z} (\hat{\mathbf{a}}_{nj} \times \hat{\mathbf{r}}_+) P^e_{nj+}(0, d_{nj}) \right]. \tag{2.70}$$

For simplicity, is is worthwhile to write these total fields as

$$\mathbf{E}_{nj}^{\mathrm{TOT}}(\mathbf{R}) = \mathbf{E}_{nj}(k_w = 0, \mathbf{R}) + \mathbf{E}_{nj}(k_w > 0, \mathbf{R}) + \mathbf{E}_{nj}(k_w < 0, \mathbf{R}) \tag{2.71}$$

$$\mathbf{H}_{nj}^{\mathrm{TOT}}(\mathbf{R}) = \mathbf{H}_{nj}(k_w = 0, \mathbf{R}) + \mathbf{H}_{nj}(k_w > 0, \mathbf{R}) + \mathbf{H}_{nj}(k_w < 0, \mathbf{R}). \tag{2.72}$$

Chapter 3

Evaluation of the Impedance Matrix

Typical elements of the impedance matrix are given by Equation (2.10) for the Z_{mn} terms, and by Equation (2.11) for the ΔZ_{mn} terms. The evaluation of the ΔZ_{mn} terms is straightforward and is presented in Section 3.1. The Z_{mn} terms are more complicated to evaluate, as will be outlined next.

Recall that expansion function n can be either a dipole ($j = 1$ and 2) or monopole ($j = 1$) expansion function. Similarly, weighting function m can be either a dipole ($i = 1$ and 2) or monopole ($i = 1$) weighting function. Therefore, there are four mutual impedance possibilities. Following the polarity convention presented in Section 2.2.1, the four mutual impedance possibilities are:

1. $i = 2, j = 2$: $Z_{mn} = Z_{m1,n1} - Z_{m1,n2} - Z_{m2,n1} + Z_{m2,n2}$,
2. $i = 1, j = 2$: $Z_{mn} = Z_{m1,n1} - Z_{m1,n2}$,
3. $i = 2, j = 1$: $Z_{mn} = Z_{m1,n1} - Z_{m2,n1}$, and
4. $i = 1, j = 1$: $Z_{mn} = Z_{m1,n1}$

where $Z_{mi,nj}$ is the mutual impedance between monopole j of expansion function n and monopole i of weighting function m.

From Equation (2.10), on a monopole to monopole basis, it is seen that

$$Z_{mi,nj} = \sum_{Q} C^{Q} Z^{Q}_{mi,nj} \tag{3.1}$$

where

$$Z^{\mathbf{Q}}_{mi,nj} = -\int_{V_{mi}} \mathbf{E}^{\mathbf{Q}}_{nj} \cdot \mathbf{W}_{mi}\, dv \tag{3.2}$$

in which $\mathbf{E}^{\mathbf{Q}}_{nj}$ is the electric field of $\mathbf{J}^{\mathbf{Q}}_{nj}$, and the integration is over V_{mi}, the volume of monopole i of weighting function m. The electric field $\mathbf{E}^{\mathbf{Q}}_{nj}$ results from both the axial and the radial components of $\mathbf{J}^{\mathbf{Q}}_{nj}$, given in Equations (2.15) and (2.16). Therefore, it is convenient to write $\mathbf{E}^{\mathbf{Q}}_{nj}$ as

$$\mathbf{E}^{\mathbf{Q}}_{nj} = \mathbf{E}^{\mathbf{Q}z}_{nj} + \mathbf{E}^{\mathbf{Q}\rho}_{nj} \tag{3.3}$$

where $\mathbf{E}^{\mathbf{Q}z}_{nj}$ is the electric field of the axial current component and $\mathbf{E}^{\mathbf{Q}\rho}_{nj}$ is the electric field of the radial current component. Similarly, it is convenient to write $Z^{\mathbf{Q}}_{mi,nj}$ as

$$Z^{\mathbf{Q}}_{mi,nj} = Z^{\mathbf{Q}z}_{mi,nj} + Z^{\mathbf{Q}\rho}_{mi,nj} \tag{3.4}$$

$$Z^{\mathbf{Q}z}_{mi,nj} = -\int_{V_{mi}} \mathbf{E}^{\mathbf{Q}z}_{nj} \cdot \mathbf{W}_{mi}\, dv \tag{3.5}$$

$$Z^{\mathbf{Q}\rho}_{mi,nj} = -\int_{V_{mi}} \mathbf{E}^{\mathbf{Q}\rho}_{nj} \cdot \mathbf{W}_{mi}\, dv. \tag{3.6}$$

The evaluation of $Z^{\mathbf{Q}\rho}_{mi,nj}$ is presented in Section 3.2.

The $Z^{\mathbf{Q}z}_{mi,nj}$ terms are evaluated for all values of $\mathbf{Q}$ at once by noting that

$$Z^{z}_{mi,nj} = \sum_{\mathbf{Q}} C^{\mathbf{Q}} Z^{\mathbf{Q}z}_{mi,nj}$$

$$= -\sum_{\mathbf{Q}} C^{\mathbf{Q}} \int_{V_{mi}} \mathbf{E}^{\mathbf{Q}z}_{nj} \cdot \mathbf{W}_{mi}\, dv = -\int_{V_{mi}} \left[\sum_{\mathbf{Q}} C^{\mathbf{Q}} \mathbf{E}^{\mathbf{Q}z}_{nj}\right] \cdot \mathbf{W}_{mi}\, dv \tag{3.7}$$

where

$$\left[\sum_{\mathbf{Q}} C^{\mathbf{Q}} \mathbf{E}^{\mathbf{Q}z}_{nj}\right] = \mathbf{E}^{\mathrm{TOT}}_{nj}$$

with $\mathbf{E}^{\mathrm{TOT}}_{nj}$ given in Equation (2.69) or (2.71). The evaluation of Equation (3.7) is rather involved, and is presented in Section 3.3.

3.1 Evaluation of ΔZ

A typical ΔZ_{mn} term is given by Equation (2.11), which involves only the expansion and weighting functions defined in the center $\mathbf{Q} = \mathbf{0}$ lattice cell. Note that the ΔZ_{mn} term will be non–zero only when expansion function n overlaps with weighting

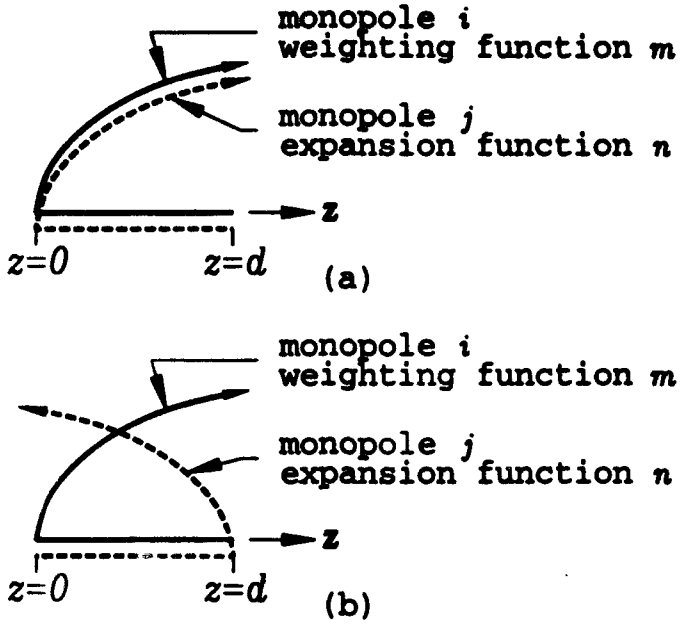

Figure 3.1: The two possible monopole to monopole overlap arrangements.

function m. Since the expansion functions are made up of monopoles, the overlapping is treated on a monopole to monopole basis. Figure 3.1 shows the two possible ways that monopole j of expansion function n, can overlap with monopole i of weighting function m, for $i, j = 1$ and/or 2.

The ΔZ contribution when monopole j of expansion function n overlaps with monopole i of weighting function m can be written as

$$\Delta Z_{mi,nj} = \frac{1}{j\omega(\epsilon_1 - \epsilon_0)} \int_0^d \int_0^{2\pi} \int_0^a \mathbf{J}_{nj}^{\theta} \cdot \mathbf{W}_{mi}\, \rho\, d\rho\, d\phi\, dz \tag{3.8}$$

where d is the length of the overlapping monopole segment. Noting the expressions for the expansion and weighting functions in Section 2.2.1, Equation (3.8) becomes

$$\Delta Z_{mi,nj} = \frac{1}{j\omega\pi a^2(\epsilon_1 - \epsilon_0)} F_{mi,nj} \tag{3.9}$$

where $F_{mi,nj}$ depends upon the axial variations of the overlapping segments, and is written as

$$F_{mi,nj} = \int_0^d F_{mi}(k_0 z)\, F_{nj}(k_0 z)\, dz. \tag{3.10}$$

In both overlapping cases of Figure 3.1, the axial variation for the weighting monopole mi is

$$F_{mi}(k_0 z) = \begin{cases} \frac{\sin(k_0 z)}{\sin(k_0 d)} & \text{if } 0 \le z \le d \\ 0 & \text{otherwise.} \end{cases} \tag{3.11}$$

If the overlapping geometry is as shown in Figure 3.1(a), then the axial variation of the expansion monopole nj is the same as for the weighting monopole mi, and Equation (3.10) becomes

$$F_{mi,nj} = \frac{k_0 d - \cos(k_0 d)\sin(k_0 d)}{2 k_0 \sin^2(k_0 d)}. \tag{3.12}$$

If the overlapping geometry is as shown in Figure 3.1(b), then the axial variation of the expansion monopole nj is

$$F_{nj}(k_0 z) = \begin{cases} -\frac{\sin(k_0 (d-z))}{\sin(k_0 d)} & \text{if } 0 \le z \le d \\ 0 & \text{otherwise,} \end{cases} \tag{3.13}$$

and Equation (3.10) becomes

$$F_{mi,nj} = -\frac{\sin(k_0 d) - k_0 d \cos(k_0 d)}{2 k_0 \sin^2(k_0 d)}. \tag{3.14}$$

The minus sign in Equations (3.13) and (3.14) account for the fact that the current on the monopoles in Figure 3.1(b) are of opposite polarity.

3.2 Evaluation of $Z^{Q\rho}$

This section evaluates $Z^{Q\rho}_{mi,nj}$ given in Equation (3.6). As indicated in Section 2.2.1, the MM expansion functions have a radial current component, J^{ρ}_{nj}, defined on a per monopole basis and given by Equation (2.16). However, the MM weighting functions, W_{mi}, given by Equations (2.20) and (2.21), contain only an axial current component. The $\hat{\rho}_{nj}$–directed current J^{ρ}_{nj} will produce an electric field, which will be highly localised to an axial field along its centerline. Therefore, $Z^{Q\rho}_{mi,nj}$ will be approximated as zero, unless if monopole j of expansion function n overlaps with monopole i of weighting function m. In this manner, only the radial currents in the center $Q = 0$ wire object contribute to the impedance matrix. In summary, $Z^{Q\rho}_{mi,nj} = 0$ for all $Q \neq 0$ and for all nonoverlapping segments.

As illustrated in Figure 3.1, and explained in Section 3.1, the overlapping is treated on a monopole to monopole basis. If monopole j of expansion function n overlaps with monopole i of weighting function m, then the contribution to the impedance matrix element Z_{mn}, resulting from J^{ρ}_{nj}, is written as

$$Z^{\rho}_{mi,nj} = \int_0^d \int_0^{2\pi} \int_0^a \mathbf{E}^{J^{\rho}}_{nj} \cdot \mathbf{W}_{mi}\, \rho\, d\rho\, d\phi\, dz \tag{3.15}$$

where d is the length of the overlapping monopole segment, and $\mathbf{E}^{J_{\rho}}_{nj}$ is the electric field of J^{ρ}_{nj}. Referencing the work of Richmond and Newman [33], this becomes

$$Z^{\rho}_{mi,nj} = -\frac{C\,[1 - J_0(k_\rho\, a)]}{j\omega\epsilon_0 k_0^2} F'_{mi,nj} \tag{3.16}$$

where

$$F'_{mi,nj} = \int_0^d F'_{mi}(k_0\, z)\, F'_{nj}(k_0\, z)\, dz. \tag{3.17}$$

The prime $'$ denotes differentiation with respect to z, and $F_{mi}(k_0 z)$ and $F_{nj}(k_0 z)$ are given by Equations (3.11) and/or (3.13), depending on the overlap geometry. If the overlap geometry is as in Figure 3.1(a), then

$$F'_{mi,nj} = \frac{k_0}{2\sin^2(k_0\, d)} \left[k_0\, d + \sin(k_0\, d)\, \cos(k_0\, d)\right] \tag{3.18}$$

and if the overlap geometry is as in Figure 3.1(b), then

$$F'_{mi,nj} = \frac{k_0}{2\sin^2(k_0\, d)} \left[k_0\, d\, \cos(k_0\, d) + \sin(k_0\, d)\right]. \tag{3.19}$$

The opposite polarity of the overlap case of Figure 3.1(b) has been included into Equation (3.19).

3.3 Evaluation of Z^z

This section evaluates the monopole to monopole impedance $Z^z_{mi,nj}$ given in Equation (3.7). In general, the scalar product of $\mathbf{E}^{\mathrm{TOT}}_{nj}$ with $\mathbf{W}_{mi}$ is integrated throughout V_{mi}, the volume of monopole i of weighting function m. Thus, the impedances require a triple volume integration throughout V_{mi}. However, in all cases this can be reduced to a single integration in the axial direction of the weighting function monopole mi.

If the monopoles mi and nj do not physically touch or overlap, then the currents can be approximated as line sources of the same axial current variation and strength, located at the centerlines of the monopole segments. In this case no stagger of the weighting monopole is necessary. However, if both monopoles are in the same plane, and that plane is parallel to the xy plane, then a slight stagger of the weighting monopole out of this plane can accelerate the convergence of the spectral summations involved in the impedance evaluation. This is due to the slight exponential decay of the evanescent waves in the spectral summation of plane waves.

If the monopoles mi and nj do physically touch or overlap, then the triple volume integration is reduced to a single integration by employing the method of equivalent wire radius, as used by Newman for thin material wires [25]. Basically, this results in the elimination of the $d\rho$ and $d\phi$ integrations by staggering the weighting monopole an *equivalent wire radius* off its centerline. The theory of this equivalent wire radius is presented in Appendix B, and the rules for staggering the weighting monopole mi are given in Appendix C.

When integrating in the axial direction of the monopole mi, it is worthwhile to note that the position vector to a point on monopole mi can be written as

$$\mathbf{R} = \mathbf{R}_{mi} + \hat{\mathbf{a}}_{mi}\, l \qquad \text{for } 0 \le l \le d_{mi} \tag{3.20}$$

where $\mathbf{R}_{mi}$ is the position vector from the origin to the reference end of monopole mi, and d_{mi} is the length of monopole mi. Recall that for the PWS monopoles used in this paper, the reference end is the zero–current end. Equation (3.20) is a direct result of Figure 2.5 applied to monopole mi instead of monopole nj, where the position variable l' has been replaced by l.

The impedance $Z^z_{mi,nj}$ involves $\mathbf{E}^{\mathrm{TOT}}_{nj}$, the electric field of the 3D array of current segments nj. $\mathbf{E}^{\mathrm{TOT}}_{nj}$ is given in Equation (2.71), where it is represented as contributions from the three ranges of the lattice summation index k_w ($k_w = 0$,$k_w > 0$ and $k_w < 0$). Thus, it is convenient to write $Z^z_{mi,nj}$ as

$$Z^z_{mi,nj} = Z^{z=}_{mi,nj} + Z^{z>}_{mi,nj} + Z^{z<}_{mi,nj} \tag{3.21}$$

$$Z^{z=}_{mi,nj} = -\int_{V_{mi}} \mathbf{E}_{nj}(k_w = 0, \mathbf{R}) \cdot \mathbf{W}_{mi}\, dv \tag{3.22}$$

$$Z^{z>}_{mi,nj} = -\int_{V_{mi}} \mathbf{E}_{nj}(k_w > 0, \mathbf{R}) \cdot \mathbf{W}_{mi}\, dv \tag{3.23}$$

$$Z^{z<}_{mi,nj} = -\int_{V_{mi}} \mathbf{E}_{nj}(k_w < 0, \mathbf{R}) \cdot \mathbf{W}_{mi}\, dv. \tag{3.24}$$

In all the above cases, the weighting monopole becomes the filament source

$$\mathbf{W}_{mi} = \hat{\mathbf{a}}_{mi}\, F_{mi}(l). \tag{3.25}$$

3.3.1 The Evaluation of $Z^{z=}_{mi,nj}$

The form of $\mathbf{E}_{nj}(k_w = 0, \mathbf{R})$ used in the evaluation of $Z^{z=}_{mi,nj}$ depends upon the geometrical arrangement of monopoles mi and nj. Figure D.1 and Appendix D describe the eight possible geometrical arrangements, which are labeled as Case 1 – Case 8. Basically, Equations (2.57),(2.58) and/or (2.60) are used to evaluate $\mathbf{E}_{nj}(k_w = 0, \mathbf{R})$ in Regions (I), (II) and/or (III), as required by the geometry of monopoles mi and nj. The eight possible cases for the evaluation of $Z^{z=}_{mi,nj}$ are analyzed here.

Case 1 and Case 2:

Cases 1 and 2 are the simplest because the electric field of expansion monopole nj across weighting monopole mi consists solely of left–going or right–going waves, respectively. For Case 1, $\mathbf{E}_{nj}(k_w = 0, \mathbf{R}) = \mathbf{E}^{(\mathrm{I})}_{nj}(\mathbf{R})$ of Equation (2.57), and for Case 2, $\mathbf{E}_{nj}(k_w = 0, \mathbf{R}) = \mathbf{E}^{(\mathrm{III})}_{nj}(\mathbf{R})$ of Equation (2.58). Since monopole mi is entirely within either Region (I) or Region (III) of expansion monopole nj, only one expression for $\mathbf{E}_{nj}(k_w = 0, \mathbf{R})$ is required, and the limits of integration are over the entire length of monopole mi in that region. The only spatial variation of $\mathbf{E}_{nj}(k_w = 0, \mathbf{R})$ is the exponential term $e^{-jk_0 \mathbf{R}\cdot\hat{\mathbf{r}}_\pm}$ inside the double spectral summation of plane waves. Thus, the integration only involves this exponential term and the weighting function variation of Equation (3.25).

Inserting $\mathbf{E}_{nj}(k_w = 0, \mathbf{R})$ and $\mathbf{W}_{mi}$ into Equation (3.22) and integrating, it is obtained for Case 1 that

$$Z^{z=}_{mi,nj} = -\frac{\eta_0}{2d_u v_y d_v} \sum_{n_u} \sum_{n_v} \frac{e^{-jk_0[\mathbf{R}_{mi} - \mathbf{R}_{nj}]\cdot\hat{\mathbf{r}}_-}}{\tau_z} \times$$

$$\times\, (\mathbf{e}_{nj-} \cdot \hat{\mathbf{a}}_{mi})\, P^{e}_{nj-}(0, d_{nj}) P^{r}_{mi-}(0, d_{mi}) \tag{3.26}$$

and for Case 2

$$Z^{z=}_{mi,nj} = -\frac{\eta_0}{2d_u v_y d_v} \sum_{n_u} \sum_{n_v} \frac{e^{-jk_0[\mathbf{R}_{mi}-\mathbf{R}_{nj}]\cdot\hat{\mathbf{r}}_+}}{\tau_z} \times$$
$$\times \left(\mathbf{e}_{nj+} \cdot \hat{\mathbf{a}}_{mi}\right) P^e_{nj+}(0, d_{nj}) P^r_{mi+}(0, d_{mi}) \tag{3.27}$$

where $P^r_{mi\pm}(a,b)$ is termed the mi^{th} *receive pattern factor* and is defined as

$$P^r_{mi\pm}(a,b) = \int_a^b F_{mi}(l)\, e^{-jk_0 l(\hat{\mathbf{a}}_{mi}\cdot\hat{\mathbf{r}}_\pm)}\, dl = C^r_{mi\pm}\left[A^r_{mi\pm}(b) - A^r_{mi\pm}(a)\right] \tag{3.28}$$

where

$$C^r_{mi\pm} = \frac{1}{k_0 \sin(k_0 d_{mi})\left[1 - (\hat{\mathbf{a}}_{mi}\cdot\hat{\mathbf{r}}_\pm)^2\right]} \tag{3.29}$$

$$A^r_{mi\pm}(x) = e^{-jk_0 x(\hat{\mathbf{a}}_{mi}\cdot\hat{\mathbf{r}}_\pm)}\left[-j(\hat{\mathbf{a}}_{mi}\cdot\hat{\mathbf{r}}_\pm)\sin(k_0 x) - \cos(k_0 x)\right]. \tag{3.30}$$

Case 3:

Case 3 is more complicated beçause $\mathbf{E}_{nj}(k_w = 0, \mathbf{R}) = \mathbf{E}^{(\mathrm{II})}_{nj}(\mathbf{R})$ of Equation (2.60), which consists of both right–going and left–going waves across weighting monopole mi. However, monopole mi is entirely within Region (II) of expansion monopole nj, so the limits of integration are over the entire length of monopole mi using the Region (II) field. The spectral summations contain the usual spatial variation of the exponential term $e^{-jk_0\mathbf{R}\cdot\hat{\mathbf{r}}_\pm}$. Moreover, the source pattern factors $P^e_{nj\pm}(a_{nj\pm}, b_{nj\pm})$ contain a spatial variation due to the z dependence of their integration limits, given in Section A.1. With these considerations for Case 3, $Z^{z=}_{mi,nj}$ becomes

$$Z^{z=}_{mi,nj} = -\frac{\eta_0}{2d_u v_y d_v} \sum_{n_u} \sum_{n_v} \left[\frac{e^{-jk_0[\mathbf{R}_{mi}-\mathbf{R}_{nj}]\cdot\hat{\mathbf{r}}_+}}{\tau_z} G_{mi,nj+}(0, d_{mi}) + \right.$$
$$\left. + \frac{e^{-jk_0[\mathbf{R}_{mi}-\mathbf{R}_{nj}]\cdot\hat{\mathbf{r}}_-}}{\tau_z} G_{mi,nj-}(0, d_{mi})\right] \tag{3.31}$$

where

$$G_{mi,nj\pm}(a,b) = \int_a^b \left(\mathbf{e}_{nj\pm}\cdot\hat{\mathbf{a}}_{mi}\right) F_{mi}(l)\, e^{-jk_0 l(\hat{\mathbf{a}}_{nj}\cdot\hat{\mathbf{r}}_\pm)}\, P^e_{nj\pm}(a_{nj\pm}, b_{nj\pm})\, dl. \tag{3.32}$$

Note that $P^e_{nj\pm}(a_{nj\pm}, b_{nj\pm})$ has an l dependence due to the source integration limits. The scalar product $(\mathbf{e}_{nj+}\cdot\hat{\mathbf{a}}_{mi})$ appears inside the integration so that open–current end charge contributions can be isolated and/or removed (see Section A.2). $G_{mi,nj\pm}(a,b)$ is a rather involved integration and is evaluated in Appendix E.

Case 4, Case 5 and Case 6:

Note from Figure D.1 that in Case 4 the weighting monopole is partially in Region (I) and partially in Region (II) of expansion monopole nj. Therefore, $\mathbf{E}_{nj}(k_w = 0, \mathbf{R}) = \mathbf{E}_{nj}^{(\mathrm{I})}(\mathbf{R})$ of Equation (2.57) when integrating over the portion of monopole mi that is in Region (I), and $\mathbf{E}_{nj}(k_w = 0, \mathbf{R}) = \mathbf{E}_{nj}^{(\mathrm{II})}(\mathbf{R})$ of Equation (2.60) when integrating over the portion of monopole mi that is in Region (II).

Similarly, for Case 5 the weighting monopole is partially in Region (III) and partially in Region (II) of expansion monopole nj. In this case, $\mathbf{E}_{nj}(k_w = 0, \mathbf{R}) = \mathbf{E}_{nj}^{(\mathrm{III})}(\mathbf{R})$ of Equation (2.58) when integrating over the portion of monopole mi that is in Region (III), and $\mathbf{E}_{nj}(k_w = 0, \mathbf{R}) = \mathbf{E}_{nj}^{(\mathrm{II})}(\mathbf{R})$ of Equation (2.60) when integrating over the portion of monopole mi that is in Region (II).

When integrating in Region (I) or Region (III), the spatial variation of $\mathbf{E}_{nj}(k_w = 0, \mathbf{R})$ consists only of the exponential term $e^{-jk_0\mathbf{R}\cdot\hat{\mathbf{r}}_\pm}$. However, when integrating in Region (II), the spatial variation of $\mathbf{E}_{nj}(k_w = 0, \mathbf{R})$ includes the exponential term and the source pattern factor. With these considerations, for Case 4 $Z_{mi,nj}^{z=}$ becomes

$$Z_{mi,nj}^{z=} = -\frac{\eta_0}{2d_u v_y d_v} \sum_{n_u} \sum_{n_v}$$

$$\left[\frac{e^{-jk_0[\mathbf{R}_{mi}-\mathbf{R}_{nj}]\cdot\hat{\mathbf{r}}_-}}{r_z} (\mathbf{e}_{nj-} \cdot \hat{\mathbf{a}}_{mi})\, P_{nj-}^{e}(0, d_{nj}) P_{mi-}^{r}(a_{mi1}, b_{mi1}) + \right.$$

$$+ \frac{e^{-jk_0[\mathbf{R}_{mi}-\mathbf{R}_{nj}]\cdot\hat{\mathbf{r}}_-}}{r_z} G_{mi,nj-}(a_{mi2}, b_{mi2}) +$$

$$\left. + \frac{e^{-jk_0[\mathbf{R}_{mi}-\mathbf{R}_{nj}]\cdot\hat{\mathbf{r}}_+}}{r_z} G_{mi,nj+}(a_{mi2}, b_{mi2}) \right] \tag{3.33}$$

and for Case 5 $Z_{mi,nj}^{z=}$ becomes

$$Z_{mi,nj}^{z=} = -\frac{\eta_0}{2d_u v_y d_v} \sum_{n_u} \sum_{n_v}$$

$$\left[\frac{e^{-jk_0[\mathbf{R}_{mi}-\mathbf{R}_{nj}]\cdot\hat{\mathbf{r}}_+}}{r_z} (\mathbf{e}_{nj+} \cdot \hat{\mathbf{a}}_{mi})\, P_{nj+}^{e}(0, d_{nj}) P_{mi-}^{r}(a_{mi3}, b_{mi3}) + \right.$$

$$+ \frac{e^{-jk_0[\mathbf{R}_{mi}-\mathbf{R}_{nj}]\cdot\hat{\mathbf{r}}_-}}{r_z} G_{mi,nj-}(a_{mi2}, b_{mi2}) +$$

$$\left. + \frac{e^{-jk_0[\mathbf{R}_{mi}-\mathbf{R}_{nj}]\cdot\hat{\mathbf{r}}_+}}{r_z} G_{mi,nj+}(a_{mi2}, b_{mi2}) \right]. \tag{3.34}$$

In either case, the limits of integration $(a_{mi1}, b_{mi1}), (a_{mi2}, b_{mi2})$ and (a_{mi3}, b_{mi3}) represent the portion of weighting monopole mi that is in Region (I),(II) or (III), respectively. These limits are defined in Appendix F.

From Figure D.1, it is seen that Case 6 is an extension of either Case 4 or Case 5 in that monopole mi extends over Regions (I),(II) and (III) of monopole nj. The same statements made above for Cases 4 and 5 hold true for Case 6, so that $Z^{z=}_{mi,nj}$ is written as

$$Z^{z=}_{mi,nj} = -\frac{\eta_0}{2d_u v_y d_v} \sum_{n_u} \sum_{n_v}$$

$$\left[\frac{e^{-jk_0[\mathbf{R}_{mi}-\mathbf{R}_{nj}]\cdot\hat{\mathbf{t}}_-}}{r_z} (\mathbf{e}_{nj-} \cdot \hat{\mathbf{a}}_{mi})\, P^e_{nj-}(0, d_{nj}) P^r_{mi-}(a_{mi1}, b_{mi1}) + \right.$$

$$+ \frac{e^{-jk_0[\mathbf{R}_{mi}-\mathbf{R}_{nj}]\cdot\hat{\mathbf{t}}_+}}{r_z} (\mathbf{e}_{nj+} \cdot \hat{\mathbf{a}}_{mi})\, P^e_{nj+}(0, d_{nj}) P^r_{mi-}(a_{mi3}, b_{mi3}) +$$

$$+ \frac{e^{-jk_0[\mathbf{R}_{mi}-\mathbf{R}_{nj}]\cdot\hat{\mathbf{t}}_-}}{r_z} G_{mi,nj-}(a_{mi2}, b_{mi2}) +$$

$$\left. + \frac{e^{-jk_0[\mathbf{R}_{mi}-\mathbf{R}_{nj}]\cdot\hat{\mathbf{t}}_+}}{r_z} G_{mi,nj+}(a_{mi2}, b_{mi2}) \right]. \qquad (3.35)$$

The limits of integration are given in Appendix F.

Case 7 and Case 8:

From Figure D.1, it is seen that Case 7 can be viewed as a special case geometry of Case 6, where Region (II) of monopole nj has vanished. Thus, $Z^{z=}_{mi,nj}$ consists of only the Region (I) and Region (III) contributions, and is written as

$$Z^{z=}_{mi,nj} = -\frac{\eta_0}{2d_u v_y d_v} \sum_{n_u} \sum_{n_v}$$

$$\left[\frac{e^{-jk_0[\mathbf{R}_{mi}-\mathbf{R}_{nj}]\cdot\hat{\mathbf{t}}_-}}{r_z} (\mathbf{e}_{nj-} \cdot \hat{\mathbf{a}}_{mi})\, P^e_{nj-}(0, d_{nj}) P^r_{mi-}(a_{mi1}, b_{mi1}) + \right.$$

$$\left. + \frac{e^{-jk_0[\mathbf{R}_{mi}-\mathbf{R}_{nj}]\cdot\hat{\mathbf{t}}_+}}{r_z} (\mathbf{e}_{nj+} \cdot \hat{\mathbf{a}}_{mi})\, P^e_{nj+}(0, d_{nj}) P^r_{mi+}(a_{mi3}, b_{mi3}) \right]. \qquad (3.36)$$

Case 8 is similar to Case 3, except that in Case 8 monopole mi does not have any extent in the z direction. However, it is still entirely within Region (II) of monopole nj. The limits of integration become independent of z, and the integrations of (3.32)

no longer are nested. For case 8, $Z^{zz}_{mi,nj}$ can still be given by Equation (3.31), except that the pattern factor integral term now simplifies to

$$G_{mi,nj\pm}(a,b) = P^r_{mi\pm}(a,b)\, P^s_{nj\pm}(a_{nj\pm}, b_{nj\pm}) \tag{3.37}$$

where the limits of integration are given in Appendix F.

3.3.2 The Evaluation of $Z^{z>}_{mi,nj}$ and $Z^{z<}_{mi,nj}$

The electric field from all planes indexed by $k_w > 0$ consists only of left–going plane waves in the center Q = 0 lattice cell, and is expressed as

$$\mathbf{E}_{nj}(k_w > 0, \mathbf{R}) = \frac{\eta_0}{2d_u v_y d_v} \sum_{n_u} \sum_{n_v} \left(\frac{e^{-j\beta_-}}{1 - e^{-j\beta_-}} \right) \frac{e^{-jk_0[\mathbf{R}-\mathbf{R}_{nj}]\cdot\hat{\mathbf{r}}_-}}{r_z} \mathbf{e}_{nj-} P^s_{nj-}(0, d_{nj}). \tag{3.38}$$

The only spatial variation of $\mathbf{E}_{nj}(k_w > 0, \mathbf{R})$ is the exponential term $e^{-jk_0\mathbf{R}\cdot\hat{\mathbf{r}}_-}$ inside the double spectral summation of plane waves. Employing Equation (3.20), $Z^{z>}_{mi,nj}$ can be expressed as

$$Z^{z>}_{mi,nj} = -\frac{\eta_0}{2d_u v_y d_v} \sum_{n_u} \sum_{n_v} \left(\frac{e^{-j\beta_-}}{1 - e^{-j\beta_-}} \right) \frac{e^{-jk_0[\mathbf{R}_{mi}-\mathbf{R}_{nj}]\cdot\hat{\mathbf{r}}_-}}{r_z} \times$$
$$\times (\mathbf{e}_{nj-} \cdot \hat{\mathbf{a}}_{mi})\, P^s_{nj-}(0, d_{nj}) P^r_{mi-}(0, d_{mi}) \tag{3.39}$$

where $P^r_{mi-}(0, d_{mi})$ is given in Equation (3.28).

Similarly, $Z^{z<}_{mi,nj}$ can be expressed as

$$Z^{z<}_{mi,nj} = -\frac{\eta_0}{2d_u v_y d_v} \sum_{n_u} \sum_{n_v} \left(\frac{e^{-j\beta_+}}{1 - e^{-j\beta_+}} \right) \frac{e^{-jk_0[\mathbf{R}_{mi}-\mathbf{R}_{nj}]\cdot\hat{\mathbf{r}}_+}}{r_z} \times$$
$$\times (\mathbf{e}_{nj+} \cdot \hat{\mathbf{a}}_{mi})\, P^s_{nj+}(0, d_{nj}) P^r_{mi+}(0, d_{mi}) \tag{3.40}$$

Chapter 4

Average Eigenfunction Electric and Magnetic Fields

This chapter presents the evaluation of the electric and magnetic eigenfunction fields averaged over the center $\mathbf{Q} = \mathbf{0}$ lattice cell. These fields, denoted as $(\mathbf{E}^{\mathbf{0}}, \mathbf{H}^{\mathbf{0}})$, are defined as

$$\mathbf{E}^{\mathbf{0}} = \frac{1}{\Delta v} \int_{V^{\mathbf{0}}} \mathbf{E}(\mathbf{R})\, dv \tag{4.1}$$

$$\mathbf{H}^{\mathbf{0}} = \frac{1}{\Delta v} \int_{V^{\mathbf{0}}} \mathbf{H}(\mathbf{R})\, dv \tag{4.2}$$

where Δv is the volume of a lattice cell in the 3D array and $V^{\mathbf{0}}$ represents the integration limits for the center $\mathbf{Q} = \mathbf{0}$ lattice cell. For the evaluation presented here, the 3D lattice array consists of perpendicular axes, i.e.,

$$\begin{aligned} \hat{\mathbf{u}} &= \hat{\mathbf{x}}, \qquad \hat{\mathbf{v}} = \hat{\mathbf{y}}, \qquad \hat{\mathbf{w}} = \hat{\mathbf{z}}, \\ d_u &= d_x, \qquad d_v = d_y, \qquad d_w = d_z \end{aligned}$$

and therefore $\Delta v = d_x\, d_y\, d_z$.

The eigenfunction fields $(\mathbf{E}, \mathbf{H})$ are the fields radiated by the eigenfunction currents, so for the PMM solution

$$\mathbf{E}(\mathbf{R}) \approx \sum_{n=1}^{N} I_n \sum_{j=1}^{1(2)} (-1)^{j+1}\, \mathbf{E}_{nj}(\mathbf{R})\, dv \tag{4.3}$$

$$\mathbf{H}(\mathbf{R}) \approx \sum_{n=1}^{N} I_n \sum_{j=1}^{1(2)} (-1)^{j+1}\, \mathbf{H}_{nj}(\mathbf{R})\, dv \tag{4.4}$$

where the summation on j is $j = 1$ for a monopole and $j = 1, 2$ for a dipole expansion function. The sign factor $(-1)^{j+1}$ accounts for the polarity convention of the

monopoles making up the expansion functions. In evaluating the fields of a given MM expansion function, the fields of the radial current component are neglected, and thus Equations (2.71) and (2.72) are used to evaluate the fields of current segment nj. Noting that Equations (2.71) and (2.72) represent the fields as contributions from three ranges of the lattice summation index k_w ($k_w = 0, k_w > 0$ and $k_w < 0$), the averaged eigenfunction fields are written as

$$\mathbf{E}^0 \approx \frac{1}{\Delta v} \sum_{n=1}^{N} I_n \sum_{j=1}^{1(2)} (-1)^{j+1} \left[\mathbf{I}_{nj}^{\mathbf{E}}(k_w = 0) + \mathbf{I}_{nj}^{\mathbf{E}}(k_w > 0) + \mathbf{I}_{nj}^{\mathbf{E}}(k_w < 0) \right] \tag{4.5}$$

$$\mathbf{H}^0 \approx \frac{1}{\Delta v} \sum_{n=1}^{N} I_n \sum_{j=1}^{1(2)} (-1)^{j+1} \left[\mathbf{I}_{nj}^{\mathbf{H}}(k_w = 0) + \mathbf{I}_{nj}^{\mathbf{H}}(k_w > 0) + \mathbf{I}_{nj}^{\mathbf{H}}(k_w < 0) \right] \tag{4.6}$$

where

$$\begin{aligned}
\mathbf{I}_{nj}^{\mathbf{E}}(k_w = 0) &= \int_{V\mathbf{0}} \mathbf{E}_{nj}(k_w = 0, \mathbf{R})\, dv \\
\mathbf{I}_{nj}^{\mathbf{E}}(k_w > 0) &= \int_{V\mathbf{0}} \mathbf{E}_{nj}(k_w > 0, \mathbf{R})\, dv \\
\mathbf{I}_{nj}^{\mathbf{E}}(k_w < 0) &= \int_{V\mathbf{0}} \mathbf{E}_{nj}(k_w < 0, \mathbf{R})\, dv \\
\mathbf{I}_{nj}^{\mathbf{H}}(k_w = 0) &= \int_{V\mathbf{0}} \mathbf{H}_{nj}(k_w = 0, \mathbf{R})\, dv \\
\mathbf{I}_{nj}^{\mathbf{H}}(k_w > 0) &= \int_{V\mathbf{0}} \mathbf{H}_{nj}(k_w > 0, \mathbf{R})\, dv \\
\mathbf{I}_{nj}^{\mathbf{H}}(k_w < 0) &= \int_{V\mathbf{0}} \mathbf{H}_{nj}(k_w < 0, \mathbf{R})\, dv.
\end{aligned} \tag{4.7}$$

Recall from Figure 2.6 that in general there are three possible regions for a field point in the center $\mathbf{Q} = \mathbf{0}$ lattice cell, due to the $k_w = 0$ array of current segments nj. These regions are defined by the z values of the current segment endpoints. Figure 4.1 shows the limits on the z integration corresponding to the three regions. It is convenient to write

$$\mathbf{I}_{nj}^{\mathbf{E}}(k_w = 0) = \mathbf{I}_{nj}^{\mathbf{E}(\mathrm{I})} + \mathbf{I}_{nj}^{\mathbf{E}(\mathrm{II})} + \mathbf{I}_{nj}^{\mathbf{E}(\mathrm{III})} \tag{4.8}$$

$$\mathbf{I}_{nj}^{\mathbf{H}}(k_w = 0) = \mathbf{I}_{nj}^{\mathbf{H}(\mathrm{I})} + \mathbf{I}_{nj}^{\mathbf{H}(\mathrm{II})} + \mathbf{I}_{nj}^{\mathbf{H}(\mathrm{III})} \tag{4.9}$$

where

$$\mathbf{I}_{nj}^{\mathbf{E}(\mathrm{I})} = \int_{V\mathrm{I}} \mathbf{E}_{nj}^{(\mathrm{I})}(\mathbf{R})\, dv$$

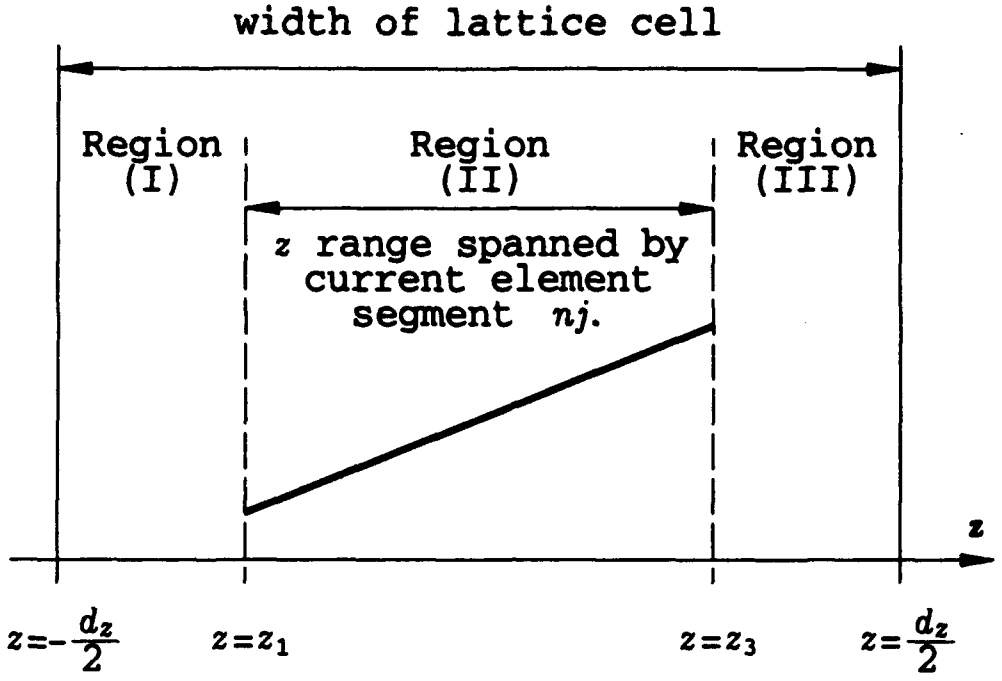

Figure 4.1: The z integration limits for evaluating the average eigenfunction fields.

$$\mathbf{I}_{nj}^{\mathbf{E}(\mathrm{II})} = \int_{V\mathrm{II}} \mathbf{E}_{nj}^{(\mathrm{II})}(\mathbf{R})\, dv$$

$$\mathbf{I}_{nj}^{\mathbf{E}(\mathrm{III})} = \int_{V\mathrm{III}} \mathbf{E}_{nj}^{(\mathrm{III})}(\mathbf{R})\, dv$$

$$\mathbf{I}_{nj}^{\mathbf{H}(\mathrm{I})} = \int_{V\mathrm{I}} \mathbf{H}_{nj}^{(\mathrm{I})}(\mathbf{R})\, dv$$

$$\mathbf{I}_{nj}^{\mathbf{H}(\mathrm{II})} = \int_{V\mathrm{II}} \mathbf{H}_{nj}^{(\mathrm{II})}(\mathbf{R})\, dv$$

$$\mathbf{I}_{nj}^{\mathbf{H}(\mathrm{III})} = \int_{V\mathrm{III}} \mathbf{H}_{nj}^{(\mathrm{III})}(\mathbf{R})\, dv. \qquad (4.10)$$

where the integration limits $V^{\mathrm{I}}, V^{\mathrm{II}}$ and V^{III} refer to the Region (I),(II) and (III) portions of the center lattice cell for the $k_w = 0$ current segment nj, respectively. The electric fields $\mathbf{E}_{nj}^{(\mathrm{I})}(\mathbf{R}), \mathbf{E}_{nj}^{(\mathrm{II})}(\mathbf{R})$ and $\mathbf{E}_{nj}^{(\mathrm{III})}(\mathbf{R})$ are given by Equations (2.57),(2.60) and (2.58), respectively, and the magnetic fields $\mathbf{H}_{nj}^{(\mathrm{I})}(\mathbf{R}), \mathbf{H}_{nj}^{(\mathrm{II})}(\mathbf{R})$ and $\mathbf{H}_{nj}^{(\mathrm{III})}(\mathbf{R})$ are given by Equations (2.61),(2.63) and (2.62), respectively. Note that if current segment nj is in a plane parallel to the xy plane, then $z_3 = z_1$, and Region (II) vanishes, and hence $\mathbf{I}_{nj}^{\mathbf{E}(\mathrm{II})} = \mathbf{I}_{nj}^{\mathbf{H}(\mathrm{II})} = 0$.

4.1 $k_w = 0$, Region (I)

From the analysis in Sections 2.4, it was found that for Region (I) and Region (III), the only spatial variation of the fields is the exponential term $e^{-jk_0\mathbf{R}\cdot\hat{\mathbf{r}}_\pm}$ inside the double spectral summation of plane waves. Thus, $\mathbf{I}_{nj}^{\mathbf{E}(\mathrm{I})}$ and $\mathbf{I}_{nj}^{\mathbf{H}(\mathrm{I})}$ can be expressed as

$$\mathbf{I}_{nj}^{\mathbf{E}(\mathrm{I})} = \frac{\eta_0}{2d_x d_y} \sum_{n_u} \sum_{n_v} \frac{e^{jk_0\mathbf{R}_{nj}\cdot\hat{\mathbf{r}}_-}}{r_z} \mathbf{e}_{nj-}\, P^s_{nj-}(0, d_{nj}) \int_{V\mathrm{I}} e^{-jk_0\mathbf{R}\cdot\hat{\mathbf{r}}_-}\, dv \qquad (4.11)$$

$$\mathbf{I}_{nj}^{\mathbf{H}(\mathrm{I})} = \frac{1}{2d_x d_y} \sum_{n_u} \sum_{n_v} \frac{e^{jk_0\mathbf{R}_{nj}\cdot\hat{\mathbf{r}}_-}}{r_z} (\hat{\mathbf{a}}_{nj} \times \hat{\mathbf{r}}_-)\, P^s_{nj-}(0, d_{nj}) \int_{V\mathrm{I}} e^{-jk_0\mathbf{R}\cdot\hat{\mathbf{r}}_-}\, dv. \qquad (4.12)$$

The limits of integration for Region (I) are

$$V^{\mathrm{I}} = \begin{cases} -\frac{d_x}{2} \le x \le \frac{d_x}{2} \\ -\frac{d_y}{2} \le y \le \frac{d_y}{2} \\ -\frac{d_z}{2} \le z \le z_1 \end{cases}$$

and thus the integration of Equations (4.11) and (4.12) becomes

$$\int_{V\mathrm{I}} e^{-jk_0\mathbf{R}\cdot\hat{\mathbf{r}}_-}\, dv = I_x\, I_y\, I_z^{\mathrm{I}}$$

where

$$I_x = \int_{-\frac{d_x}{2}}^{\frac{d_x}{2}} e^{-jk_0 r_x x}\, dx = \begin{cases} d_x & \text{if } r_x = 0 \\ \frac{2}{k_0 r_x} \sin(k_0 r_x \frac{d_x}{2}) & \text{otherwise} \end{cases}$$

$$I_y = \int_{-\frac{d_y}{2}}^{\frac{d_y}{2}} e^{-jk_0 r_y y}\, dy = \begin{cases} d_y & \text{if } r_y = 0 \\ \frac{2}{k_0 r_y} \sin(k_0 r_y \frac{d_y}{2}) & \text{otherwise} \end{cases}$$

$$I_z^{\mathrm{I}} = \int_{-\frac{d_z}{2}}^{z_1} e^{jk_0 r_z z}\, dz = \begin{cases} z_1 + \frac{d_z}{2} & \text{if } r_z = 0 \\ \frac{\exp(jk_0 r_z z_1) - \exp(-jk_0 r_z \frac{d_z}{2})}{jk_0 r_z} & \text{otherwise.} \end{cases}$$

Due to the product $\mathbf{e}_{nj-}\, P^s_{nj-}(0, d_{nj})$ appearing in Equation (4.11), the integrated electric field $\mathbf{I}_{nj}^{\mathbf{E}(\mathrm{I})}$ does include the electric field resulting from the open–current end charge. However, since the product $\mathbf{e}_{nj-}\, P^s_{nj-}(0, d_{nj})$ occurs outside of the spatial integration of Equation (4.11), the electric field of the open–current end charge can be easily isolated and/or removed using the technique presented in Section A.2. This will not affect the values of I_x, I_y or I_z^{I}.

4.2 $k_w = 0$, Region (III)

In a similar manner, $\Gamma_{nj}^{\mathbf{E}(\mathrm{III})}$ and $\Gamma_{nj}^{\mathbf{H}(\mathrm{III})}$ can be expressed as

$$\Gamma_{nj}^{\mathbf{E}(\mathrm{III})} = \frac{\eta_0}{2d_x d_y} \sum_{n_u} \sum_{n_v} \frac{e^{jk_0 \mathbf{R}_{nj} \cdot \hat{\mathbf{t}}_+}}{\tau_z} \mathbf{e}_{nj+} P^e_{nj+}(0, d_{nj}) \int_{V\mathrm{III}} e^{-jk_0 \mathbf{R} \cdot \hat{\mathbf{t}}_+} \, dv \qquad (4.13)$$

$$\Gamma_{nj}^{\mathbf{H}(\mathrm{III})} = \frac{1}{2d_x d_y} \sum_{n_u} \sum_{n_v} \frac{e^{jk_0 \mathbf{R}_{nj} \cdot \hat{\mathbf{t}}_+}}{\tau_z} (\hat{\mathbf{a}}_{nj} \times \hat{\mathbf{t}}_+) P^e_{nj+}(0, d_{nj}) \int_{V\mathrm{III}} e^{-jk_0 \mathbf{R} \cdot \hat{\mathbf{t}}_+} \, dv. \qquad (4.14)$$

The limits of integration for Region (III) are

$$V^{\mathrm{III}} = \begin{cases} -\frac{d_x}{2} \leq x \leq \frac{d_x}{2} \\ -\frac{d_y}{2} \leq y \leq \frac{d_y}{2} \\ z_3 \leq z \leq \frac{d_z}{2} \end{cases}$$

and thus the integration of Equations (4.13) and (4.14) becomes

$$\int_{V\mathrm{III}} e^{-jk_0 \mathbf{R} \cdot \hat{\mathbf{t}}_+} \, dv = I_x I_y I_z^{\mathrm{III}}$$

where I_x and I_y are the same as above and

$$I_z^{\mathrm{III}} = \int_{z_3}^{\frac{d_z}{2}} e^{-jk_0 \tau_z z} \, dz = \begin{cases} \frac{d_z}{2} - z_3 & \text{if } \tau_z = 0 \\ \frac{\exp(-jk_0 \tau_z \frac{d_z}{2}) - \exp(-jk_0 \tau_z z_3)}{-jk_0 \tau_z} & \text{otherwise.} \end{cases}$$

Note that a similar statement can be made concerning the electric field resulting from the open-current end charge for the integrated Region (III) electric field as was made above, for the Region (I) electric field.

4.3 $k_w = 0$, Region (II)

In Region (II), the spatial variation of the fields consists of both the exponential term $e^{-jk_0 \mathbf{R} \cdot \hat{\mathbf{t}}_\pm}$, and also the pattern factor $P^e_{nj\pm}(a, b)$ due to the z dependence of its integration limits, given in Section A.1. Thus, $\Gamma_{nj}^{\mathbf{E}(\mathrm{II})}$ and $\Gamma_{nj}^{\mathbf{H}(\mathrm{II})}$ can be expressed as

$$\Gamma_{nj}^{\mathbf{E}(\mathrm{II})} = \frac{\eta_0}{2d_x d_y} \sum_{n_u} \sum_{n_v}$$

$$\left[\frac{e^{jk_0 \mathbf{R}_{nj} \cdot \hat{\mathbf{t}}_-}}{\tau_z} \int_{V\mathrm{II}} \mathbf{e}_{nj-} P^e_{nj-}(a_{nj-}, b_{nj-}) e^{-jk_0 \mathbf{R} \cdot \hat{\mathbf{t}}_-} \, dv + \right.$$

$$+\frac{e^{jk_0\mathbf{R}_{nj}\cdot\hat{\mathbf{r}}_+}}{r_z}\int_{V\mathrm{II}}\mathbf{e}_{nj+}\,P^e_{nj+}(a_{nj+},b_{nj+})\,e^{-jk_0\mathbf{R}\cdot\hat{\mathbf{r}}_+}\,dv\Bigg] \tag{4.15}$$

$$\mathbf{I}^{\mathbf{H}(\mathrm{II})}_{nj}=\frac{1}{2d_xd_y}\sum_{n_x}\sum_{n_y}$$

$$\Bigg[\frac{e^{jk_0\mathbf{R}_{nj}\cdot\hat{\mathbf{r}}_-}}{r_z}(\hat{\mathbf{a}}_{nj}\times\hat{\mathbf{r}}_-)\int_{V\mathrm{II}}P^e_{nj-}(a_{nj-},b_{nj-})\,e^{-jk_0\mathbf{R}\cdot\hat{\mathbf{r}}_-}\,dv+$$

$$+\frac{e^{jk_0\mathbf{R}_{nj}\cdot\hat{\mathbf{r}}_+}}{r_z}(\hat{\mathbf{a}}_{nj}\times\hat{\mathbf{r}}_+)\int_{V\mathrm{II}}P^e_{nj+}(a_{nj+},b_{nj+})\,e^{-jk_0\mathbf{R}\cdot\hat{\mathbf{r}}_+}\,dv\Bigg]. \tag{4.16}$$

The electric field resulting from the open-current end charge is embedded in the product $\mathbf{e}_{nj\pm}\,P^e_{nj\pm}(a_{nj\pm},b_{nj\pm})$. Thus the vector $\mathbf{e}_{nj\pm}$ appears inside the integral of Equation (4.15) so that the charge electric field can be isolated and/or removed. The limits of integration for Region (II) are

$$V^{\mathrm{II}}=\begin{cases}-\frac{d_x}{2}\;\le\;x\;\le\;\frac{d_x}{2}\\ -\frac{d_y}{2}\;\le\;y\;\le\;\frac{d_y}{2}\\ z_1\;\le\;z\;\le\;z_3,\end{cases}$$

and therefore the integrations of Equations (4.15) and (4.16) can be written as

$$\int_{V\mathrm{II}}\mathbf{e}_{nj\pm}\,P^e_{nj\pm}(a_{nj\pm},b_{nj\pm})\,e^{-jk_0\mathbf{R}\cdot\hat{\mathbf{r}}_\pm}\,dv=I_x\,I_y\,\mathbf{I}^{\mathbf{E}(\mathrm{II})}_{z\pm}$$

$$\int_{V\mathrm{II}}P^e_{nj\pm}(a_{nj\pm},b_{nj\pm})\,e^{-jk_0\mathbf{R}\cdot\hat{\mathbf{r}}_\pm}\,dv=I_x\,I_y\,I^{\mathbf{H}(\mathrm{II})}_{z\pm}$$

where I_x and I_y are the same as above, and

$$\mathbf{I}^{\mathbf{E}(\mathrm{II})}_{z\pm}=\int_{z_1}^{z_3}\mathbf{e}_{nj\pm}\,P^e_{nj\pm}(a_{nj\pm},b_{nj\pm})\,e^{\mp jk_0r_zz}\,dz$$

$$I^{\mathbf{H}(\mathrm{II})}_{z\pm}=\int_{z_1}^{z_3}P^e_{nj\pm}(a_{nj\pm},b_{nj\pm})\,e^{\mp jk_0r_zz}\,dz.$$

For the evaluation of these integrals, the notation of Appendix A will be utilised, as follows:

Figure A.1(b) Geometry		Figure A.1(c) Geometry	
$B^s_{nj+}(b_{nj+})$	$= B^s_{nj+}(\alpha_{nj} + \beta_{nj}\, z)$	$B^s_{nj+}(b_{nj+})$	$= C^s_{1nj+}$
$B^s_{nj+}(a_{nj+})$	$= C^s_{1nj+}$	$B^s_{nj+}(a_{nj+})$	$= B^s_{nj+}(\alpha_{nj} + \beta_{nj}\, z)$
$Q^s_{nj+}(b_{nj+})$	$= Q^s_{nj+}(\alpha_{nj} + \beta_{nj}\, z)$	$Q^s_{nj+}(b_{nj+})$	$= Q^s_{nj+}$
$Q^s_{nj+}(a_{nj+})$	$= Q^s_{nj+} = 0$	$Q^s_{nj+}(a_{nj+})$	$= Q^s_{nj+}(\alpha_{nj} + \beta_{nj}\, z)$
$A^s_{nj+}(b_{nj+})$	$= A^s_{nj+}(\alpha_{nj} + \beta_{nj}\, z)$	$A^s_{nj+}(b_{nj+})$	$= C^s_{2nj+}$
$A^s_{nj+}(a_{nj+})$	$= C^s_{2nj+}$	$A^s_{nj+}(a_{nj+})$	$= A^s_{nj+}(\alpha_{nj} + \beta_{nj}\, z)$
$B^s_{nj-}(b_{nj-})$	$= C^s_{1nj-}$	$B^s_{nj-}(b_{nj-})$	$= B^s_{nj-}(\alpha_{nj} + \beta_{nj}\, z)$
$B^s_{nj-}(a_{nj-})$	$= B^s_{nj-}(\alpha_{nj} + \beta_{nj}\, z)$	$B^s_{nj-}(a_{nj-})$	$= C^s_{1nj-}$
$Q^s_{nj-}(b_{nj-})$	$= Q^s_{nj-}$	$Q^s_{nj-}(b_{nj-})$	$= Q^s_{nj-}(\alpha_{nj} + \beta_{nj}\, z)$
$Q^s_{nj-}(a_{nj-})$	$= Q^s_{nj-}(\alpha_{nj} + \beta_{nj}\, z)$	$Q^s_{nj-}(a_{nj-})$	$= Q^s_{nj-} = 0$
$A^s_{nj-}(b_{nj-})$	$= C^s_{2nj-}$	$A^s_{nj-}(b_{nj-})$	$= A^s_{nj-}(\alpha_{nj} + \beta_{nj}\, z)$
$A^s_{nj-}(a_{nj-})$	$= A^s_{nj-}(\alpha_{nj} + \beta_{nj}\, z)$	$A^s_{nj-}(a_{nj-})$	$= C^s_{2nj-}$.

(4.17)

The terms $C^s_{1nj\pm}$ and $C^s_{2nj\pm}$ are constants with respect to z which result from the endpoints of segment nj. Similarly, the terms $Q^s_{nj\pm}$ are the charge terms associated with the open–current at the endpoints of segment nj, and are independent of z. The charge terms $Q^s_{nj\pm}(\alpha_{nj} + \beta_{nj}\, z)$ must be removed from the integral for the answer to be right, but I'm not sure why this is so. Using the definition of $\mathbf{e}_{nj\pm}$ from Equation (2.54), and $P^s_{nj\pm}(a_{nj\pm}, b_{nj\pm})$ from Appendix A, along with the notation of Equation (4.17)

$$\begin{aligned} \mathbf{I}^{\mathbf{E(II)}}_{s\pm} &= C^s_{nj\pm}\, S\, [-\hat{\mathbf{r}}_\pm\, (\hat{\mathbf{a}}_{nj} \cdot \hat{\mathbf{r}}_\pm) + \hat{\mathbf{a}}_{nj}]\, I^{\mathrm{II}}_{cs\pm} + \\ &+ C^s_{nj\pm}\, S\, [j\, \hat{\mathbf{r}}_\pm - j\, \hat{\mathbf{a}}_{nj}\, (\hat{\mathbf{a}}_{nj} \cdot \hat{\mathbf{r}}_\pm)]\, I^{\mathrm{II}}_{ss\pm} + \\ &+ C^s_{nj\pm}\, S\, \left[-\hat{\mathbf{r}}_\pm\, (C^s_{1nj\pm} + Q^s_{nj\pm}) + \hat{\mathbf{a}}_{nj}\, C^s_{2nj\pm}\right] I^{\mathrm{II}}_{s\pm} \end{aligned} \tag{4.18}$$

$$I^{\mathbf{H(II)}}_{s\pm} = C^s_{nj\pm}\, S\, \left[j\, (\hat{\mathbf{a}}_{nj} \cdot \hat{\mathbf{r}}_\pm)\, I^{\mathrm{II}}_{ss\pm} - I^{\mathrm{II}}_{cs\pm} - C^s_{2nj\pm}\, I^{\mathrm{II}}_{s\pm}\right] \tag{4.19}$$

where

$$S = \begin{cases} +1 & \text{if Figure A.1(b) geometry and + integration} \\ & \text{or Figure A.1(c) geometry and } - \text{ integration,} \\ -1 & \text{if Figure A.1(b) geometry and } - \text{ integration} \\ & \text{or Figure A.1(c) geometry and + integration,} \end{cases}$$

$$I^{\mathrm{II}}_{cz\pm} = \int_{z_1}^{z_3} e^{\mp jk_0 r_z z}\, e^{jk_0(\alpha_{nj}+\beta_{nj}z)(\hat{\mathbf{a}}_{nj}\cdot\hat{\mathbf{r}}_\pm)} \cos\left[k_0(\alpha_{nj}+\beta_{nj}z)\right] dz$$

$$= e^{jk_0\alpha_{nj}(\hat{\mathbf{a}}_{nj}\cdot\hat{\mathbf{r}}_\pm)} \left[\frac{e^{jk_0\alpha_{nj}}}{2} I_+ + \frac{e^{-jk_0\alpha_{nj}}}{2} I_-\right] \tag{4.20}$$

$$I^{\mathrm{II}}_{sz\pm} = \int_{z_1}^{z_3} e^{\mp jk_0 r_z z}\, e^{jk_0(\alpha_{nj}+\beta_{nj}z)(\hat{\mathbf{a}}_{nj}\cdot\hat{\mathbf{r}}_\pm)} \sin\left[k_0(\alpha_{nj}+\beta_{nj}z)\right] dz$$

$$= e^{jk_0\alpha_{nj}(\hat{\mathbf{a}}_{nj}\cdot\hat{\mathbf{r}}_\pm)} \left[\frac{e^{jk_0\alpha_{nj}}}{2j} I_+ - \frac{e^{-jk_0\alpha_{nj}}}{2j} I_-\right] \tag{4.21}$$

where

$$\omega_{nj} = \mp r_z + \beta_{nj}\left(\hat{\mathbf{a}}_{nj}\cdot\hat{\mathbf{r}}_\pm\right) = \frac{r_x\, a_{njx} + r_y\, a_{njy}}{a_{njz}}$$

$$I_\pm = \int_{z_1}^{z_3} e^{jk_0(\omega_{nj}\pm\beta_{nj})z}\, dz$$

$$= \begin{cases} z_3 - z_1 & \text{if } \omega_{nj} = -\beta_{nj} \\ \frac{\exp[jk_0(\omega_{nj}\pm\beta_{nj})z_3] - \exp[jk_0(\omega_{nj}\pm\beta_{nj})z_1]}{jk_0(\omega_{nj}\pm\beta_{nj})} & \text{otherwise} \end{cases}$$

and

$$I^{\mathrm{II}}_{z\pm} = \int_{z_1}^{z_3} e^{\mp jk_0 r_z z}\, dz = \begin{cases} z_3 - z_1 & \text{if } r_z = 0 \\ \frac{\exp[\mp jk_0 r_z z_3] - \exp[\mp jk_0 r_z z_1]}{\mp jk_0 r_z} & \text{otherwise.} \end{cases}$$

If it is desired to remove the electric field resulting from the open–current end charge, then $Q^s_{nj\pm}$ needs to be removed from Equation (4.18).

4.4 $k_w > 0$ and $k_w < 0$

The only spatial variation of the fields of the planar arrays where $k_w > 0$ is the exponential term $e^{-jk_0\mathbf{R}\cdot\hat{\mathbf{r}}_-}$ inside the double spectral summation of plane waves. Thus $\mathbf{I}^{\mathbf{E}}_{nj}(k_w > 0)$ and $\mathbf{I}^{\mathbf{H}}_{nj}(k_w > 0)$ can be expressed as

$$\mathbf{I}^{\mathbf{E}}_{nj}(k_w > 0) = \frac{\eta_0}{2d_x d_y} \sum_{n_u} \sum_{n_v} \left(\frac{e^{-j\beta_-}}{1 - e^{-j\beta_-}}\right) \frac{e^{jk_0\mathbf{R}_{nj}\cdot\hat{\mathbf{r}}_-}}{r_z} \times$$

$$\times \mathbf{e}_{nj-}\, P^{e}_{nj-}(0, d_{nj}) \int_{V^0} e^{-jk_0 \mathbf{R}\cdot\hat{\mathbf{r}}_-}\, dv \tag{4.22}$$

$$\mathbf{I}^{\mathbf{H}}_{nj}(k_w > 0) = \frac{1}{2d_x d_y} \sum_{n_u} \sum_{n_v} \left(\frac{e^{-j\beta_-}}{1 - e^{-j\beta_-}} \right) \frac{e^{jk_0 \mathbf{R}_{nj}\cdot\hat{\mathbf{r}}_-}}{\tau_z} \times$$

$$\times (\hat{\mathbf{a}}_{nj} \times \hat{\mathbf{r}}_-)\, P^{e}_{nj-}(0, d_{nj}) \int_{V^0} e^{-jk_0 \mathbf{R}\cdot\hat{\mathbf{r}}_-}\, dv. \tag{4.23}$$

A similar statement can be made about the fields of the planar arrays where $k_w < 0$, and thus $\mathbf{I}^{\mathbf{E}}_{nj}(k_w < 0)$ and $\mathbf{I}^{\mathbf{H}}_{nj}(k_w < 0)$ can be expressed as

$$\mathbf{I}^{\mathbf{E}}_{nj}(k_w < 0) = \frac{\eta_0}{2d_x d_y} \sum_{n_u} \sum_{n_v} \left(\frac{e^{+j\beta_+}}{1 - e^{+j\beta_+}} \right) \frac{e^{jk_0 \mathbf{R}_{nj}\cdot\hat{\mathbf{r}}_+}}{\tau_z} \times$$

$$\times \mathbf{e}_{nj+}\, P^{e}_{nj+}(0, d_{nj}) \int_{V^0} e^{-jk_0 \mathbf{R}\cdot\hat{\mathbf{r}}_+}\, dv \tag{4.24}$$

$$\mathbf{I}^{\mathbf{H}}_{nj}(k_w < 0) = \frac{1}{2d_x d_y} \sum_{n_u} \sum_{n_v} \left(\frac{e^{+j\beta_+}}{1 - e^{+j\beta_+}} \right) \frac{e^{jk_0 \mathbf{R}_{nj}\cdot\hat{\mathbf{r}}_+}}{\tau_z} \times$$

$$\times (\hat{\mathbf{a}}_{nj} \times \hat{\mathbf{r}}_+)\, P^{e}_{nj+}(0, d_{nj}) \int_{V^0} e^{-jk_0 \mathbf{R}\cdot\hat{\mathbf{r}}_+}\, dv. \tag{4.25}$$

The integration limits are over the entire $\mathbf{Q} = 0$ lattice cell and are symmetric, i.e.,

$$V^0 = \begin{cases} -\frac{d_x}{2} \le x \le \frac{d_x}{2} \\ -\frac{d_y}{2} \le y \le \frac{d_y}{2} \\ -\frac{d_z}{2} \le z \le \frac{d_z}{2}. \end{cases}$$

The integrations of Equations (4.22)–(4.25) can be written as

$$\int_{V^0} e^{-jk_0 \mathbf{R}\cdot\hat{\mathbf{r}}_\pm}\, dv = I_x\, I_y\, I_z$$

where I_x and I_y are the same as above and

$$I_z = \int_{-\frac{d_z}{2}}^{\frac{d_z}{2}} e^{\mp jk_0 \tau_z z}\, dz = \begin{cases} d_z & \text{if } \tau_z = 0 \\ \frac{2}{k_0 \tau_z} \sin(k_0 \tau_z \frac{d_z}{2}) & \text{otherwise.} \end{cases}$$

The electric field of open–current end charges can be isolated and/or removed by operating on the $\mathbf{e}_{nj\pm}\, P^{e}_{nj\pm}(0, d_{nj})$ product as outlined in Section A.2.

Chapter 5

Numerical Results

5.1 A 3D Array of Short PEC Dipoles

The first set of data illustrate the convergence of the effective permittivity and the current shape of a simple artificial dielectric with respect to the number of MM expansion functions. The data also illustrate the ability of the PMM solution to account for the mutual coupling effects between wire objects in the artificial dielectric. Finally, it is shown that the effective wavenumber can vary greatly with the direction of propagation, whereas the effective permittivity is typically independent of the direction of propagation, provided the current shape does not change very much.

As shown in the insert to Figure 5.1, the geometry of the artificial dielectric consists of a 3D periodic array of short perfect electric conducting (PEC) dipoles in a host medium of free space. The dipoles have radius $a = 0.001\lambda_0$ and length $2h = 0.2\lambda_0$, and are oriented parallel to the x–axis. They are arranged in a lattice structure where $d_x = 2h + d$ and $d_y = d_z = d$. For this uniaxial structure, the only non–unity diagonal element of the permittivity tensor is ϵ_{xx}^{cr}, i.e., the solution will have an $\hat{\mathbf{x}}$ polarized electric current and electric field. The plane wave is propagating in the $\hat{\mathbf{u}}_k = -(\hat{\mathbf{y}} + \hat{\mathbf{z}})/\sqrt{2}$ direction. The computed relative effective permittivity ϵ_{xx}^{cr} is plotted for lattice spacing d ranging up to $0.1\lambda_0$ with N = 1,7 and 15 MM expansion functions for the current on each wire dipole. The $N = 1$ curve corresponds identically with the results obtained by Blanchard [21, Ch. 5]. Also, an $N = 1$ static approximation for the relative effective permittivity is given. This static approximation is based upon methods presented by Collin [20, Ch. 12].

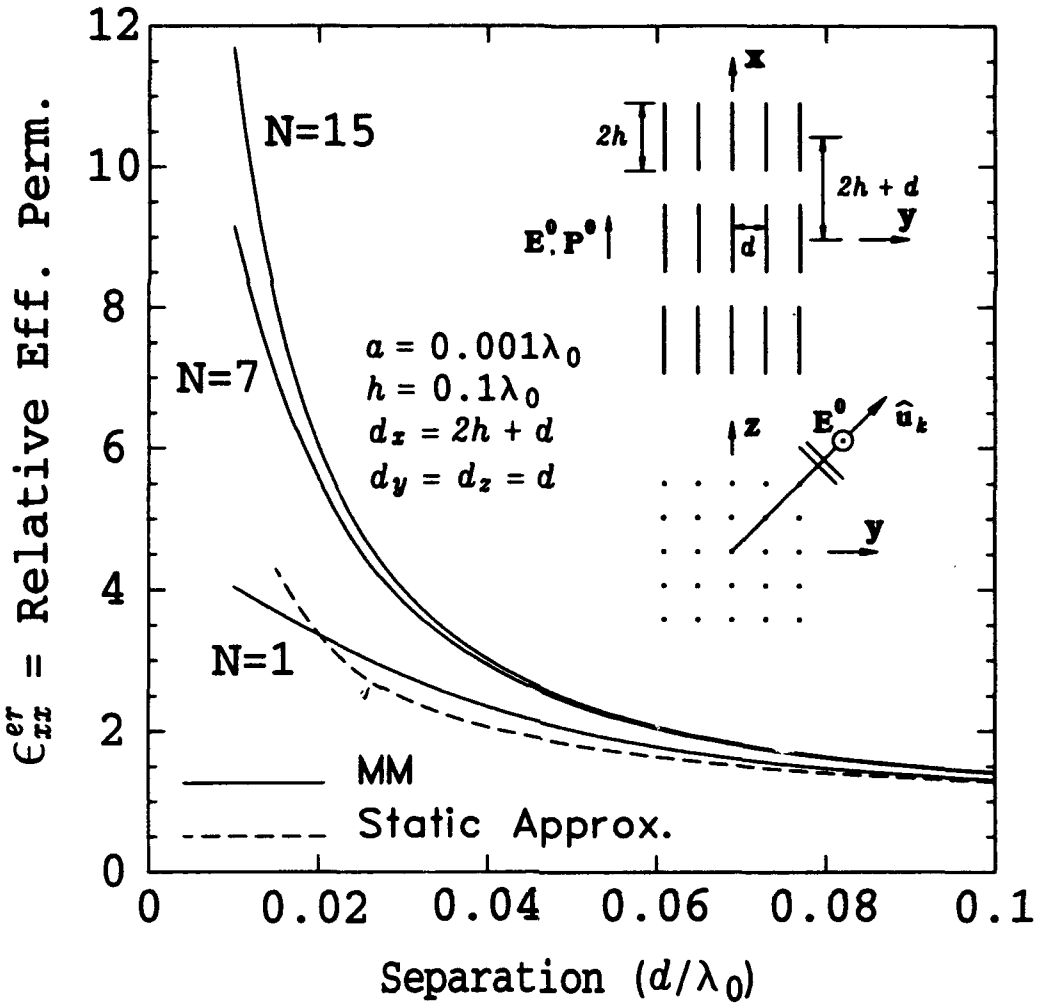

Figure 5.1: Relative effective permittivity versus lattice spacing for a 3D array of perfectly conducting short dipoles.

Figure 5.2 shows the shape of the normalized current induced on the same 3D array of dipoles, at the specific value of $d = 0.02\lambda_0$, for N = 1,7 and 15. Note that the PMM solution predicts a rounded off pulse shape for the current, and several MM PWS expansion functions are needed to accurately model the current. This illustrates that the moment method solution accounts for a change in *shape* in the dipole current caused by mutual coupling effects in the 3D array. In contrast, typically, static solutions employ a *polarizability* of the objects. This polarizability is a characteristic parameter of the objects, and is not influenced by the 3D array [20, Sec. 12.1].

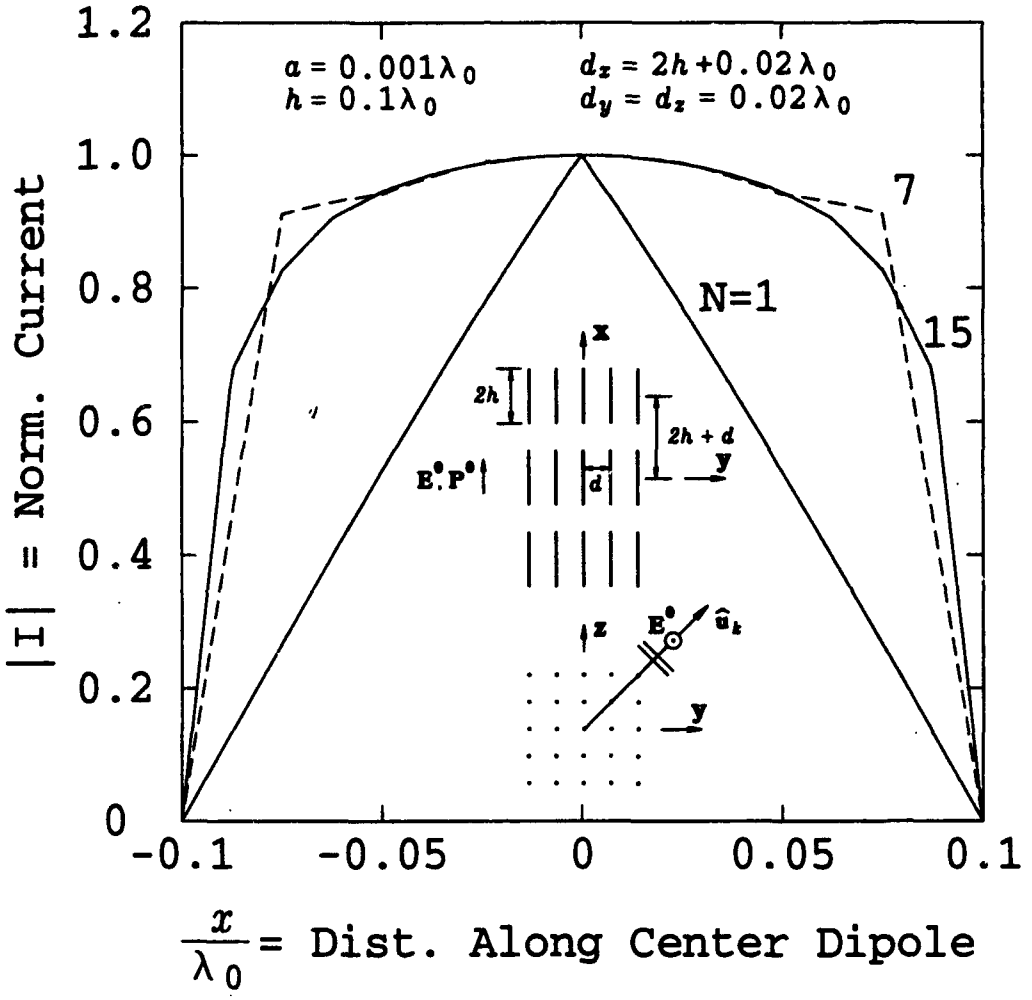

Figure 5.2: The normalized current induced on the dipoles in a 3D array of perfectly conducting short dipoles.

Now consider the 3D array of PEC dipoles in free space shown in the insert to Figure 5.3. As before, the dipoles have radius $a = 0.001\lambda_0$ and length $2h = 0.2\lambda_0$. This time they are arranged in a fixed lattice where $d_x = 0.25\lambda_0$ and $d_y = d_z = 0.05\lambda_0$. Again, the artificial dielectric is uniaxial, and ϵ_{xx}^{er} is the only non-unity diagonal permittivity tensor component. The direction of propagation $\hat{\mathbf{u}}_k$ varies with the angle θ from 0 to 80°, measured from the z-axis, as indicated in the insert to Figure 5.3. The data in Figures 5.3 and 5.4 were computed with 7 MM expansion functions.

Figure 5.3 shows the relative effective permittivity ϵ_{xx}^{er} (computed by both the polarization method of Equations (2.32) or (2.38), and the Maxwell's equations method of Equation (2.37)) and the normalized effective wavenumber (k_e/k_0) as a function of the propagation angle θ. These data illustrate that, in general, the effective permittivity tensor components will be almost constant, whereas the effective wavenumber can vary quite noticeably with different propagation directions. This is exactly true for real anisotropic media, and it holds reasonably well for many typical artificial anisotropic media. See Appendix G for a discussion of the wavenumber predicted by the ellipsoid of wave normals. Figure 5.4 shows the current shape on the center dipole for various angles θ. Note that the magnitude of the current shape is essentially the same for different propagation direction directions, whereas the phase of the current shape exhibits a slight odd symmetry about the center of the dipoles.

5.2 Dispersion of a 3D Array of Dipoles

The data in Figure 5.5 illustrate the dispersion characteristics of an artificial dielectric composed of PEC dipoles. As shown in the insert to Figure 5.5, the dipoles are of length $2h = 0.6$cm, radius $a = 0.01$cm, and are arranged in a 3D lattice array with spacings $d_x = 0.7$cm and $d_y = d_z = 0.1$cm. The dipoles are parallel to the x-axis, and therefore the electric current and electric field are $\hat{\mathbf{s}}$ polarized. This artificial dielectric is uniaxial, and the only non-unity diagonal component of the permittivity tensor is ϵ_{xx}^{er}. The direction of propagation is along the z-axis. The relative effective permittivity ϵ_{xx}^{er} is plotted versus frequency for $N = 1$,5 and 11 MM expansion functions for the current on each dipole. The frequency varies up to 24

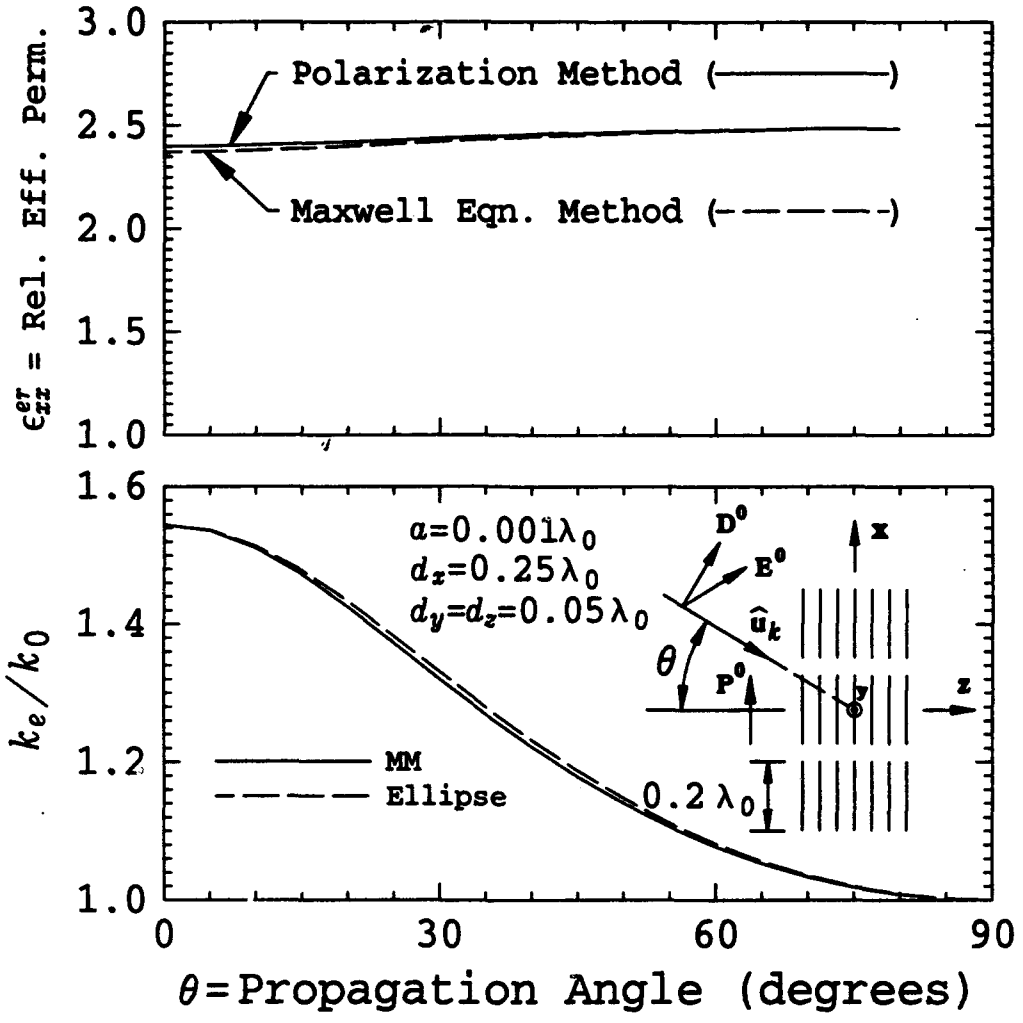

Figure 5.3: The normalized effective wavenumber (k_e/k_0) and the relative effective permittivity versus propagation angle θ, for an array of perfectly conducting short dipoles.

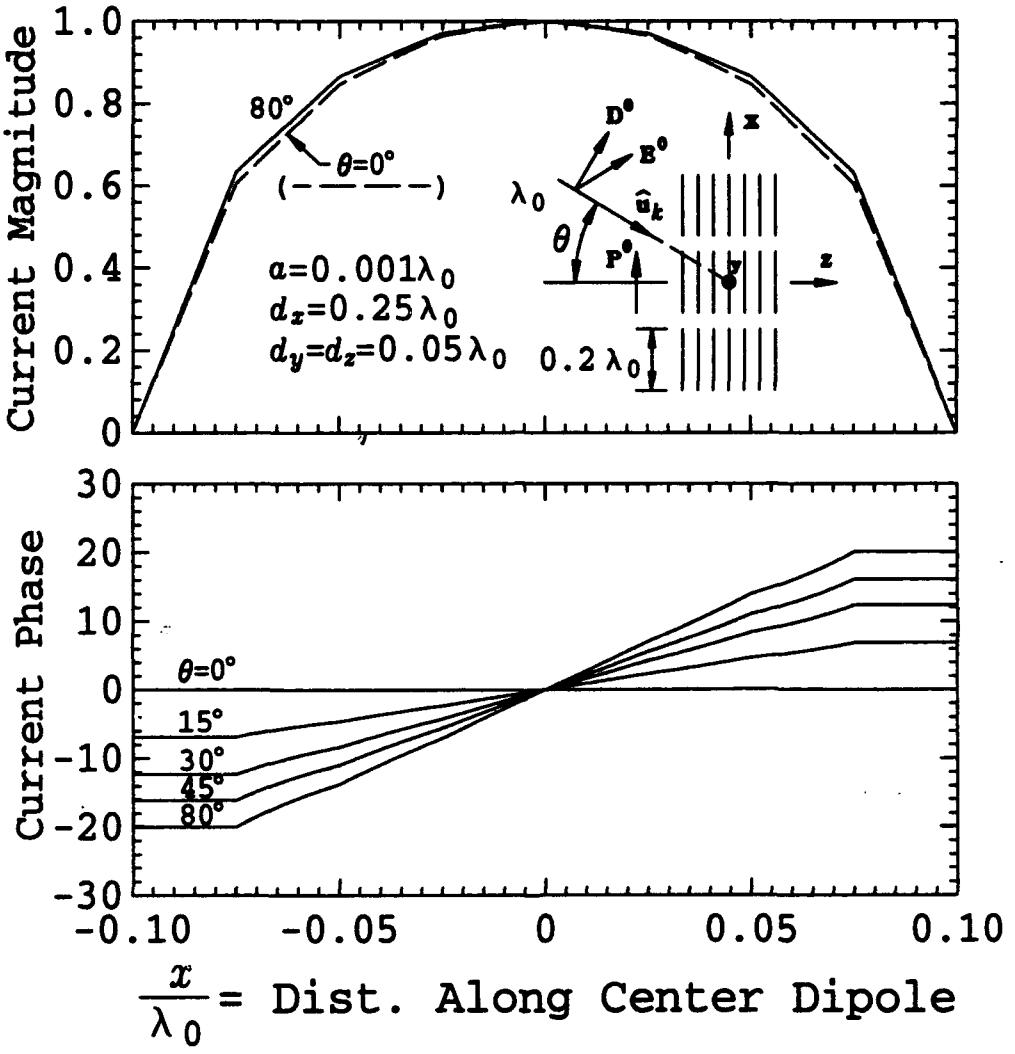

Figure 5.4: Magnitude and phase of the current on the center dipole for several different propagation angles θ, for an array of perfectly conducting short dipoles.

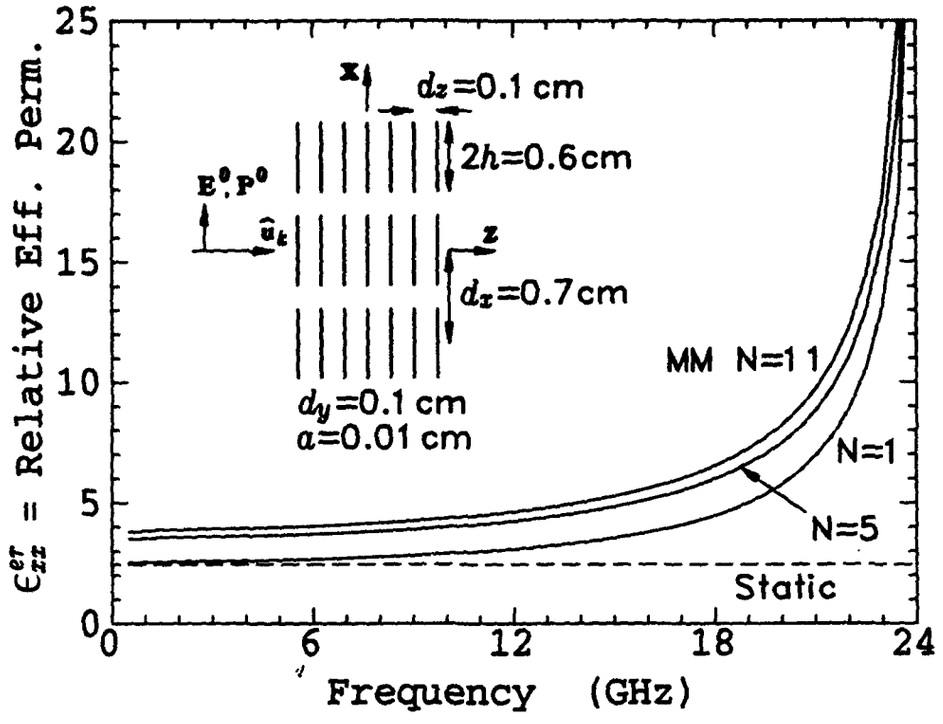

Figure 5.5: Dispersion curve for a 3D array of perfectly conducting dipoles.

GHz, corresponding to a dipole length of $0.48\lambda_0$. At low frequencies, the effective permittivity approaches a constant value, and the $N = 1$ solution approaches the static approximation of Collin [20]. As the frequency increases, the scattered field of each dipole increases, and thus the effective permittivity increases, especially as the half wavelength resonance of the dipoles is approached.

5.3 Array of Dipoles Oriented at Angle ϕ

The data in this section show an example of a simple artificial dielectric that is not uniaxial, i.e., the effective permittivity tensor has non-zero off-diagonal components. It is shown that the two eigenfunction solutions (one being a solution with a free space root $k_e = k_0$) are needed to solve for the permittivity tensor. As shown in the insert sketch to Figure 5.6, the artificial dielectric consists of straight PEC dipoles of length $2h = 0.2\lambda_0$ and radius $a = 0.001\lambda_0$, oriented in the direction of the angle ϕ.

The dipoles are arranged in a 3D lattice array with spacings $d_x = d_y = 0.21\lambda_0$ and $d_z = 0.01\lambda_0$. The direction of propagation is along the z–axis.

Figure 5.6 shows the normalized effective wavenumber (k_e/k_0) as a function of the orientation angle ϕ, for $N = 7$ and 15 MM expansion functions. (Recall that another free space root solution exists, too.) Note that for the indicated effective wavenumber, the electric dipole moment $\mathbf{P}_1^0$ and the average eigenfunction electric field $\mathbf{E}_1^0$ are oriented parallel to the dipoles. The magnetic dipole moment $\mathbf{M}_1^0$ vanishes and the average eigenfunction magnetic field $\mathbf{H}_1^0$ is oriented perpendicular to the dipoles in the xy–plane. Corresponding to the free space root $k_e = k_0$, the dipole moments $(\mathbf{P}_2^0, \mathbf{M}_2^0)$ vanish and the eigenfunction fields may be written as

$$\mathbf{E}_2^0 = \hat{\mathbf{x}}\eta_0 \sin\phi - \hat{\mathbf{y}}\eta_0 \cos\phi$$

$$\mathbf{H}_2^0 = \hat{\mathbf{x}} \cos\phi + \hat{\mathbf{y}} \sin\phi \tag{5.1}$$

where η_0 is the characteristic impedance of free space. Using the current moment and eigenfunction fields above in Equations (2.32) or (2.37), the polarization method and the Maxwell's equations method yield virtually identical results for the permittivity tensor components, shown in Figure 5.7. Note that the artificial dielectric degenerates to a uniaxial dielectric when the dipoles are oriented along a principle axis, i.e., when $\phi = 0$ or $\phi = 90°$.

5.4 Resistive Loaded Dipoles

This data in this section show the effect of resistive loading on a 3D array of dipoles. As shown in the insert to Figure 5.8, the geometry consists of PEC dipoles of length $2h = 0.2\lambda_0$ and radius $a = 0.001\lambda_0$, arranged in a 3D lattice with spacings $d_x = 0.23\lambda_0$ and $d_y = d_z = 0.03\lambda_0$. A purely resistive load R_L is located at the center of each dipole. Propagation is in the $\hat{\mathbf{u}}_k = \hat{\mathbf{z}}$ direction, and polarization is in the $\hat{\mathbf{x}}$ direction. Figure 5.8 shows the relative effective permittivity ϵ_{xx}^{er} and effective loss tangent $\tan\delta_{xx}^{e}$ of the artificial medium versus load resistance for $10\Omega \leq R_L \leq 100\text{K}\Omega$, for solutions with $N = 7$ and $N = 13$ MM expansion functions. Note that at low resistive loading ($R_L < 200\Omega$) the effective permittivity is close to that for

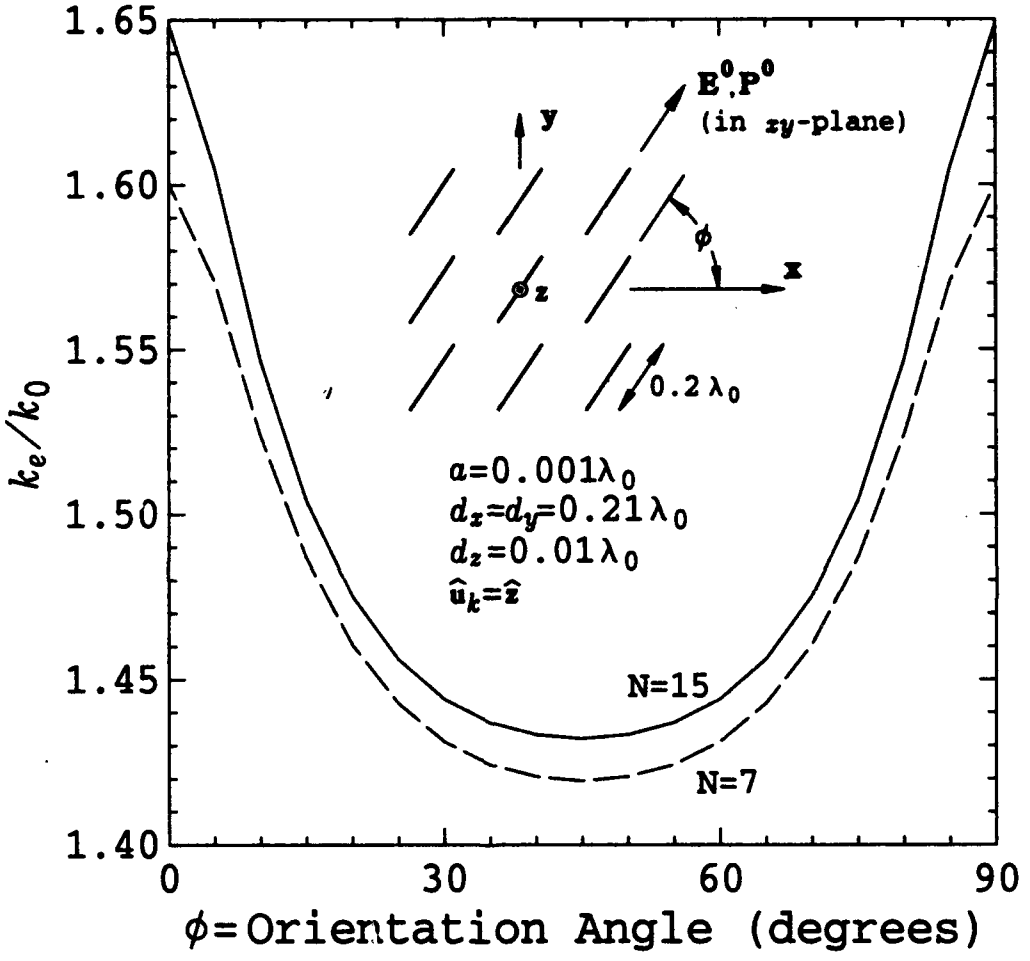

Figure 5.6: The normalized effective wavenumber (k_e/k_0) versus orientation angle ϕ for an array of perfectly conducting short dipoles.

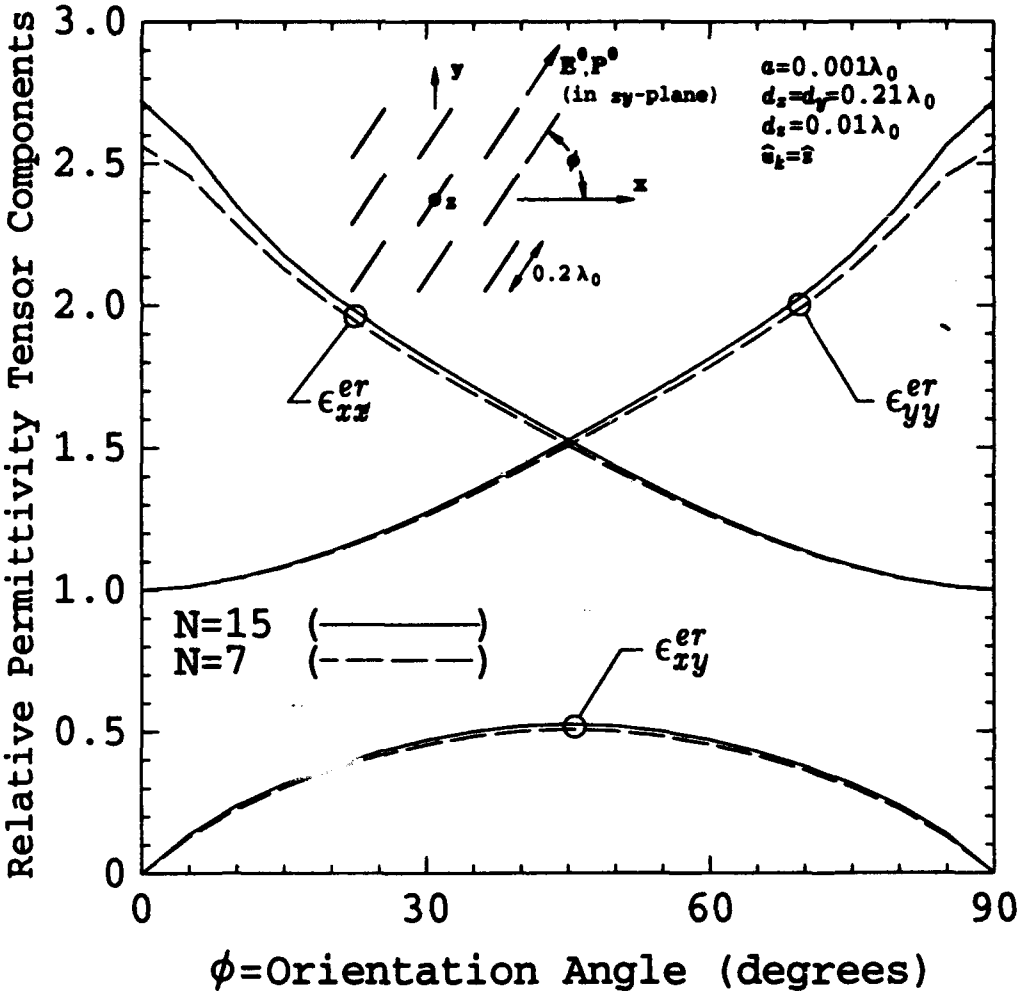

Figure 5.7: The effective permittivity tensor components versus orientation angle ϕ for an array of perfectly conducting short dipoles.

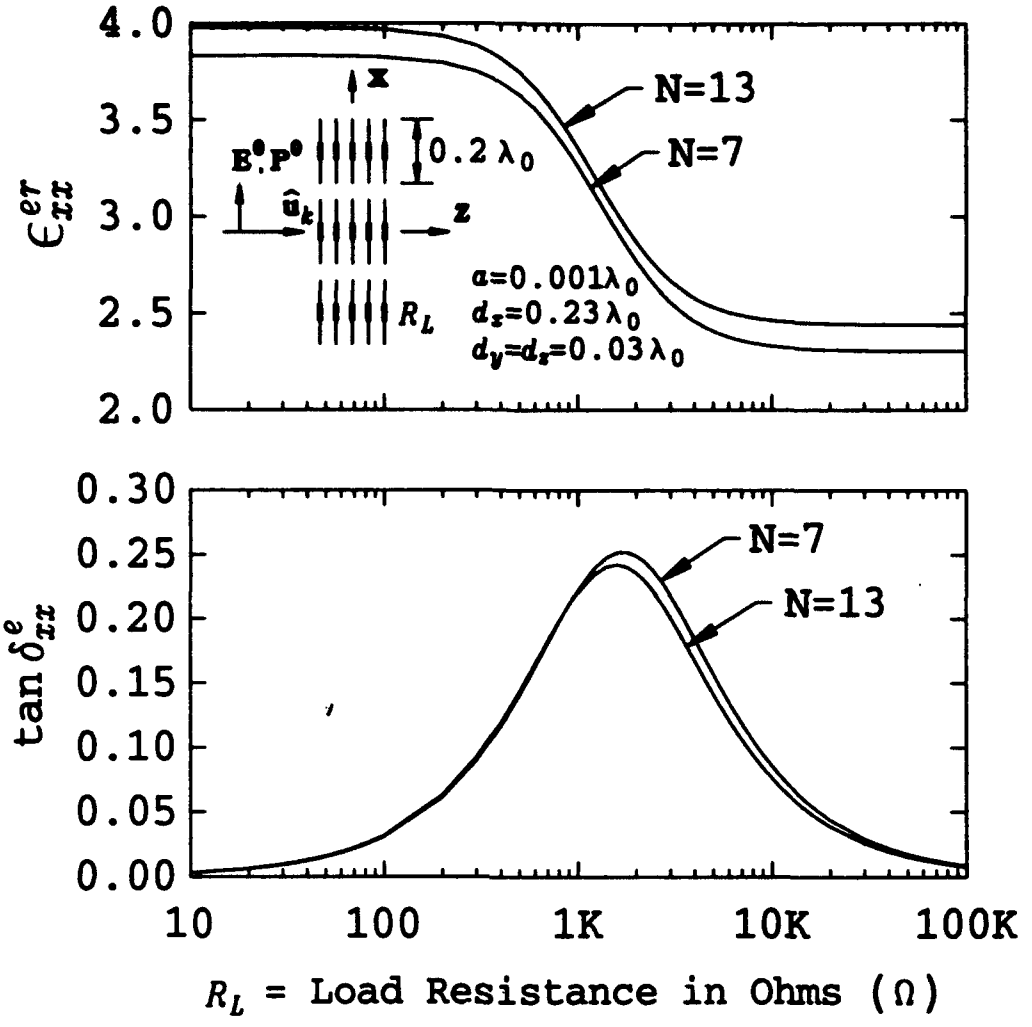

Figure 5.8: Relative effective permittivity and loss tangent for a 3D array of resistive loaded PEC dipoles.

PEC dipoles of length $2h$, and at high resistive loading ($R_L > 10\text{K}\Omega$) the effective permittivity is close to that for two disconnected PEC dipoles, each of length h. The maximum loss of the artificial medium occurs near $R_L = 1.5\text{K}\Omega$, corresponding to the maximum I^2R_L loss in the load resistance of the dipoles.

Figure 5.9 shows the magnitude and phase of the current shape on the center dipole for $N = 13$ MM expansion functions and for load resistances of $R_L = 100\Omega$, $1\text{K}\Omega$ and $10\text{K}\Omega$. Note that as the load resistance increases, the current at the terminals of the dipole (at R_L) decreases, until for large R_L the dipole is essentially disconnected at its center, effectively forming two dipoles.

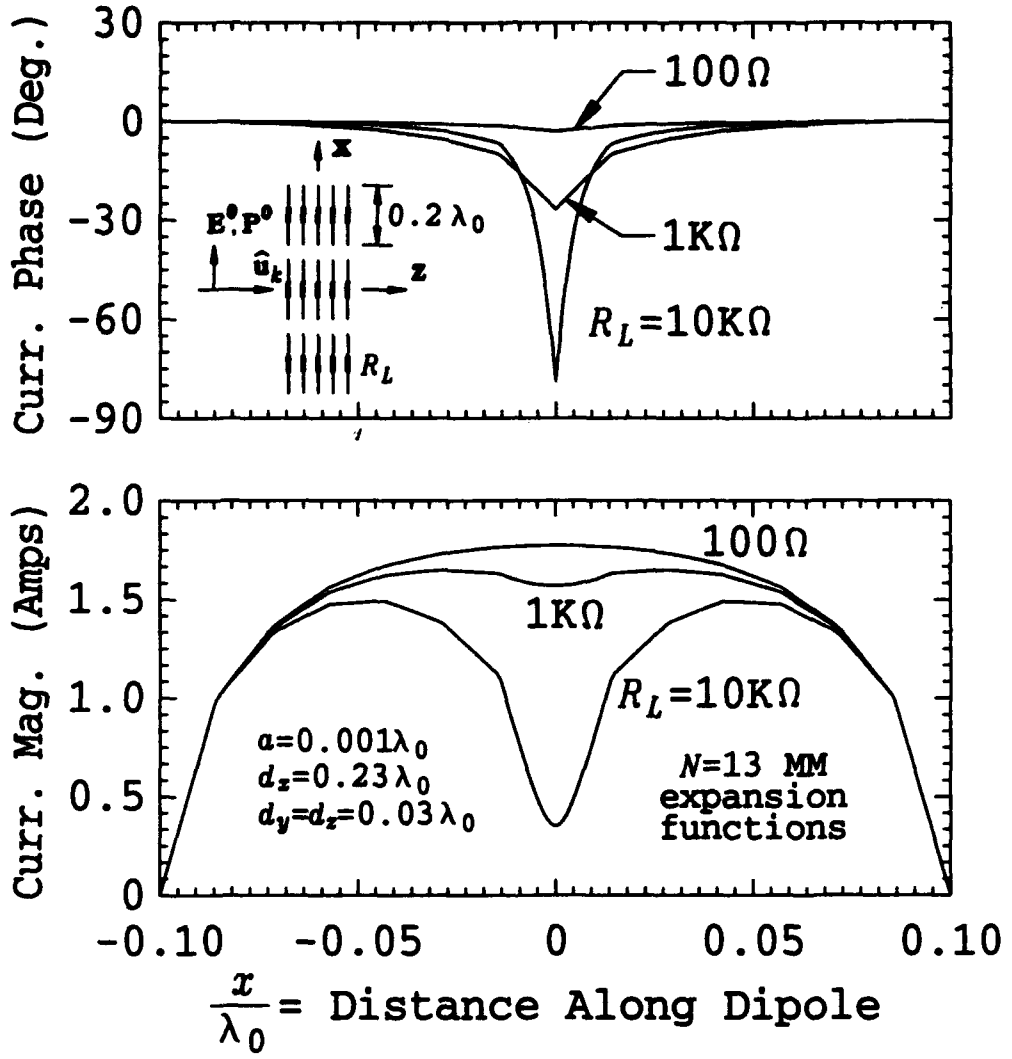

Figure 5.9: Magnitude and phase of the current on the center dipole at $R_L = 100\Omega$, 1KΩ and 10KΩ, for a 3D array of resistive loaded PEC dipoles.

5.5 Lossy Dielectric Dipoles

The data in this section show the effects of dielectric loss in a 3D array of dipoles. For simplicity of dimensions, the data are computed at 300 MHz with a free space host medium so that λ_0 =1 meter. As shown in the insert to Figure 5.10, the geometry consists of lossy dielectric dipoles of length $2h = 0.2\lambda_0$ and radius $a = 0.001\lambda_0$, arranged in a 3D lattice with spacings $d_x = 0.23\lambda_0$ and $d_y = d_z = 0.03\lambda_0$. The dipoles have relative dielectric constant $\epsilon_{1r} = 1$ and loss tangent $\tan\delta_1$. Propagation is in the $\hat{\mathbf{u}}_k = \hat{\mathbf{z}}$ direction, and polarization is in the $\hat{\mathbf{x}}$ direction. Figure 5.10 shows the relative effective permittivity ϵ_{xx}^{er} and effective loss tangent $\tan\delta_{xx}^{e}$ of the artificial medium versus dipole loss tangent for $10 \leq \tan\delta_1 \leq 100,000$ and for solutions with $N = 9$ and $N = 15$ MM expansion functions. Note that a monopole expansion function, with its associated open–current end charge contribution, was included at each end of the dielectric dipoles.

Figure 5.11 shows the magnitude and phase of the current shape on the center dipole at $N = 15$ MM expansion functions for dipole loss tangent values of $\tan\delta_1 =$ 50, 500 and 5000. Note that for a low dipole loss tangent, the current is fairly uniform across the dipole. As the dipole loss tangent increases, the current shape approaches that of a PEC dipole.

5.6 Square PEC Loops

The data in this section involves an artificial medium that is slightly magnetic. It is shown that the eigenfunction current shape on the wire objects can be a strong function of the direction of propagation. As shown in the insert to Figure 5.12, the geometry of the artificial medium consists of a 3D periodic array of PEC square loops arranged in a host medium of free space. The loop wires have radius $a = 0.001\lambda_0$ and the sides are of length $l = 0.1\lambda_0$. The loops are arranged perpendicular to the z–axis in a lattice structure where $d_x = d_y = 0.12\lambda_0$ and $d_z = 0.02\lambda_0$. Propagation is in the $\hat{\mathbf{u}}_k$ direction, always in the the yz–plane, measured by the angle θ from the z–axis. θ varies from 0° (broadside to the the loops) to 90° (edge–on to the loops). For all the

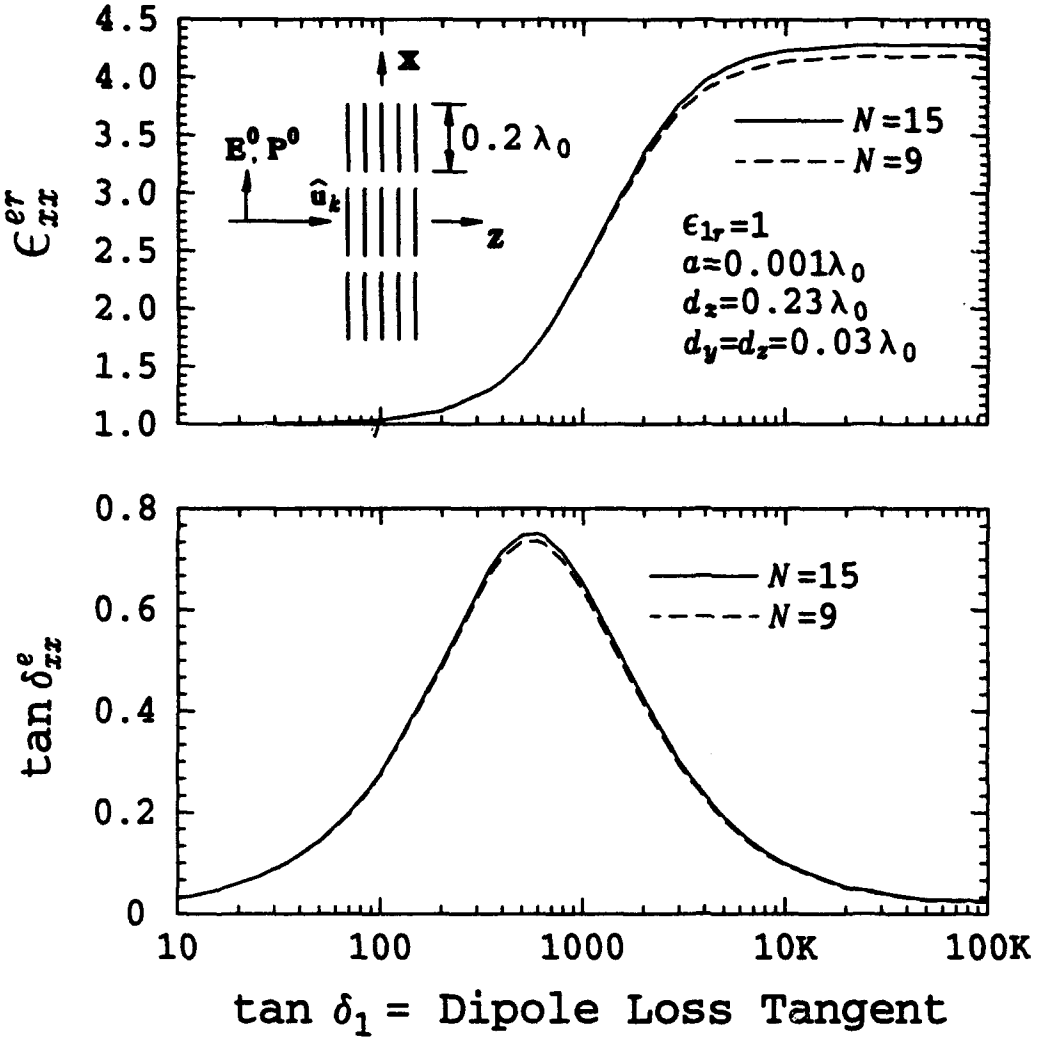

Figure 5.10: Relative effective permittivity and loss tangent for a 3D array of lossy dielectric dipoles.

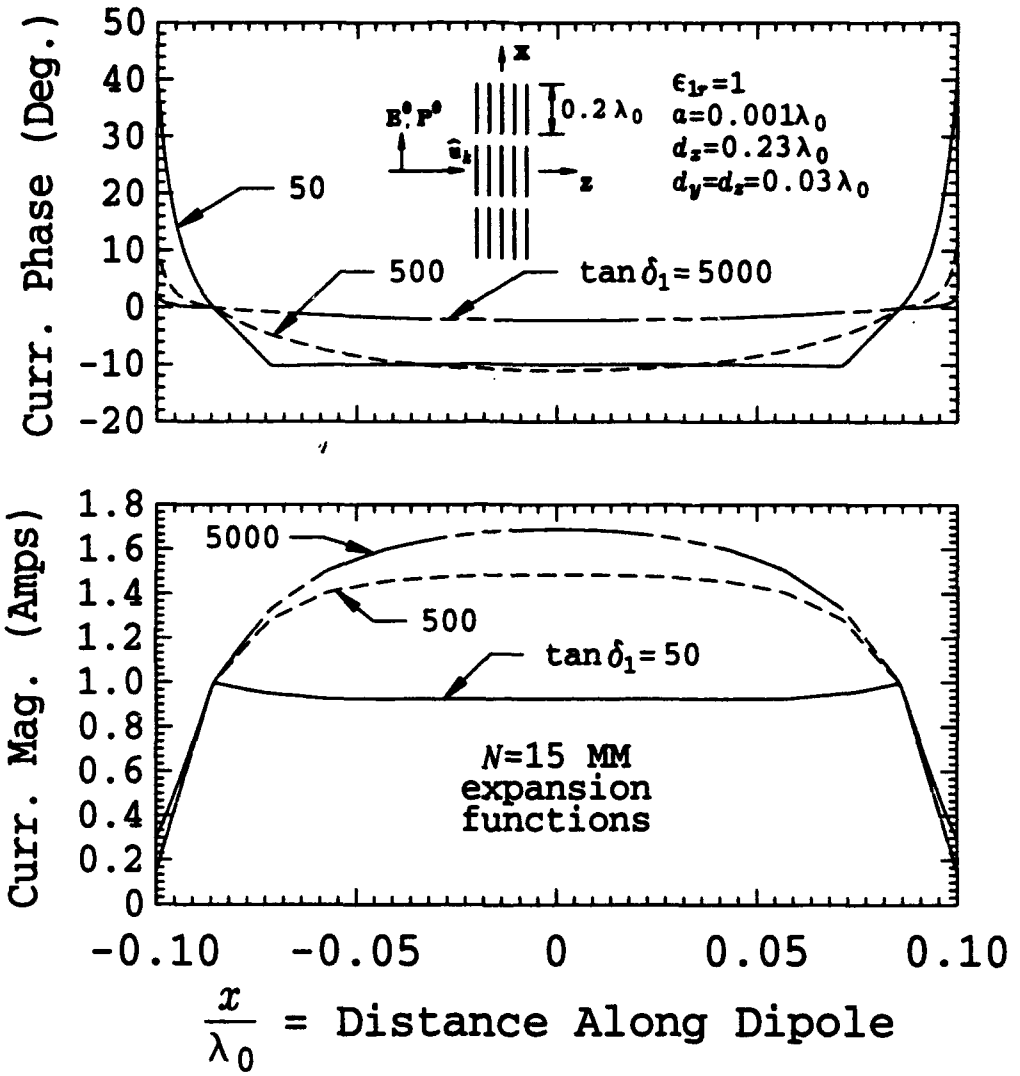

Figure 5.11: Magnitude and phase of the current on the center dipole at $\tan\delta_1 = 50$, 500 and 5000, for a 3D array of lossy dielectric dipoles.

data shown in this section, there are 8 MM expansion functions distributed equally around the square loop.

Figure 5.12 shows the normalized effective wavenumber (k_e/k_0) corresponding to each of the two roots (see Section 2.3.1) as a function of the propagation angle θ. The roots were computed by two methods. The first method determines the roots by the PMM solution. The second method employs a technique from crystal optics known as the *ellipsoid of wave normals* (see Appendix G) [23, Ch. 4],[24, Ch. 14]. The ellipsoid of wave normals uses the roots computed by the PMM for $\theta = 0°$ and $\theta = 90°$. Figure 5.13 shows the magnitude of the determinant of the impedance matrix $|\mathcal{Z}|$ versus the normalized effective wavenumber for propagation angles $\theta = 0, 15, 30, 60$ and $90°$. The roots are indicated by the sharp minima of $|\mathcal{Z}|$. Note the occurrence of a double root due to symmetry considerations only at $\theta = 0°$. Also, note that the $\theta = 90°$ curve only indicates one root; the other root being a free space root at $k_e = k_0$.

Figures 5.14 and 5.15 show the current shape on the center loop for both roots 1 and 2, respectively, for several propagation angles θ. The sketch at the top of Figure 5.15 shows how the current is plotted in relation to the geometry of the loop. The phase of the current shape corresponding to root 2 is not plotted because it is $0°$ for positive x and $180°$ for negative x. Note that the current shape corresponding to root 1 changes with propagation angle θ, whereas the current shape corresponding to root 2 does not change with propagation angle. Also, note that at propagation angle $\theta = 0°$ the two current shapes are orthogonal to each other, corresponding to the double root from symmetry. The current shape for root 1 has net electric dipole moment $\mathbf{P}^0$ oriented in the x–direction, whereas the current shape for root 2 has $\mathbf{P}^0$ oriented in the y–direction.

Figures 5.16 and 5.17 show the effective relative permittivity and permeability tensor components, respectively, computed as a function of the propagation angle θ. Observe that this artificial medium is uniaxial. The permittivity tensor components were computed using both the polarization method of Equations (2.32) or (2.38), and the Maxwell's equations method of Equation (2.37). There is good agreement

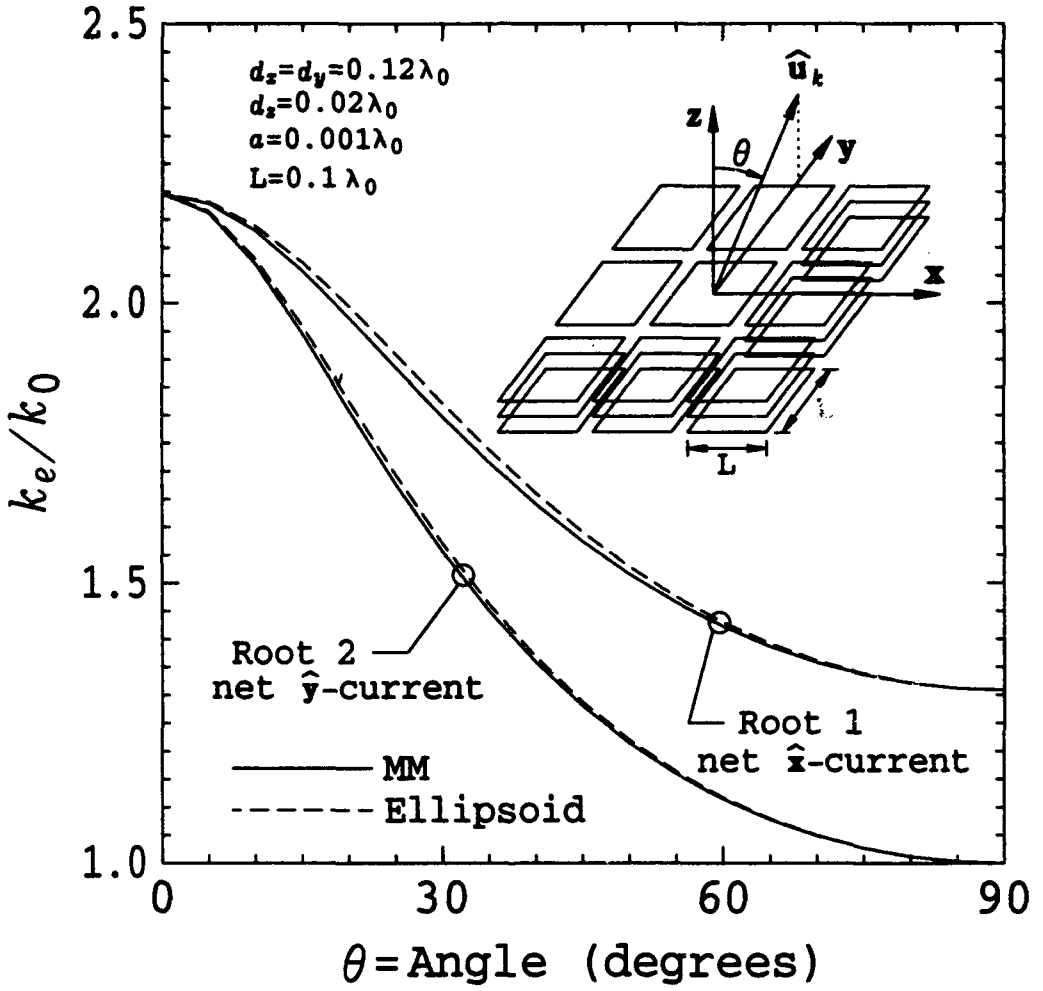

Figure 5.12: Normalized effective wavenumber (k_e/k_0) for both roots versus propagation angle θ, for an array of square PEC loops.

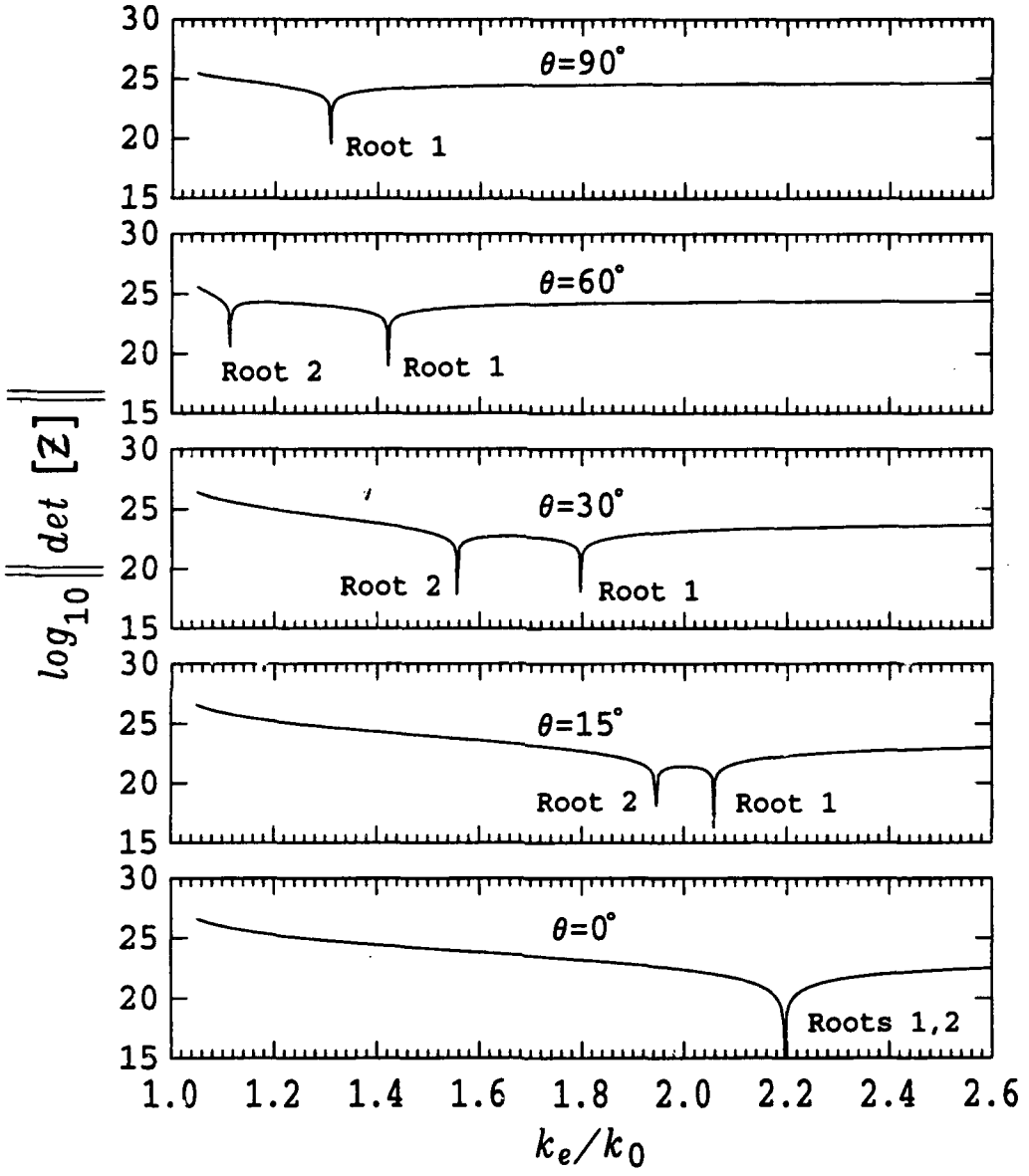

Figure 5.13: Magnitude of $|\mathcal{Z}|$ versus normalized effective wavenumber at $\theta = 0, 15, 30, 60$ and 90°, for an array of square PEC loops.

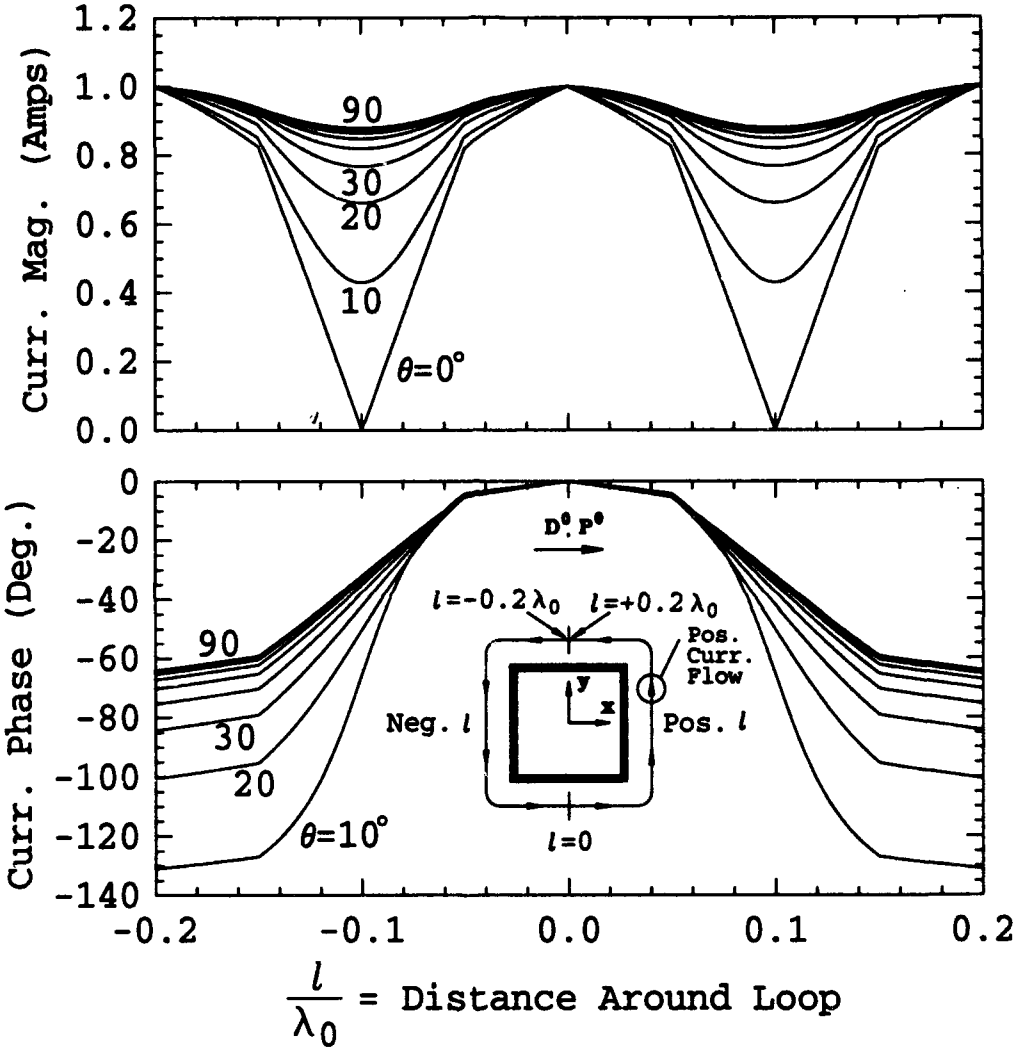

Figure 5.14: The root 1 current mode shape at $\theta = 0, 10, 20, 30, \ldots, 90°$, for an array of square PEC loops.

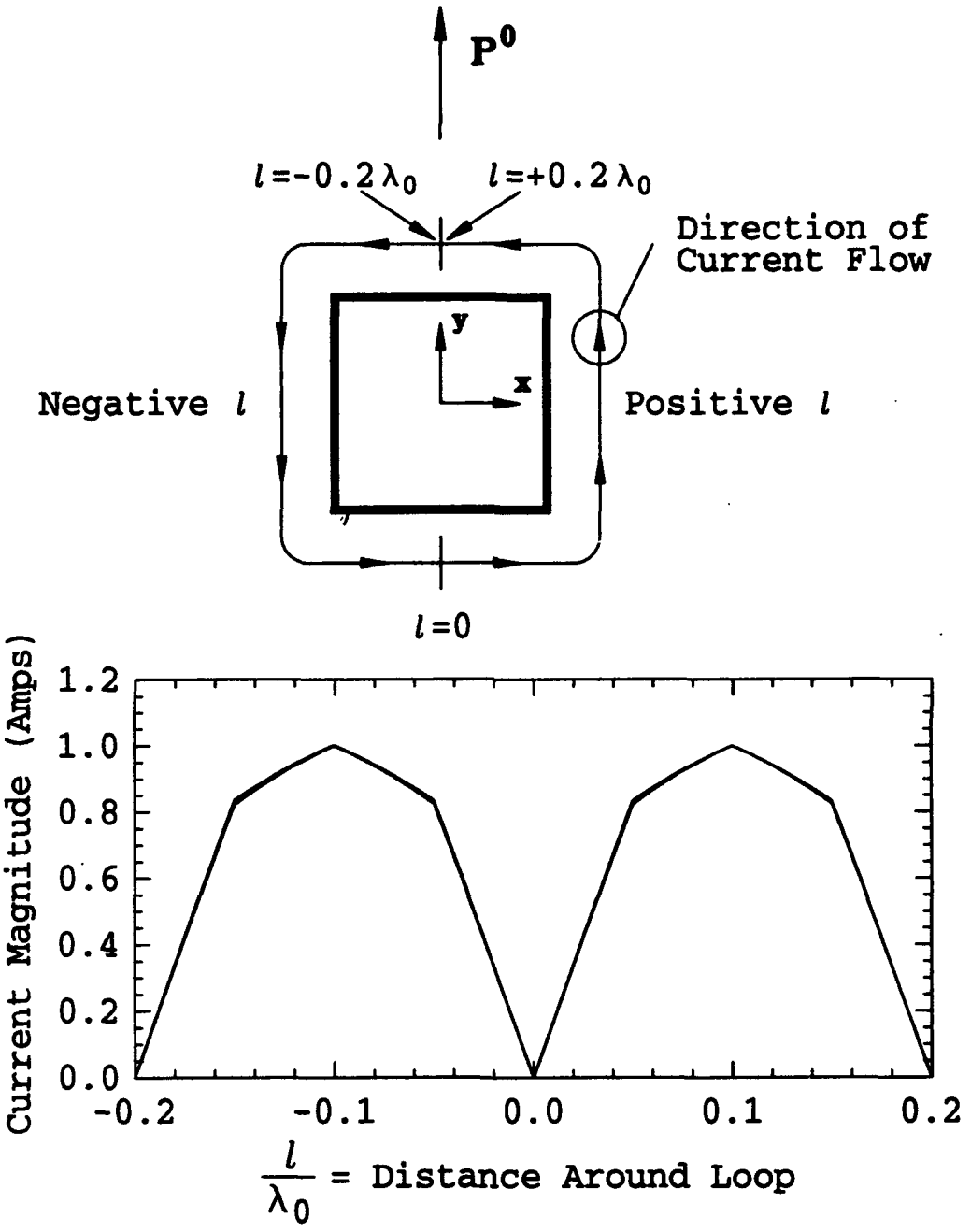

Figure 5.15: The root 2 current mode shape at all θ, for an array of square PEC loops.

between the two methods for ϵ_{yy}^{er} and ϵ_{zz}^{er}, but not for ϵ_{xx}^{er}. Note that ϵ_{yy}^{er} and ϵ_{zz}^{er} are solely determined from the root 2 solution, whose current shape does not change with propagation angle θ. On the other hand, ϵ_{xx}^{er} is determined solely from the root 1 solution, where the current shape does change with propagation angle θ. This discrepancy between the two solutions for ϵ_{xx}^{er} has not been resolved. However, it is interesting to note one possible major difference between real anisotropic media and artificial media. In a real anisotropic medium, the permittivity tensor components will not change with propagation direction. In an artificial medium, the permittivity tensor components may change with propagation direction since the eigenfunction currents may change.

5.7 PEC Wire Crosses

The data in this section illustrate the effect of the horizontal cross member on the dispersion characteristics for an array of PEC wire crosses. As shown in the insert to Figure 5.18, the wire crosses have vertical extent from $y = -L/2$ to $y = +L/2$, and horizontal extent from $x = -L/4$ to $x = +L/4$, with $L = 5$cm. The horizontal cross member is located at $y = +L/4$, and the wire radius is $a = 1$mm. The wire crosses are arranged in a 3D lattice with $d_x = 3.75$cm, $d_y = 7.5$cm and $d_z = 1$cm. This artificial dielectric is uniaxial with non–unity values for both ϵ_{xx}^{er} and ϵ_{yy}^{er}. The direction of propagation is along the z–axis. There are 7 vertical expansion functions, 3 horizontal expansion functions, and 1 horizontal to vertical expansion function, for a total of $N = 11$. Data are also included for the vertical and horizontal members alone (arrays of dipoles), as shown in the inserts for the lower two curves of Figure 5.19.

Figure 5.18 shows the dispersion variation of ϵ_{xx}^{er} and ϵ_{yy}^{er} for frequencies up to 3 GHz, corresponding to $L = 0.5\lambda_0$, for the 3D array of wire crosses. Also, shown are the dispersion variations of ϵ_{xx}^{er} for the array of horizontal dipoles, and ϵ_{yy}^{er} for the array of vertical dipoles. Corresponding to the horizontally polarized ($\hat{\mathbf{x}}$–polarized) wave, note that ϵ_{xx}^{er} is identical for the array of wire crosses and the array of horizontal dipoles. The horizontal eigenfunction current is the same for both cases because the vertical member is symmetrically located with respect to the horizontal member.

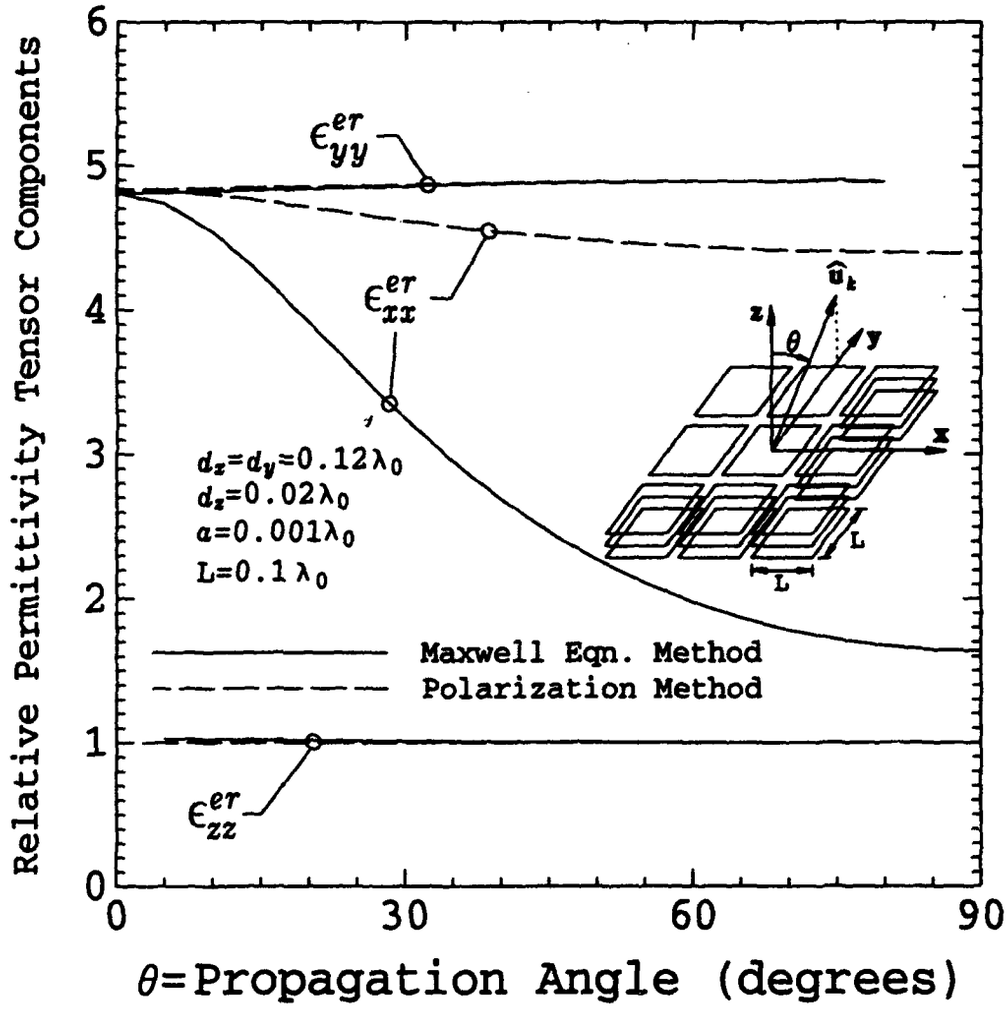

Figure 5.16: The permittivity tensor components versus propagation angle θ, for an array of square PEC loops.

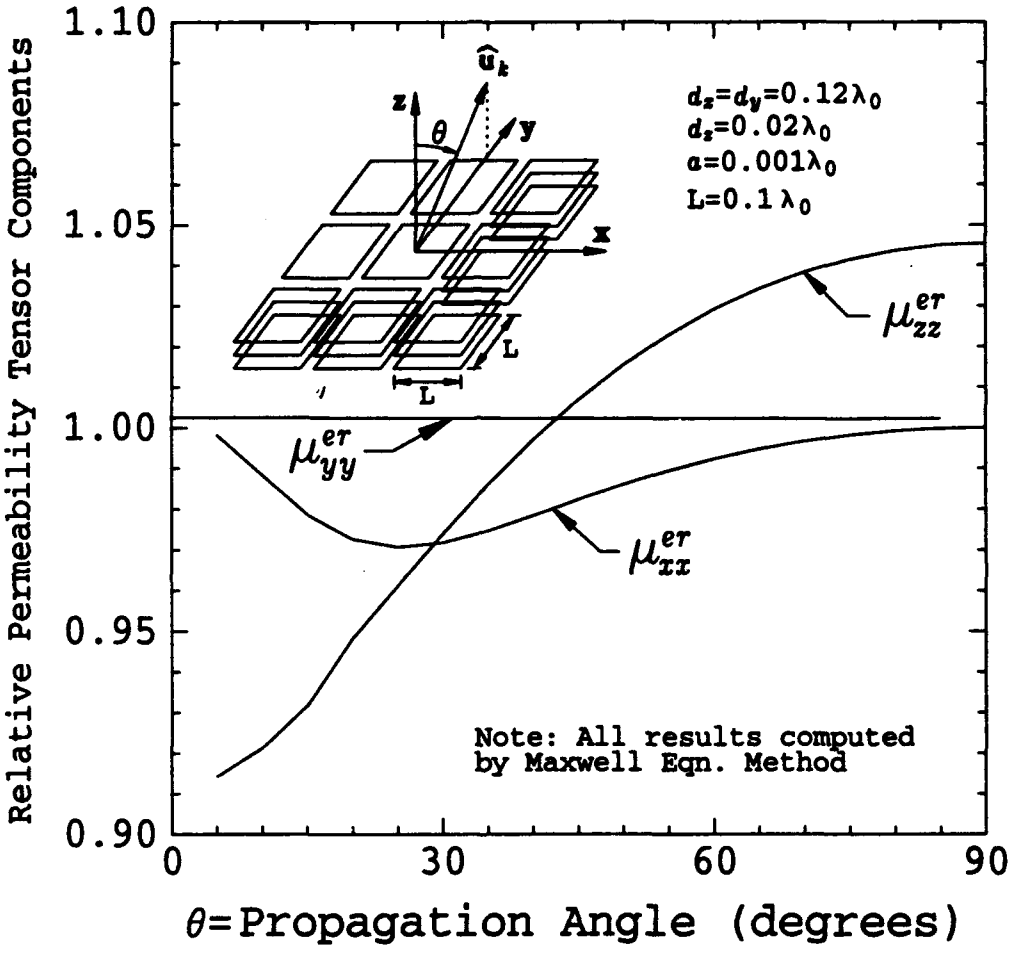

Figure 5.17: The permeability tensor components versus propagation angle θ, for an array of square PEC loops.

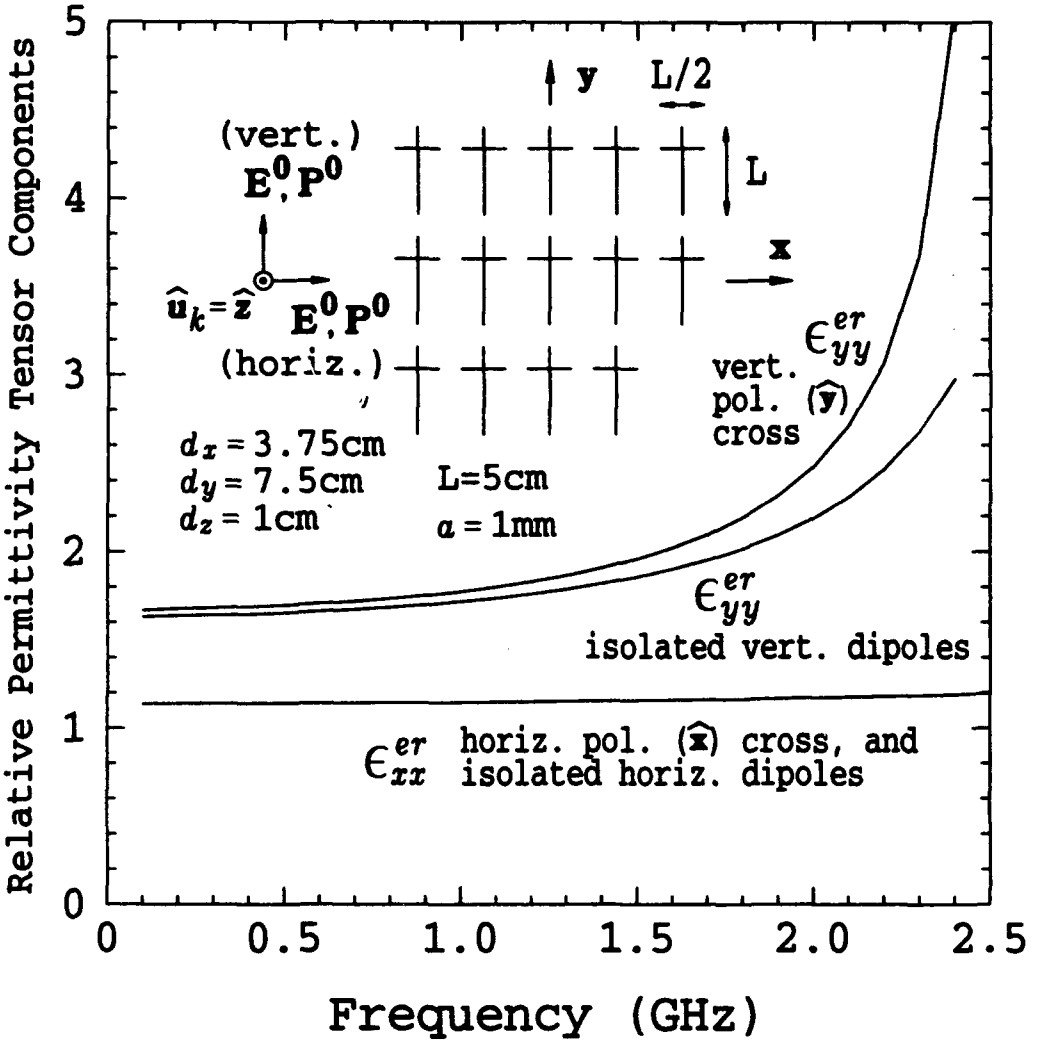

Figure 5.18: Dispersion curve for a 3D array of PEC wire crosses.

However, for vertical polarization, ϵ_{yy}^{cr} is greater for the array of wire crosses than for the array of vertical dipoles. The horizontal member is not symmetrically located with respect to the vertical member, allowing for a greater net y–directed current in the case of the wire crosses. This effect can also be observed in Figure 5.19, which shows the magnitude of the determinant of the impedance matrix $|\mathcal{Z}|$ versus the normalized effective wavenumber for the array of PEC wire crosses, as well as for the arrays of vertical and horizontal dipoles, at the frequency of 2 GHz. Note that the horizontal polarization root does not change from the array of wire crosses to the array of horizontal dipoles, whereas the vertical polarization root occurs at a greater effective wavenumber for the array of wire crosses than for the array of vertical dipoles.

5.8 Graphite–Epoxy 2D Composite Medium

This section presents the analysis of a modern composite material consisting of very thin graphite fibers embedded in an epoxy host binding material. Figure 5.20 shows the geometry of this composite material. The graphite fibers are modeled as material wires of infinite length in the x direction with radius $a = 3.2\mu$m, spaced in a square 2D lattice with $d_y = d_z = 7.5\mu$m. The conductivity of the graphite fibers is 71.4 K(Ω^{-1})/meter and the permittivity of the host epoxy material is $\epsilon_{0r} = 2.5$. As shown in Figure 5.20, the PMM solution uses 3 expansion functions; 1 dipole expansion function and two monopole expansion functions without open–current end charges. (The charges cancel between adjacent x direction cells.) To model this 2D material, the x direction lattice spacing was chosen as $d_x = 75\mu$m.

Figure 5.21 shows the computed dispersion characteristics of the composite material. Note that at low frequencies, the effective conductivity is very close to what results from using a simple *fill factor* formula based on a ratio of the area occupied by the graphite fibers to the area occupied by a 2D lattice cell, i.e., for low frequencies, the effective conductivity is approximately given by

$$\sigma_{xx}^{e} \approx \frac{A_{fiber}}{A_{cell}} \sigma_{fiber} = \frac{\pi a^2}{d_y d_z} \sigma_1. \tag{5.2}$$

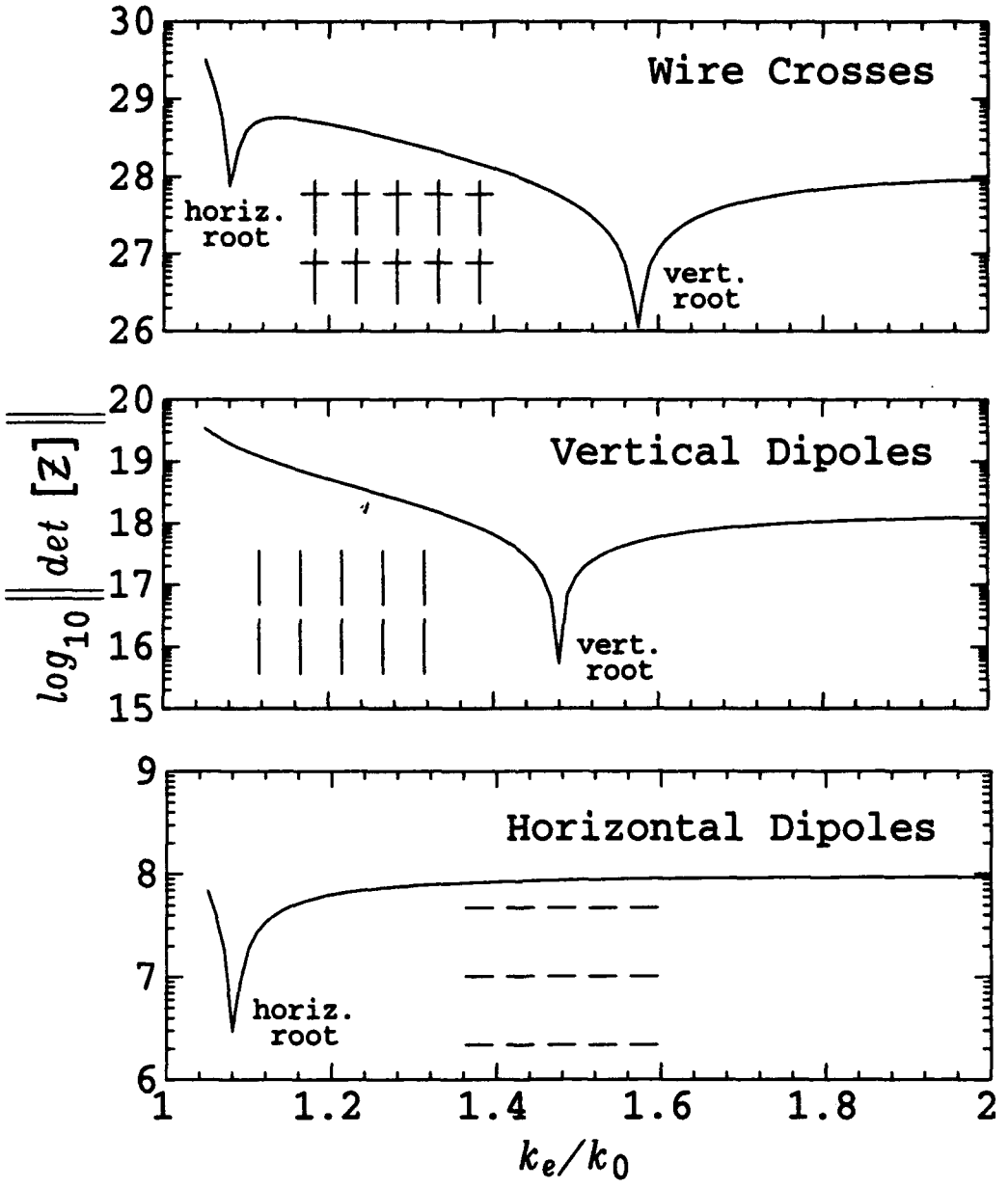

Figure 5.19: Magnitude of $|Z|$ versus normalized effective wavenumber for an array of PEC wire crosses, and for the isolated vertical and horizontal dipole members.

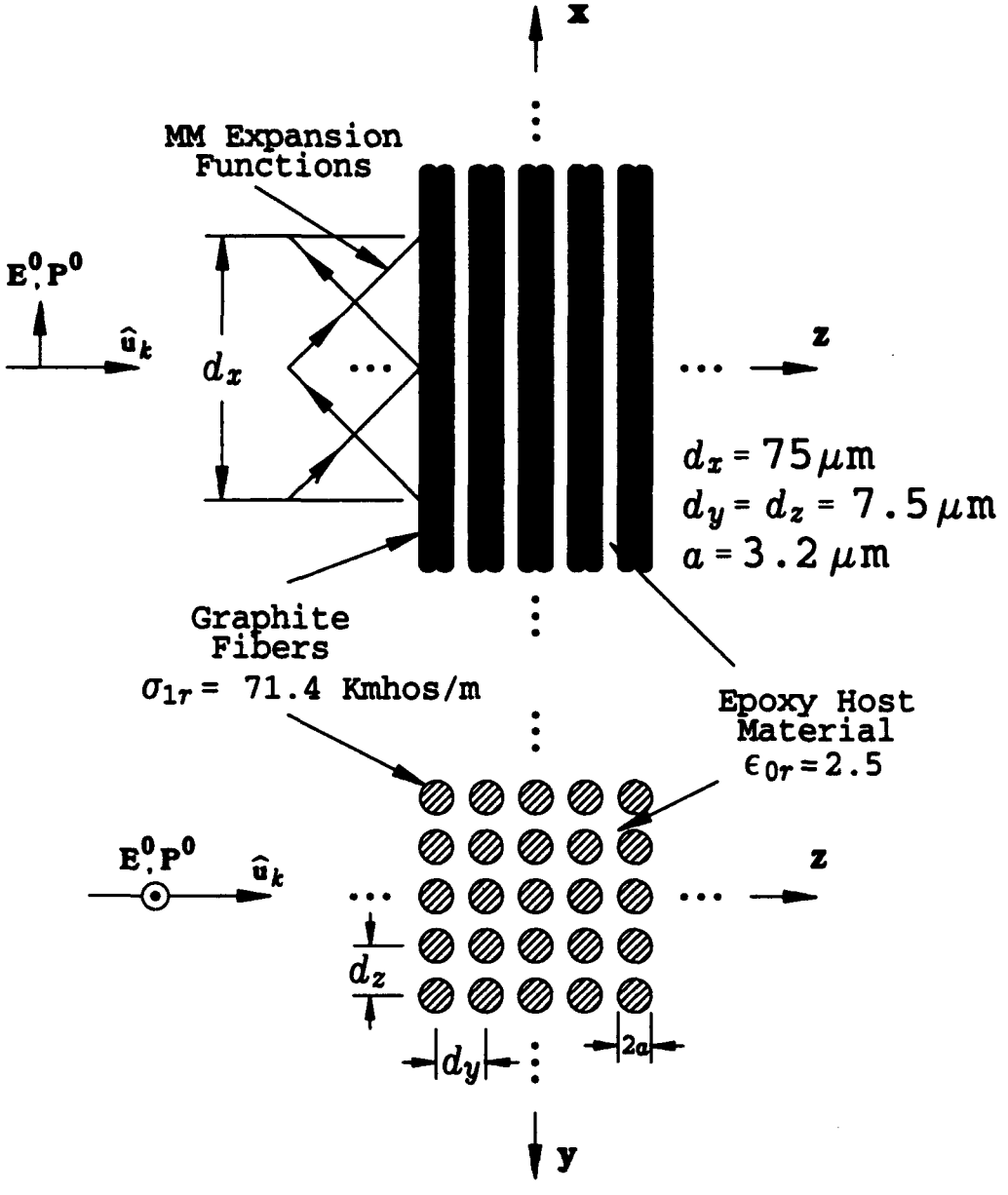

Figure 5.20: The geometry of the graphite–epoxy 2D composite medium.

Applying Equation (5.2) to the graphite–epoxy composite medium results in $\sigma^e_{zz} =$ 40.8 K(Ω^{-1})/meter, agreeing very closely with the results of Figure 5.21.

5.9 Dielectric Weave

The data in this section show the dispersion characteristics of the effective permittivity of a *dielectric weave*, a geometry which has current that flows between adjacent lattice cells. As shown in the insert to Figure 5.22, the geometry consists of stacked or layered square grids of dielectric rods. The dielectric rods have relative permittivity $\epsilon_{1r} = 10$, loss tangent $\tan\delta_1 = 0$ or 1, and radius $a = 2$mm. The grid dimensions are $d_x = d_y = L = 5$cm, and are spaced a distance of $d_z = 6$mm apart. Propagation is along the z–axis, and due to symmetry considerations, the medium is uniaxial with $\epsilon^{er}_{xx} = \epsilon^{er}_{yy}$ and $\epsilon^{er}_{zz} = 1$. All data was computed with $N = 11$ expansion functions, including 4 monopole expansion functions to enforce continuity of current between adjacent lattice cells. Figure 5.22 shows the relative effective permittivity $\epsilon^{er}_{xx} = \epsilon^{er}_{yy}$ and effective loss tangent $\tan\delta^e_{xx} = \tan\delta^e_{yy}$ of the artificial medium for frequency varying up to 3 GHz (corresponding to a grid size of $L = 0.5\lambda_0$) for dielectric rod loss tangent values of $\tan\delta_1 = 0$ and 1. Note that the relative effective permittivity and effective loss tangent are almost constant across the given frequency range. This is due to the fact that the current is essentially constant in the dielectric rods from continuity of current between adjacent lattice cells.

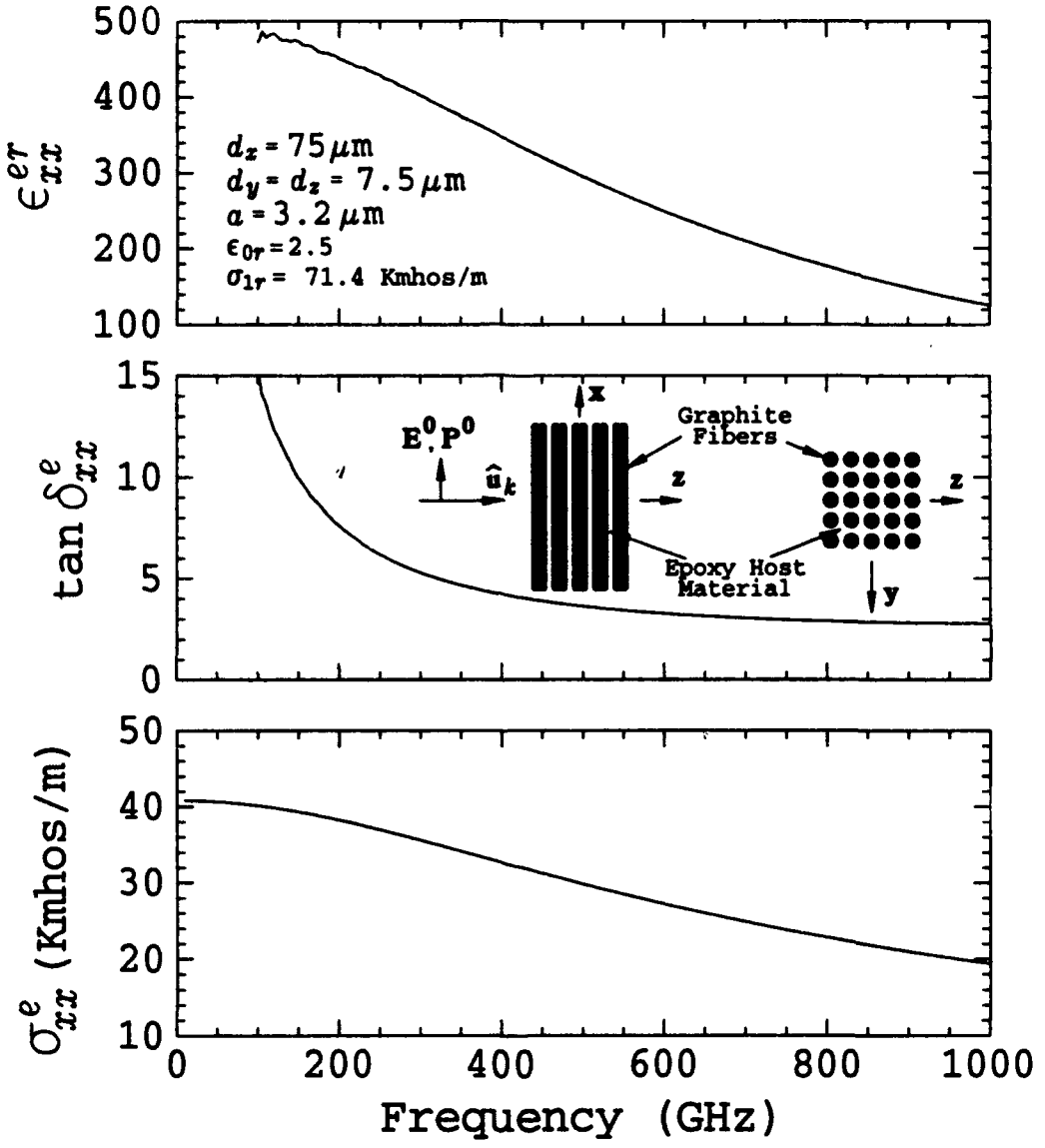

Figure 5.21: Dispersion curves for a composite graphite–epoxy material.

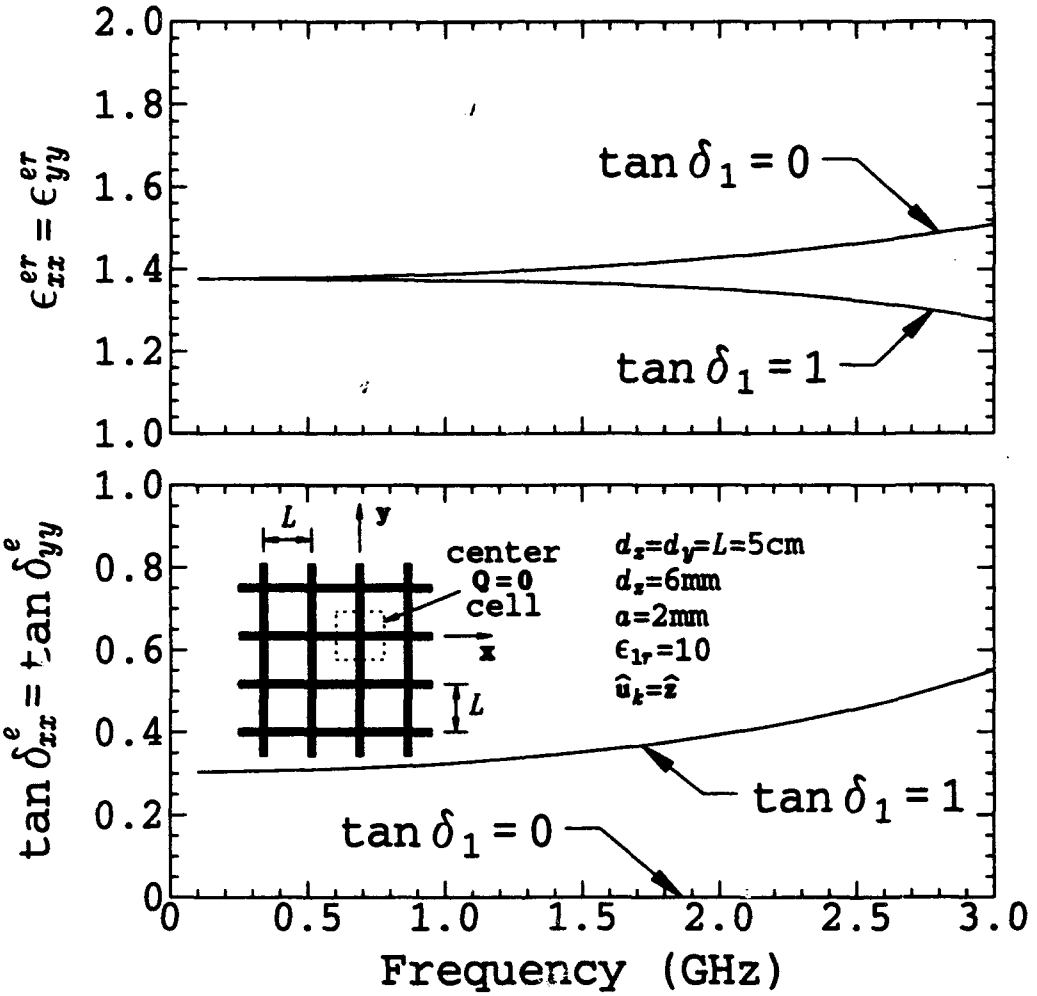

Figure 5.22: Dispersion curves for a *dielectric weave* geometry.

Chapter 6

Computer Program ADWIRS

This chapter presents the usage of the computer program **ADWIRS**. The program **ADWIRS** can analyze an artificial medium composed of a 3D periodic array of identical arbitrarily–shaped thin conductive or dielectric wire objects arranged in a homogeneous host medium. **ADWIRS** computes such parameters as the effective wavenumber k_e corresponding to the root, the shape of the eigenfunction currents in the wire objects, the average electric and magnetic dipole moments per unit cell $(\mathbf{P}^0, \mathbf{M}^0)$, and the average electric and magnetic fields per unit cell $(\mathbf{E}^0, \mathbf{H}^0)$.

Concerning the effective constitutive parameters of the artificial medium, **ADWIRS** only computes the effective permittivity ϵ_e as given in Equation (2.41). Note that this equation for evaluating ϵ_e is only valid when polarization and direction of propagation are along one of the principle axes. The effective permittivity ϵ_e can be written as

$$\epsilon_e = \epsilon_{ii}^{er}\,\epsilon_0 - j\,\frac{\sigma_{ii}^e}{\omega} = \epsilon_{ii}^{er}\,\epsilon_0\,(1 - j\,\tan\delta_{ii}^e) \tag{6.1}$$

where the $ii = xx, yy$ or zz, as determined by the principle axis of polarization. **ADWIRS** computes the three values $\epsilon_{ii}^{er}, \tan\delta_{ii}^e$ and σ_{ii}^e. Often Equation (2.41) does not apply, and/or the polarization method (Section 2.3.2) and Maxwell's equations method (Section 2.3.3) are used to compute the effective constitutive parameters. In this case, $(\mathbf{P}^0, \mathbf{M}^0)$ and $(\mathbf{E}^0, \mathbf{H}^0)$ must be used in another program to be written by the user, which solves for $\bar{\epsilon}_e$ and $\bar{\mu}_e$ using the polarization method or the Maxwell's equations method.

```
C READ 1:
      Read (8,*) ConTol,Derr,Ipv,Iwrz,Iwrc,Iqz,Isum,Nmaxz,Nmaxe
C READ 2:
      Read (8,*) Iswp,Nswpts,Parami,Dparam
C READ 3:
      Read (8,*) FGHz,Eps0r,Tand0,Epser1,Tande1,Epser2,Tande2
C READ 4:
      Read (8,*) Np,Ns,Nload
C READ 5:
      Do N = 1,Np
        Read (8,*) X(N),Y(N),Z(N)
      End Do
C READ 6:
      Do N = 1,Ns
        Read (8,*) Ia(N),Ib(N),Iloss(N),Radwire(N),Epsrwire(N),Loss
                   < FORTRAN statements to process Loss >
      End Do
C READ 7:
      Do N = 1,Nload
        Read (8,*) Iload(N),Zload(N)
      End Do
C READ 8:
      V(3) = 0.0
      Read (8,*) V(1),V(2)
C READ 9:
      Read (8,*) W(1),W(2),W(3)
C READ 10:
      Read (8,*) D(1),D(2),D(3)
C READ 11:
      Read (8,*) Uk(1),Uk(2),Uk(3)
```

Figure 6.1: The ADWIRS program READ statements.

6.1 Inputs To ADWIRS

The inputs to the computer program **ADWIRS** are read via 11 unformatted FORTRAN 77 READ statements from an input file on logical unit 8. These READ statements are shown in Figure 6.1. The values defined in the READ statements are explained in the sections that follow, along with the type of FORTRAN variable the input value must be in the input file (Integer, Real or Complex.)

6.1.1 READ 1: Run Control Parameters

ConTol = Convergence test tolerance for the spectral evaluation of the impedance matrix term contributions Z^s, given in Section 3.3, and for the average eigenfunction fields $(\mathbf{E}^0, \mathbf{H}^0)$, given in Section 4. Note that all spectral self and mutual impedance terms Z^s_{mn} are evaluated to within a tolerance of **ConTol**. Also, the average eigenfunction fields $(\mathbf{E}^0, \mathbf{H}^0)$ have converged to within a tolerance of **ConTol**. If **ConTol** is set greater than 0.1, then **ConTol** is automatically

set equal to 0.1, so there is never worse than 10% accuracy. Typically ConTol = 0.01, corresponding to 1% accuracy. (Real)

Derr = Convergence test tolerance for the evaluation of the root k_e, i.e., the root search for k_e continues until k_e is determined to within a tolerance of Derr. If Derr is set greater than 0.1, then Derr is automatically set equal to 0.1, so there is never worse than 10% accuracy. Typically Derr = 0.01, corresponding to 1% accuracy. (Real)

Ipv = Indicator for a 2D planar lattice or a 3D volume lattice impedance calculation. A 2D planar lattice includes only the $k_w = 0$ planar array of wire objects. A 3D volume lattice includes all the planar arrays indexed by k_w ($k_w = 0, k_w > 0$ and $k_w < 0$). (See Section 3.3.) (Integer)

= 1 implies only compute the 2D planar lattice impedances from the $k_w = 0$ plane of wire objects.

= 2 implies compute the 3D volume lattice impedances from all planar array indexed by k_w ($k_w = 0, k_w > 0$ and $k_w < 0$).

Note that for propagation through a 3D array of wire objects, set Ipv = 2.

Iwrz = Indicator for printing the impedance matrix. (Integer)

= 0 implies do NOT print the impedance matrix.

= 1 implies print the impedance matrix.

Note that setting Iwrz = 1 will result in all the different contributions to the impedance matrix being printed at each value of k_e during the root search iteration procedure.

Iwrc = Indicator for printing the current solution. (Integer)

= 0 implies do NOT print the current solution.

= 1 implies print the current solution.

Note that setting Iwrc = 1 will result in the current solution being printed for all possible choices of current coefficients I_n set to unity (see Section 2.2.2).

Iqz = Indicator for including open–current end charge contributions in the evaluation of the electric fields and impedance matrix terms. (Integer)

= 0 implies do NOT include open–current end charge contributions.

= 1 implies include open–current end charge contributions.

Note that the user can always set Ipv = 1 to include open–current end charge contributions and get theoretically correct results. However, including open–current end charge contributions usually makes the impedance matrix converge much more slowly, and thus it is recommended to set Ipv = 0 when possible. In general, the user can set Ipv = 0 *except when*: 1) open–current end monopole basis functions exist in the material wire scattering object (for example with dielectric wires), *and* 2) these open–current end monopole basis functions do NOT connect with adjoining monopole basis function from an adjacent lattice cell (for example with a dielectric weave).

Isum = Indicator for performing an approximate spectral summation on root search values beyond the initial guess. (Integer)

= 0 implies perform exact spectral summation on all root search values.

= 1 implies perform approximate spectral summation beyond the initial root search guess.

The user can always set Isum = 0 to obtain a solution. However, setting Isum = 1 can save considerable CPU time, without much loss in accuracy, when the initial root guess is close to the final root. Typically, the user can set Ipv = 1 and obtain a solution. Then the user should check that the final root is within a few percent the initial root guess. If not, the user should use the final root of this solution as the initial root guess of a new solution, and then compute the new solution.

Nmaxz = Maximum double summation spectral index limit for the evaluation of the spectral impedance matrix contributions Z^z, i.e., n_u and n_v in Sections 3.3.1 and 3.3.2 shall not exceed Nmaxz, even in the event that all the spectral impedance matrix terms Z^z_{mn} have not converged to ConTol by this point.

Typically, **Nmaxz** = 50, if no open–current end monopole basis functions exist in the scattering object geometry. If open–current end monopole basis functions do exist in the scattering object geometry, then fields converge much more slowly, and hence **Nmaxz** = 100 or greater. (Integer)

Nmaxe = Maximum double summation spectral index limit for the evaluation of the average eigenfunction fields $(\mathbf{E}^0, \mathbf{H}^0)$, i.e., n_u and n_v in Chapter 4 shall not exceed **Nmaxz**, even in the event that all the average eigenfunction fields have not converged to **ConTol** by this point. The average eigenfunction fields are much easier to evaluate, and converge more quickly than the spectral impedance matrix contributions, and hence typically **Nmaxe** = 20. (Integer)

6.1.2 READ 2: Parameter Sweep Inputs

Iswp = Indicator for what type of a parameter sweep to perform. (Integer)

= -1 implies sweep k_e, and evaluate impedance matrix determinant only.

= 0 implies no parameter sweep, i.e., evaluate a single solution.

= 1 implies sweep frequency in GHz.

= 2 implies sweep d_u (in meters) where d_v and d_w remain fixed.

= 3 implies sweep d_v (in meters) where d_u and d_w remain fixed.

= 4 implies sweep d_w (in meters) where d_u and d_v remain fixed.

= 5 implies sweep $d_u = d_v$ (in meters) where d_w remains fixed.

= 6 implies sweep $d_u = d_w$ (in meters) where d_v remains fixed.

= 7 implies sweep $d_v = d_w$ (in meters) where d_u remains fixed.

= 8 implies sweep ϵ_{0r} = relative permittivity of the host medium.

= 9 implies sweep $\tan\delta_0$ = loss tangent of the host medium.

= 10 implies sweep a = radius (in meters) of every wire segment. (All wire segments are set the same.)

= 11 implies sweep ϵ_{1r} = relative permittivity of every wire segment. (All wire segments are set the same.)

= 12 implies sweep $\tan\delta_1$ = loss tangent of every wire segment. (All wire segments are set the same.)

= 13 implies sweep σ_1 = conductivity (in Ω^{-1}/ meter) of every wire segment. (All wire segments are set the same.)

Nswpts = Number of points in the parameter sweep. (Integer)

Parami = Initial value of the parameter being varied. (Real)

Dparam = Increment step size of the parameter being varied. (Real)

Note that if an impedance matrix determinant sweep is performed (**Iswp** = -1) then the variables **Parami** and **Dparam** refer to normalised wavenumber values, i.e., k_e/k_0. Also, the effective wavenumber k_e must be a purely real value.

6.1.3 READ 3: Frequency, Host Media and Initial Root Guess

FGHz = Frequency in GHz. (Real)

Eps0r = ϵ_{0r} = relative permittivity of the host medium. (Real)

Tand0 = $\tan\delta_0$ = loss tangent of the host medium. (Real)

Epser1 = Initial guess at ϵ_{er} = relative effective permittivity, corresponding to the initial value in the parameter sweep (if **Iswp** > 0) or at the single computed value (if **Iswp** = 0.) (Real)

Tande1 = Initial guess at $\tan\delta_e$ = effective loss tangent, corresponding to the initial value in the parameter sweep (if **Iswp** > 0) or at the single computed value (if **Iswp** = 0.) (Real)

Epser2 = Initial guess at ϵ_{er}, corresponding to the second value in the parameter sweep (if **Iswp** > 0.) (Real)

Tande2 = Initial guess at $\tan\delta_e$, corresponding to the second value in the parameter sweep (if **Iswp** > 0.) (Real)

Note that the exact complex permittivity of the host medium is

$$\epsilon_0 = \epsilon_{0r}\,\epsilon(1 - j\tan\delta_0)$$

where ϵ is the free space permittivity. Also, in the program **ADWIRS**, the root k_e is related to the effective permittivity as

$$k_e = \omega\sqrt{\mu_0\epsilon_e} \quad \text{where} \quad \epsilon_e = \epsilon_{er}\,\epsilon(1 - j\tan\delta_e).$$

If a parameter sweep is computed (**Iswp** > 0 in READ 2) then the initial guess at the first two roots are defined through the input variables **Epser1**, **Tande1**, **Epser2** and **Tande2**. The initial guess at subsequent roots is generated automatically within the program **ADWIRS**. If only a single value is computed (**Iswp** = 0 in READ 2) then the initial guess at the root is defined by **Epser1** and **Tande1**. Finally, if an impedance matrix determinant sweep is computed (**Iswp** = −1 in READ 2) then no initial root guess is required, but **Epser1**, **Tande1**, **Epser2** and **Tande2** must be input anyway for consistency.

6.1.4 READ 4: Number of Points, Segments and Lumped Loads

READ statements 4,5 and 6 define the geometry of the wire objects. The method of wire geometry input used by **ADWIRS** is too complicated to explain here, but has been used before and is well documented. The reader is referred to [34], [35] and/or [36] for a detailed description of the wire geometry input method. The input parameters are briefly explained below.

Np = Total number of wire points defining the scattering object. (Integer)

Ns = Total number of wire segments defining the scattering object. (Integer)

Nload = Total number of lumped loads defining the wire object. (Integer)

6.1.5 READ 5: Wire Point Coordinates

X(N) = x–coordinate (in meters) of wire point N, for N = 1,2,...,Np. (Real)

Y(N) = y–coordinate (in meters) of wire point N, for N = 1,2,...,Np. (Real)

Z(N) = z–coordinate (in meters) of wire point N, for N = 1,2,...,Np. (Real)

6.1.6 READ 6: Wire Segments

Ia(N) = Endpoint A of wire segment N, for N = 1,2,...,Ns. (Integer)

Ib(N) = Endpoint B of wire segment N, for N = 1,2,...,Ns. (Integer)

Iloss(N) = Indicator for the material composition of wire segment N,
for N = 1,2,...,Ns. (Integer)
= 1 implies the parameter **Loss** is $\tan\delta_1$ = loss tangent of wire segment N.
= 2 implies the parameter **Loss** is σ_1 = conductivity of wire segment N (in Ω^{-1}/ meter).
= 3 implies wire segment N is PEC, and DO NOT use monopole end-modes on this segment.
= 4 implies wire segment N is PEC, and DO use monopole end-modes on this segment.
Note that for PEC wire segments, the user should only set **Iloss(N)** = 4 when wire segment N physically connects with a corresponding wire segment in an adjacent lattice cell. This enables the monopole end-modes to account for continuity of current across lattice cell boundaries when PEC wire segments are used. For lossy and/or dielectric wire segments (**Iloss(N)** = 1 or 2) monopole end-modes are always enabled.

Radwire(N) = a = radius (in meters) of wire segment N, for N = 1,2,...,Ns. (Real)

Epsrwire(N) = ϵ_{1r} = relative permittivity of wire segment N,
for N = 1,2,...,Ns. (Real)
Note that **Epsrwire(N)** only has meaning for lossy and/or dielectric wire segments, i.e., when **Iloss(N)** = 1 or 2.

Loss = Loss parameter of wire segment N, for N = 1,2,...,Ns. (Real)
= $\tan\delta_1$ of wire segment N if **Iloss(N)** = 1.

$= \sigma_1$ of wire segment N (in Ω^{-1}/ meter) if Iloss(N) = 2.

Note that Loss only has meaning for lossy and/or dielectric wire segments, i.e., when Iloss(N) = 1 or 2.

6.1.7 READ 7: Lumped Loads

Iload(N) = Location of lumped load N, for N = 1,2,...,Nload. (Integer)

Zload(N) = Complex impedance of lumped load N, for N = 1,2,...,Nload. (Complex)

Note that wire "location" L is defined as follows:

- by endpoint A of segment L if: $L \leq Ns$.
- by endpoint B of segment (L − Ns) if: $(Ns + 1) \leq L \leq 2\ Ns$.

6.1.8 READs 8, 9 and 10: Lattice Geometry

V(1) = v_x = x–component of the lattice defining vector $\hat{\mathbf{v}}$. (Real)

V(2) = v_y = y–component of the lattice defining vector $\hat{\mathbf{v}}$. (Real)

W(1) = w_x = x–component of the lattice defining vector $\hat{\mathbf{w}}$. (Real)

W(2) = w_y = y–component of the lattice defining vector $\hat{\mathbf{w}}$. (Real)

W(3) = w_z = z–component of the lattice defining vector $\hat{\mathbf{w}}$. (Real)

D(1) = Lattice spacing (in meters) in the $\hat{\mathbf{u}} = \hat{\mathbf{x}}$ direction. (Real)

D(2) = Lattice spacing (in meters) in the $\hat{\mathbf{v}} = v_x\,\hat{\mathbf{x}} + v_y\,\hat{\mathbf{y}}$ direction. (Real)

D(3) = Lattice spacing (in meters) in the $\hat{\mathbf{w}} = w_x\,\hat{\mathbf{x}} + w_y\,\hat{\mathbf{y}} + w_z\,\hat{\mathbf{z}}$ direction. (Real)

Note that the lattice defining vectors $\hat{\mathbf{v}}$ and $\hat{\mathbf{w}}$ do not need to be normalized to unit vectors in the input file, only the direction needs to be defined. Also if the lattice is perpendicular, then set:

- V(1) = 0,
- V(2) = 1,
- W(1) = 0,
- W(2) = 0,
- W(3) = 1.

6.1.9 READ 11: Direction of Propagation

Uk(1) = x–component of propagation direction $\hat{\mathbf{u}}_k$. (Real)

Uk(2) = y–component of propagation direction $\hat{\mathbf{u}}_k$. (Real)

Uk(3) = z–component of propagation direction $\hat{\mathbf{u}}_k$. (Real)

Note that the propagation direction defining vector $\hat{\mathbf{u}}_k$ does not need to be normalized to a unit vector in the input file, only its direction needs to be defined.

6.2 Output From ADWIRS

6.2.1 The Output File.

The program ADWIRS writes its output file to standard output on logical unit 6. This output file includes such information as:

1. Input data and any errors in the input data.
2. Any errors encountered during the computations.
3. The impedance matrix, if requested.
4. The effective wavenumber k_e, and the constitutive parameters as calculated by the simple formula of Equation (6.1).
5. The eigenfunction currents, dipole moments per unit cell ($\mathbf{P}^0, \mathbf{M}^0$), and the average electric and magnetic fields per unit cell ($\mathbf{E}^0, \mathbf{H}^0$).
6. The CPU times.

6.2.2 The Eigenfunction Solution File.

The program **ADWIRS** writes the eigenfunction solutions to a file on logical unit 9. This is the file to be used when Equation (6.1) is not valid and the polarization method or the Maxwell's equations method is to be implemented by the user. The data can be read by the following FORTRAN 77 READ statements.

```
READ (9,*) NSWPTS,NUMMODES
DO I = 1,NSWPTS
   READ (9,*) PARAM(I),OMEGA(I)
   DO J = 1,NUMMODES
      READ (9,*) KE(I,J,1),KE(I,J,2),KE(I,J,3)
      READ (9,*) EPL(I,J,1),EPL(I,J,2),EPL(I,J,3)
      READ (9,*) HPL(I,J,1),HPL(I,J,2),HPL(I,J,3)
      READ (9,*) PO(I,J,1),PO(I,J,2),PO(I,J,3)
      READ (9,*) MO(I,J,1),MO(I,J,2),MO(I,J,3)
   END DO
END DO
```

The above variables are defined here.

NSWPTS = the number of points in the parameter sweep.

NUMMODES = the number of MM expansion functions on the wire geometry.

PARAM(I) = the value of the parameter that is being swept at sweep point I.

OMEGA(I) = the angular frequency (in radians / second) at sweep point I.

KE(I,J,1),KE(I,J,2),KE(I,J,3) = the x, y, z components of the effective wave-vector at current mode solution J and sweep point I.

EPL(I,J,1),EPL(I,J,2),EPL(I,J,3) = the x, y, z components of $\mathbf{E}^0$ at current mode solution J and sweep point I.

HPL(I,J,1),HPL(I,J,2),HPL(I,J,3) = the x, y, z components of $\mathbf{H}^0$ at current mode solution J and sweep point I.

P0(I,J,1),P0(I,J,2),P0(I,J,3) = the x, y, z components of $\mathbf{P}^0$ at current mode solution J and sweep point I.

M0(I,J,1),M0(I,J,2),M0(I,J,3) = the x, y, z components of $\mathbf{M}^0$ at current mode solution J and sweep point I.

6.2.3 The Parameter Sweep Files

When a parameter sweep is performed (either a standard parameter sweep, or a determinant versus k_e sweep) then data are output to specific files for plotting. In a standard parameter sweep run, tabular listings of ϵ_{ii}^{er}, $\tan\delta_{ii}^{e}$ and σ_{ii}^{e} (as computed by Equation (6.1)) versus the parameter being swept are written to files on logical units 41, 42 and 43, respectively. In a determinant versus k_e sweep, tabular listings of the absolute value, the real part, and the imaginary part of $|\mathcal{Z}|$ versus k_e/k_0 are written to files on logical units 20, 21 and 22, respectively.

Chapter 7

Summary

An artificial medium can be viewed as a macroscopic model of a real medium. Typically, an artificial medium consists of a large number of scattering objects distributed in a host medium. For example, the artificial media treatable by the solution in this dissertation are composed of a 3D periodic array of identical arbitrarily–shaped thin conductive or dielectric wire objects arranged in the homogeneous host medium. In general, the wire objects perturb the eigenfunction solution for a plane wave in the host medium such that a plane wave with a different *effective* wavenumber propagates in the artificial medium. Thus, artificial media are characterized by effective constitutive parameters, and in general are anisotropic media. The effective constitutive parameters can be a function of frequency, the direction of propagation, the size, shape, and orientation of the wire objects, and the constitutive parameters of both the wire objects and the host medium.

The topic of this dissertation is the solution of the plane wave that propagates in the artificial medium, and the determination of the effective constitutive parameters from this solution. The solution is obtained by formulating an integral equation for the plane wave that propagates in the artificial medium. This integral equation is solved by the periodic moment method (PMM), and yields the complex effective wavenumber, the eigenfunction currents in the wire objects, and the eigenfunction fields in the artificial medium.

Three methods are presented for determining the effective constitutive parameters of the artificial medium. The simplest method employs the effective wavenumber and

characteristic impedance of the artificial medium, and applies only to uniaxial media with propagation and polarization along principle axes. The other two methods apply to general anisotropic media at any direction of propagation. One method enforces the constitutive relationship equations and the other method enforces Maxwell's source-free equations in the artificial medium. Both methods use quantities averaged over the volume of a lattice cell.

The solution of this dissertation has several distinguishing characteristics setting it apart from other solutions to artificial media. First of all, no static approximations are made, and the only limitation on frequency is that the wire objects and lattice spacing are not too electrically large. This solution satisfies Maxwell's equations, in an average sense, inside the artificial medium. Secondly, this solution includes the mutual coupling effects of the 3D array. Mutual coupling affects the fields acting on the reference wire object and the current shape in the wire objects. Finally, artificial media composed of complex wire shapes in a periodic arrangement can be analyzed.

One important property of artificial media is that for a given direction of propagation, there are two distinct plane wave modes that can propagate without excitation. Note that for some artificial media, at certain directions of propagation, one or both of the plane wave modes may be the same as a plane wave in the host medium. As the direction of propagation changes, the plane wave modes that propagate also change. This phenomenon is seen by observing that the effective wavenumber for a plane wave mode of propagation is a strong function of the direction of propagation. This is also true for real anisotropic media. Also, in a real anisotropic medium, the permittivity tensor components are independent of the direction of propagation. It appears that the effective permittivity tensor components, and the current shape on the wire objects, *can* be a function of the direction of propagation. Several examples with numerical results verify these observations.

Appendix A

The Source Pattern Factor for PWS Current Functions

This section evaluates the source pattern factor $P^s_{nj\pm}(a,b)$ given by Equation (2.59) for the MM expansion functions. The axial variation along the length of the straight current elements used in the MM expansion functions is the piecewise sinusoidal variation given in Equation (2.18). Inserting this current variation into Equation (2.59), and integrating, it is obtained that

$$P^s_{nj\pm}(a,b) = C^s_{nj\pm}\left[A^s_{nj\pm}(b) - A^s_{nj\pm}(a)\right] \tag{A.1}$$

where

$$C^s_{nj\pm} = \frac{1}{k_0 \sin(k_0 d_{nj})\left[1-(\hat{\mathbf{a}}_{nj}\cdot\hat{\mathbf{r}}_\pm)^2\right]} \tag{A.2}$$

$$A^s_{nj\pm}(x) = e^{jk_0 x(\hat{\mathbf{a}}_{nj}\cdot\hat{\mathbf{r}}_\pm)}\left[j(\hat{\mathbf{a}}_{nj}\cdot\hat{\mathbf{r}}_\pm)\sin(k_0 x) - \cos(k_0 x)\right]. \tag{A.3}$$

In the event that $a = 0$ and $b = d_{nj}$, as in the Region (I) and Region (III) fields, the source pattern factor simplifies to

$$A^s_{nj\pm}(a) = -1$$

and

$$A^s_{nj\pm}(b) = e^{jk_0 d_{nj}(\hat{\mathbf{a}}_{nj}\cdot\hat{\mathbf{r}}_\pm)}\left[j(\hat{\mathbf{a}}_{nj}\cdot\hat{\mathbf{r}}_\pm)\sin(k_0 d_{nj}) - \cos(k_0 d_{nj})\right].$$

A.1 Source Pattern Factor Limits of Integration

Figure A.1 shows the three primary geometrical arrangements for source current segment nj. The geometrical arrangement of current segment nj depends upon the z

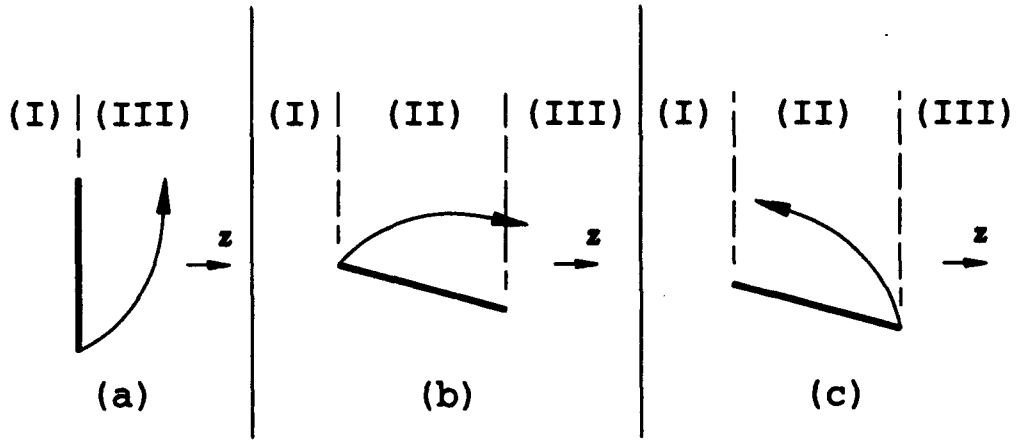

Figure A.1: The three geometrical arrangements for a source current segment.

values of its endpoints, which dictate the expressions for the electric fields and the corresponding limits of integration for the source pattern factor, $P^{s}_{nj\pm}(a,b)$.

The arrangement shown in Figure A.1(a) has current segment nj located in a plane parallel to the xy plane. Region (II) has vanished and there are only Region (I) and Region (III) type fields. Thus, for either case, the limits of integration for $P^{s}_{nj\pm}(a,b)$ are $a = 0$ and $b = d_{nj}$, the length of current segment nj.

Similarly, for the arrangements shown in Figure A.1(b) and (c), if the field point is either in Region (I) or Region (III), then the limits of integration are $a = 0$ and $b = d_{nj}$. However, if the field point is in Region (II), then the electric and magnetic fields consist of both right–going and left–going waves, as given in Equations (2.60) and (2.63). If the vector from the origin to the field point is R, then the point l' on current segment nj of the same z value as R can be determined by solving

$$\hat{\mathbf{z}} \cdot \mathbf{R} = \hat{\mathbf{z}} \cdot [\mathbf{R}_{nj} + l' \, \hat{\mathbf{a}}_{nj}]$$

for l', resulting in

$$l' = -\frac{R_{njz}}{a_{njz}} + \frac{1}{a_{njz}} z = \alpha_{nj} + \beta_{nj} z$$

where R_{njz} and a_{njz} are the z–components of $\mathbf{R}_{nj}$ and $\hat{\mathbf{a}}_{nj}$, respectively. Employing the notation of Equation (2.60), if the current segment geometry is as shown in Figure

A.1(b), then the limits of integration are

$$\begin{aligned} a_{nj+} &= 0 \\ b_{nj+} &= \alpha_{nj} + \beta_{nj} z \\ a_{nj-} &= \alpha_{nj} + \beta_{nj} z \\ b_{nj-} &= d_{nj}. \end{aligned}$$

Similarly, if the current segment is as shown in Figure A.1(c), then the limits of integration are

$$\begin{aligned} a_{nj-} &= 0 \\ b_{nj-} &= \alpha_{nj} + \beta_{nj} z \\ a_{nj+} &= \alpha_{nj} + \beta_{nj} z \\ b_{nj+} &= d_{nj}. \end{aligned}$$

A.2 Open–Current End Charge Terms

The monopole expansion functions have a discontinuous current distribution in which the current rises sinusoidally to unity, and then abruptly falls to zero. This results in a charge distribution existing at the open–current end of monopole expansion functions. These charge terms will cancel when two monopoles are placed together to form a dipole expansion function, of if monopole expansion functions are used to model continuous current across adjacent lattice cells. In both these cases, the physical current is continuous and does not contain charges resulting from an open–current end.

Since the geometry of interest is a 3D periodic array of wire objects, with MM current expansions similar (to within a constant) on each wire object, then there exists a 3D array of charges corresponding to the open–current monopole expansion functions. It is often desirable to isolate and/or remove the contribution to the electric field from this 3D charge array. This can be done by rearranging the product $\mathbf{e}_{nj\pm} P^s_{nj\pm}(a,b)$, which occurs in the expression for the total electric field of Equation (2.69), as

$$\mathbf{e}_{nj\pm} P^s_{nj\pm}(a,b) = C^s_{nj\pm} \left\{ \left[B^s_{nj\pm}(b) + Q^s_{nj\pm}(b) - B^s_{nj\pm}(a) - Q^s_{nj\pm}(a) \right] \hat{\mathbf{r}}_{\pm} -$$

$$- \left[A^e_{nj\pm}(b) - A^e_{nj\pm}(a) \right] \hat{\mathbf{a}}_{nj} \Big\} \tag{A.4}$$

where $C^e_{nj\pm}$ and $A^e_{nj\pm}(x)$ are given by Equations (A.2) and (A.3), respectively, and

$$B^e_{nj\pm}(x) = e^{jk_0 x(\hat{\mathbf{a}}_{nj} \cdot \hat{\mathbf{r}}_\pm)} \left[-(\hat{\mathbf{a}}_{nj} \cdot \hat{\mathbf{r}}_\pm) \cos(k_0 x) + j \sin(k_0 x) \right] \tag{A.5}$$

and

$$Q^e_{nj\pm}(x) = \frac{-j}{k_0 C^e_{nj\pm}} \frac{\sin(k_0 x)}{\sin(k_0 d_{nj})} e^{jk_0 x(\hat{\mathbf{a}}_{nj} \cdot \hat{\mathbf{r}}_\pm)}. \tag{A.6}$$

The term $Q^e_{nj\pm}(x)$ is the contribution to the total electric field from the charge array located at endpoint x. Thus, $Q^e_{nj\pm}(x)$ can be omitted to remove the electric field resulting from the charge array at endpoint x. Note that the charge contribution vanishes when $x = 0$, corresponding to zero charge at the zero current end $x = 0$.

Appendix B

Equivalent Wire Radius

This appendix evaluates a_e, the equivalent wire radius, as defined by Newman [25]. Basically, the mutual impedance between two filament line sources separated by the equivalent wire radius is the same as the mutual impedance between two volumetric cylindrical current sources, corresponding to the thin material wires.

Consider a 2D case where both the expansion and weighting current sources are of radius a and are oriented along the z–axis, with $\hat{\mathbf{s}}$–directed current. The radial variations are defined as

$$J_e = C\, J_0(k_\rho\, \rho) \qquad \text{A / m}^2$$

$$J_w = \frac{1}{\pi a^2} \qquad \text{A / m}^2$$

where the constant C is given in Equation (2.17) so that J_e and J_w have unit current. The mutual impedance between these two current sources was determined by Newman to be

$$Z_{tw} = \left(\frac{\eta_0\, H_1^{(2)}(k_0\, a)}{2a}\right)\left(\frac{k_\rho}{k_\rho^2 - k_0^2}\right)\left(k_\rho\, J_0(k_0\, a) - k_0\, J_1(k_0\, a)\frac{J_0(k_\rho\, a)}{J_1(k_\rho\, a)}\right) - \frac{j\,\eta_0}{\pi\, k_0\, a^2}. \tag{B.1}$$

where η_0 and k_0 are the characteristic impedance and wavenumber of the host medium, and may be complex. Next, Z_{tw} is equated to the mutual impedance between two filament line sources spaced a_e apart from each other, where $|k_0\, a_e| \ll 1$, i.e.,

$$Z_{tw} = \frac{k_0\,\eta_0}{4} H_0^{(2)}(k_0\, a_e) \sim \frac{k_0\,\eta_0}{4}\left[1 - j\frac{2}{\pi}\ln(k_0\, a_e)\right] \tag{B.2}$$

This expression is solved for a_e, resulting in

$$a_e = \text{Real}\left[\frac{\exp[j\,\pi\,(\frac{2Z_{in}}{k_0\,\eta_0} - \frac{1}{2})]}{k_0}\right]. \qquad \text{(B.3)}$$

The real part is taken since a_e represents a real physical displacement.

Appendix C

Stagger of Weighting Monopole

This appendix presents the method of staggering the weighting monopole segment mi. The rules for staggering the weighting monopole segment mi depend upon the relative geometrical arrangement of both monopoles segments mi and nj. The weighting monopole segment mi is staggered by an equivalent wire radius, a_e, in a direction perpendicular to its centerline, and then the integration is performed along this staggered monopole. In decreasing order of priority the rules are:

1. If monopole segments mi and nj are both in the same plane, and that plane is parallel to the xy plane, then monopole segment mi is staggered a distance of a_e in the negative x direction. This stagger is not absolutely necessary if monopole segments mi and nj do not touch or overlap. However, this stagger will increase the convergence of the spectral summation due to the slight distance of exponential decay for the evanescent waves.

2. If monopole segments mi and nj are collinear and touching, and are parallel to the z-axis, then monopole segment mi is staggered a distance of a_e in the negative x direction.

3. If monopole segments mi and nj are collinear and touching, but are neither parallel to the z-axis, nor parallel to the xy plane, then monopole segment mi is staggered a distance of a_e in the unit direction of the vector $\hat{\mathbf{a}}_{mi} \times (\hat{\mathbf{a}}_{nj} \times \hat{\mathbf{z}})$.

4. If monopole segments mi and nj are touching, but are neither collinear, nor both parallel to the xy plane, then monopole segment mi is staggered a distance of a_e in the unit direction of the vector $\hat{\mathbf{a}}_{mi} \times \hat{\mathbf{a}}_{nj}$.

5. For all other arrangements, monopole segment mi is not staggered at all, and the integration is performed along its centerline.

Appendix D

Monopole to Monopole Arrangements

As shown in Figure D.1, there are eight possible geometrical arrangements for the segment mi to segment nj impedance evaluation. These possible arrangements depend upon the z values of the endpoints of the segments, denoted as z_{mia}, z_{mib}, z_{nja} and z_{njb}. Conditions on the endpoints are indicated in Figure D.1, where, in general, endpoint b has a greater or equal z value than endpoint a. The additional criteria for choosing which case the segment to segment impedance evaluation falls under can be summarized as:

Case 1: $z_{mib} \leq z_{nja}$

Case 2: $z_{njb} \leq z_{mia}$

Case 3: $z_{mia} \geq z_{nja}$ and $z_{mib} \leq z_{njb}$

Case 4: $z_{mia} < z_{nja}$ and $z_{nja} < z_{mib} \leq z_{njb}$

Case 5: $z_{mib} > z_{njb}$ and $z_{nja} \leq z_{mia} < z_{njb}$

Case 6: $z_{mia} < z_{nja}$ and $z_{mib} > z_{njb}$

Case 7: $z_{mia} < (z_{nja} = z_{njb}) < z_{mib}$

Case 8: $z_{nja} < (z_{mia} = z_{mib}) < z_{njb}$

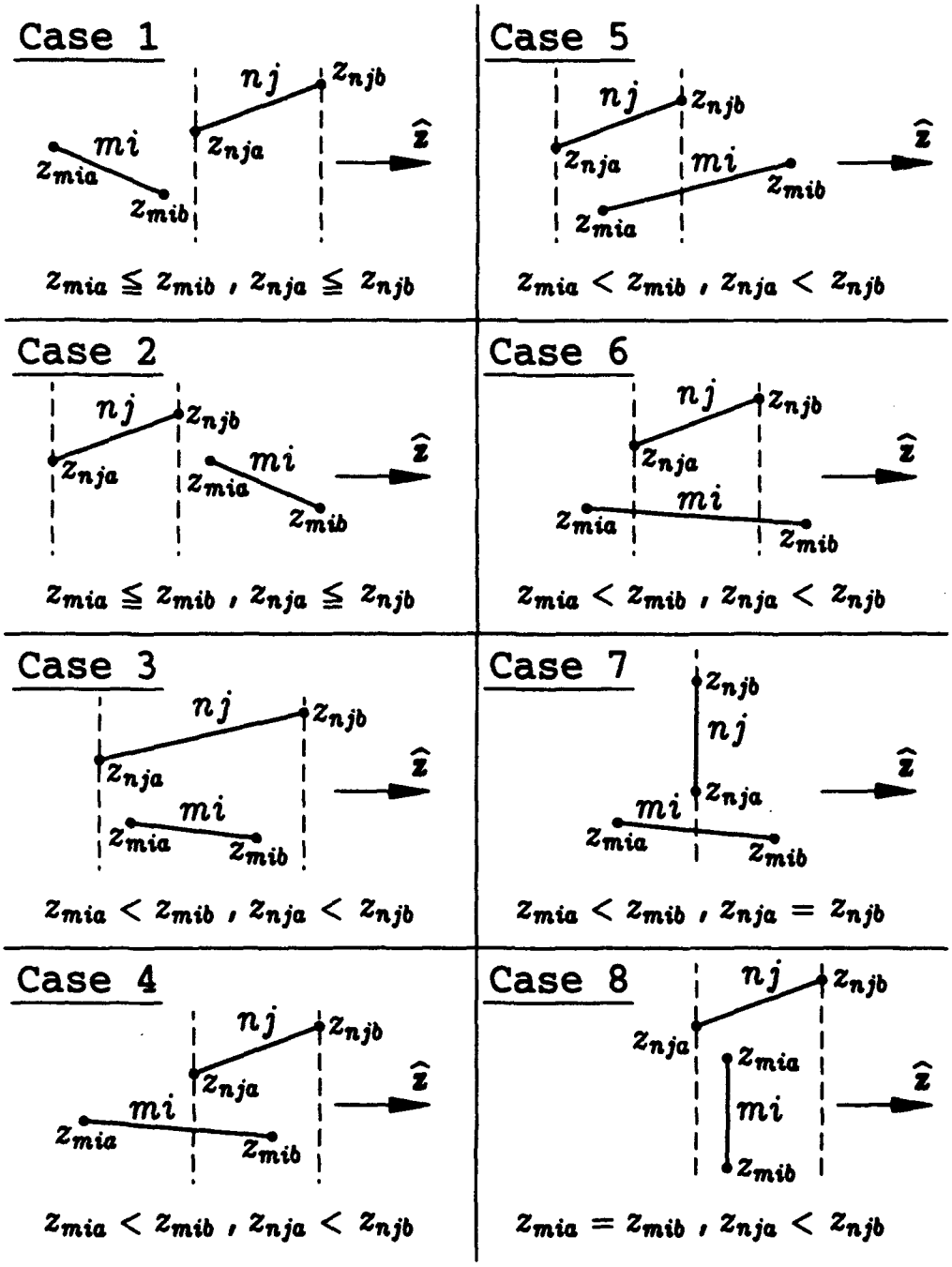

Figure D.1: The eight possible segment *mi* to segment *nj* geometry arrangements.

Appendix E

The Evaluation of $G_{mi,nj\pm}(a,b)$

This appendix evaluates $G_{mi,nj\pm}(a,b)$, defined in Equation (3.32), and used in the evaluation of the impedance matrix element contribution $Z^{z=}_{mi,nj}$. In general, $G_{mi,nj\pm}(a,b)$ requires evaluation when at least a portion of weighting monopole mi is within Region (II) of expansion monopole nj. To repeat Equation (3.32), $G_{mi,nj\pm}(a,b)$ is defined as

$$G_{mi,nj\pm}(a,b) = \int_a^b (\mathbf{e}_{nj\pm} \cdot \hat{\mathbf{a}}_{mi})\, F_{mi}(l)\, e^{-jk_0 l(\hat{\mathbf{a}}_{nj}\cdot\hat{\mathbf{r}}_\pm)}\, P^e_{nj\pm}(a_{nj\pm}, b_{nj\pm})\, dl.$$

The function $P^e_{nj\pm}(a_{nj\pm}, b_{nj\pm})$ is evaluated in Appendix A. Also, the scalar product $(\mathbf{e}_{nj\pm} \cdot \hat{\mathbf{a}}_{mi})$ is incorporated into $G_{mi,nj\pm}(a,b)$ so that the contribution from open-current end charges can be isolated and/or removed. As shown in Figure E.1, the limits of integration $(a_{nj\pm}, b_{nj\pm})$ depend upon the position vector to a point on the weighting monopole mi, and hence they have an l dependence. For a given value of l, the integration limits are determined by solving

$$\hat{\mathbf{z}} \cdot [\mathbf{R}_{nj} + l'\hat{\mathbf{a}}_{nj}] = \hat{\mathbf{z}} \cdot [\mathbf{R}_{mi} + l\hat{\mathbf{a}}_{mi}]$$

for l', resulting in

$$l' = \frac{R_{miz} - R_{njz}}{a_{njz}} + \frac{a_{miz}}{a_{njz}} l = \alpha_{mi} + \beta_{mi} l \qquad \text{(E.1)}$$

where R_{miz}, R_{njz}, a_{miz} and a_{njz} are the z-components of $\mathbf{R}_{mi}$, $\mathbf{R}_{nj}$, $\hat{\mathbf{a}}_{mi}$ and $\hat{\mathbf{a}}_{nj}$, respectively.

As was shown in Figure A.1(b) and A.1(c), there are two possible arrangements of monopole nj such that a Region (II) field exists. This results in two different cases of integration limits for the nj^{th} source pattern factor. For the geometry of

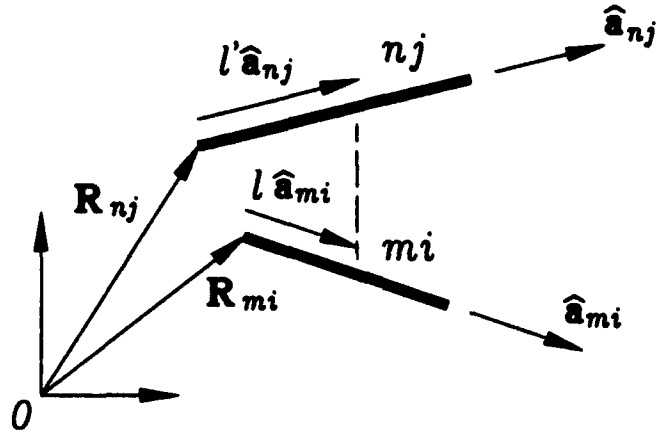

Figure E.1: Vector relationship for the center Q = 0 monopoles mi and nj.

Figure A.1(b), the integration limits are

$$\begin{aligned} a_{nj+} &= 0 \\ b_{nj+} &= \alpha_{mi} + \beta_{mi} l \\ a_{nj-} &= \alpha_{mi} + \beta_{mi} l \\ b_{nj-} &= d_{nj} \end{aligned}$$

and for the geometry shown in Figure A.1(c) the limits of integration are

$$\begin{aligned} a_{nj-} &= 0 \\ b_{nj-} &= \alpha_{mi} + \beta_{mi} l \\ a_{nj+} &= \alpha_{mi} + \beta_{mi} l \\ b_{nj+} &= d_{nj}. \end{aligned}$$

When substituting $P^s_{nj\pm}(a_{nj\pm}, b_{nj\pm})$ into the defining equation for $G_{mi,nj\pm}(a,b)$, the notation of Appendix A will be utilized, as follows:

Figure A.1(b) Geometry		Figure A.1(c) Geometry	
$B^s_{nj+}(b_{nj+})$	$= B^s_{nj+}(\alpha_{mi} + \beta_{mi}\, l)$	$B^s_{nj+}(b_{nj+})$	$= C^s_{1nj+}$
$B^s_{nj+}(a_{nj+})$	$= C^s_{1nj+}$	$B^s_{nj+}(a_{nj+})$	$= B^s_{nj+}(\alpha_{mi} + \beta_{mi}\, l)$
$Q^s_{nj+}(b_{nj+})$	$= Q^s_{nj+}(\alpha_{mi} + \beta_{mi}\, l)$	$Q^s_{nj+}(b_{nj+})$	$= Q^s_{nj+}$
$Q^s_{nj+}(a_{nj+})$	$= Q^s_{nj+} = 0$	$Q^s_{nj+}(a_{nj+})$	$= Q^s_{nj+}(\alpha_{mi} + \beta_{mi}\, l)$
$A^s_{nj+}(b_{nj+})$	$= A^s_{nj+}(\alpha_{mi} + \beta_{mi}\, l)$	$A^s_{nj+}(b_{nj+})$	$= C^s_{2nj+}$
$A^s_{nj+}(a_{nj+})$	$= C^s_{2nj+}$	$A^s_{nj+}(a_{nj+})$	$= A^s_{nj+}(\alpha_{mi} + \beta_{mi}\, l)$
$B^s_{nj-}(b_{nj-})$	$= C^s_{1nj-}$	$B^s_{nj-}(b_{nj-})$	$= B^s_{nj-}(\alpha_{mi} + \beta_{mi}\, l)$
$B^s_{nj-}(a_{nj-})$	$= B^s_{nj-}(\alpha_{mi} + \beta_{mi}\, l)$	$B^s_{nj-}(a_{nj-})$	$= C^s_{1nj-}$
$Q^s_{nj-}(b_{nj-})$	$= Q^s_{nj-}$	$Q^s_{nj-}(b_{nj-})$	$= Q^s_{nj-}(\alpha_{mi} + \beta_{mi}\, l)$
$Q^s_{nj-}(a_{nj-})$	$= Q^s_{nj-}(\alpha_{mi} + \beta_{mi}\, l)$	$Q^s_{nj-}(a_{nj-})$	$= Q^s_{nj-} = 0$
$A^s_{nj-}(b_{nj-})$	$= C^s_{2nj-}$	$A^s_{nj-}(b_{nj-})$	$= A^s_{nj-}(\alpha_{mi} + \beta_{mi}\, l)$
$A^s_{nj-}(a_{nj-})$	$= A^s_{nj-}(\alpha_{mi} + \beta_{mi}\, l)$	$A^s_{nj-}(a_{nj-})$	$= C^s_{2nj-}$.

(E.2)

The terms $C^s_{1nj\pm}$ and $C^s_{2nj\pm}$ are constants with respect to z which result from the endpoints of segment nj. Similarly, the terms $Q^s_{nj\pm}$ are the charge terms associated with the open–current at the endpoints of segment nj, and are independent of l. The charge terms $Q^s_{nj\pm}(\alpha_{mi} + \beta_{mi}\, l)$ must be removed from the integral for the answer to be right, but I'm not sure why this is so. Substituting $F_{mi}(l)$ and the above notation for $P^s_{nj\pm}(a_{nj\pm}, b_{nj\pm})$ into the defining equation for $G_{mi,nj\pm}(a,b)$, and rearranging,

$$G_{mi,nj\pm}(a,b) = S\, C_{nj} \frac{e^{-jk_0[\mathbf{R}_{mi} - \mathbf{R}_{nj}]\cdot \mathbf{r}_\pm}}{r_z} \left[C_{1\pm}\, I_{1\pm} + C_{2\pm}\, I_{2\pm} + C_{3\pm}\, I_{3\pm} \right]$$

where S is given in Equation (4.19), and

$$C_{1\pm} = \frac{jK_\pm}{\sin(k_0 d_{mi})} \left[(\hat{\mathbf{a}}_{mi} \cdot \hat{\mathbf{r}}_\pm) - j(\hat{\mathbf{a}}_{mi} \cdot \hat{\mathbf{a}}_{nj})(\hat{\mathbf{a}}_{nj} \cdot \hat{\mathbf{r}}_\pm) \right]$$

$$C_{2\pm} = \frac{K_\pm}{\sin(k_0 d_{mi})} \left[(\hat{\mathbf{a}}_{mi} \cdot \hat{\mathbf{a}}_{nj}) - j(\hat{\mathbf{a}}_{mi} \cdot \hat{\mathbf{r}}_\pm)(\hat{\mathbf{a}}_{nj} \cdot \hat{\mathbf{r}}_\pm) \right]$$

$$C_{3\pm} = C^s_{2nj\pm} (\hat{\mathbf{a}}_{mi} \cdot \hat{\mathbf{a}}_{nj}) - \left(C^s_{1nj\pm} + Q_{nj\pm} \right) (\hat{\mathbf{a}}_{mi} \cdot \hat{\mathbf{r}}_\pm)$$

$$K_{\pm} = e^{jk_0\alpha_{mi}(\hat{\mathbf{a}}_{nj}\cdot\hat{\mathbf{r}}_{\pm})}$$

$$I_{1\pm} = \int_a^b \exp\left(-jk_0 l[\hat{\mathbf{a}}_{mi} - \beta_{mi}\hat{\mathbf{a}}_{nj}]\cdot\hat{\mathbf{r}}_{\pm}\right)\sin\left[k_0(\alpha_{mi}+\beta_{mi}\,l)\right]\sin(k_0 l)\,dl$$

$$I_{2\pm} = \int_a^b \exp\left(-jk_0 l[\hat{\mathbf{a}}_{mi} - \beta_{mi}\hat{\mathbf{a}}_{nj}]\cdot\hat{\mathbf{r}}_{\pm}\right)\cos\left[k_0(\alpha_{mi}+\beta_{mi}\,l)\right]\sin(k_0 l)\,dl$$

$$I_{3\pm} = \int_a^b \exp\left[-jk_0 l(\hat{\mathbf{a}}_{mi}\cdot\hat{\mathbf{r}}_{\pm})\right]\sin(k_0 l)\,dl.$$

Note that the definition of $C_{3\pm}$ contains the open-current end charge term $Q_{nj\pm}$. This term can be omitted when two monopoles are placed together to form a dipole expansion function. In this case the charges from the two monopoles will cancel exactly.

In the evaluation of $I_{1\pm}$ and $I_{2\pm}$ it is worthwhile to define

$$\omega_{mi\pm} = jk_0[\hat{\mathbf{a}}_{mi} - \beta_{mi}\hat{\mathbf{a}}_{nj}]\cdot\hat{\mathbf{r}}_{\pm}.$$

Also, the trigonometry identities

$$\sin(A+B) = \sin A\cos B + \cos A\sin B$$

$$\cos(A+B) = \cos A\cos B - \sin A\sin B$$

$$2\sin A\sin B = -\cos(A+B) + \cos(A-B)$$

$$2\cos A\sin B = \sin(A+B) - \sin(A-B)$$

are applied to the $I_{1\pm}$ and $I_{2\pm}$ integrands to obtain

$$I_{1\pm} = \frac{1}{2}\sin(k_0\alpha_{mi})\left[I_{\pm}^{s+} - I_{\pm}^{s-}\right] - \frac{1}{2}\cos(k_0\alpha_{mi})\left[I_{\pm}^{c+} - I_{\pm}^{c-}\right]$$

$$I_{2\pm} = \frac{1}{2}\cos(k_0\alpha_{mi})\left[I_{\pm}^{s+} - I_{\pm}^{s-}\right] + \frac{1}{2}\cos(k_0\alpha_{mi})\left[I_{\pm}^{c+} - I_{\pm}^{c-}\right]$$

where

$$I_{\pm}^{s+} = \int_a^b e^{-\omega_{mi\pm}l}\sin[k_0(\beta_{mi}+1)l]\,dl = \frac{1}{(\omega_{mi\pm})^2 + [k_0(\beta_{mi}+1)]^2}\times$$

$$\times\left[e^{-\omega_{mi\pm}b}\left(-\omega_{mi\pm}\sin[k_0(\beta_{mi}+1)b] - k_0(\beta_{mi}+1)\cos[k_0(\beta_{mi}+1)b]\right) -\right.$$

$$\left. - e^{-\omega_{mi\pm}a}\left(-\omega_{mi\pm}\sin[k_0(\beta_{mi}+1)a] - k_0(\beta_{mi}+1)\cos[k_0(\beta_{mi}+1)a]\right)\right]$$

$$I_{\pm}^{s-} = \int_a^b e^{-\omega_{mi\pm}l}\sin[k_0(\beta_{mi}-1)l]\,dl = \frac{1}{(\omega_{mi\pm})^2 + [k_0(\beta_{mi}-1)]^2}\times$$

$$\times \left[e^{-\omega_{mi\pm} b} \left(-\omega_{mi\pm} \sin[k_0(\beta_{mi}-1)b] - k_0(\beta_{mi}-1)\cos[k_0(\beta_{mi}-1)b] \right) - \right.$$

$$\left. - e^{-\omega_{mi\pm} a} \left(-\omega_{mi\pm} \sin[k_0(\beta_{mi}-1)a] - k_0(\beta_{mi}-1)\cos[k_0(\beta_{mi}-1)a] \right) \right]$$

$$I_{\pm}^{c+} = \int_a^b e^{-\omega_{mi\pm} l} \cos[k_0(\beta_{mi}+1)l]\, dl = \frac{1}{(\omega_{mi\pm})^2 + [k_0(\beta_{mi}+1)]^2} \times$$

$$\times \left[e^{-\omega_{mi\pm} b} \left(k_0(\beta_{mi}+1)\sin[k_0(\beta_{mi}+1)b] - \omega_{mi\pm}\cos[k_0(\beta_{mi}+1)b] \right) - \right.$$

$$\left. - e^{-\omega_{mi\pm} a} \left(k_0(\beta_{mi}+1)\sin[k_0(\beta_{mi}+1)a] - \omega_{mi\pm}\cos[k_0(\beta_{mi}+1)a] \right) \right]$$

$$I_{\pm}^{c-} = \int_a^b e^{-\omega_{mi\pm} l} \cos[k_0(\beta_{mi}-1)l]\, dl = \frac{1}{(\omega_{mi\pm})^2 + [k_0(\beta_{mi}-1)]^2} \times$$

$$\times \left[e^{-\omega_{mi\pm} b} \left(k_0(\beta_{mi}-1)\sin[k_0(\beta_{mi}-1)b] - \omega_{mi\pm}\cos[k_0(\beta_{mi}-1)b] \right) - \right.$$

$$\left. - e^{-\omega_{mi\pm} a} \left(k_0(\beta_{mi}-1)\sin[k_0(\beta_{mi}-1)a] - \omega_{mi\pm}\cos[k_0(\beta_{mi}-1)a] \right) \right]$$

The above forms of $I_{1\pm}$ and $I_{2\pm}$ are valid as long as $\beta_{mi} \neq \pm 1$, in which case

$$I_{\pm}^{s+} = I_{\pm}^{s-} = 0 \qquad \text{always}$$

$$I_{\pm}^{c+} = I_{\pm}^{c-} = \begin{cases} b-a & \text{if } \omega_{mi\pm} = 0 \\ \frac{\exp(-\omega_{mi\pm} b) - \exp(-\omega_{mi\pm} a)}{-\omega_{mi\pm}} & \text{otherwise.} \end{cases}$$

The $I_{3\pm}$ integral can be evaluated directly as

$$I_{3\pm} = \int_a^b \exp\left[-jk_0 l(\hat{\mathbf{a}}_{mi}\cdot\hat{\mathbf{r}}_{\pm})\right] \sin(k_0 l)\, dl = \frac{1}{k_0[1-(\hat{\mathbf{a}}_{mi}\cdot\hat{\mathbf{r}}_{\pm})^2]} \times$$

$$\times \left[e^{-jk_0 b(\hat{\mathbf{a}}_{mi}\cdot\hat{\mathbf{r}}_{\pm})} \left(-j(\hat{\mathbf{a}}_{mi}\cdot\hat{\mathbf{r}}_{\pm})\sin(k_0 b) - \cos(k_0 b) \right) - \right.$$

$$\left. - e^{-jk_0 a(\hat{\mathbf{a}}_{mi}\cdot\hat{\mathbf{r}}_{\pm})} \left(-j(\hat{\mathbf{a}}_{mi}\cdot\hat{\mathbf{r}}_{\pm})\sin(k_0 a) - \cos(k_0 a) \right) - \right].$$

Appendix F

Integration Limits for Evaluating $Z^{z=}_{mi,nj}$

This appendix defines the limits of integration over the expansion monopole nj and weighting monopole mi, as needed in the evaluation of the impedance term $Z^{z=}_{mi,nj}$. In general, this includes the integration limits for the following terms:

$$P^{s}_{nj-}(a_{nj-}, b_{nj-})\, P^{r}_{mi\pm}(a_{mi1}, b_{mi1}),$$
$$P^{s}_{nj+}(a_{nj+}, b_{nj+})\, P^{r}_{mi\pm}(a_{mi3}, b_{mi3}) \quad \text{and}$$
$$G_{mi,nj\pm}(a_{mi2}, b_{mi2}).$$

Recall from Figure D.1 that there are eight possible geometrical arrangements for the monopole mi to monopole nj mutual impedance contribution $Z^{z=}_{mi,nj}$. Furthermore, as shown in Figure A.1, there are three primary arrangements for each of monopoles mi and nj. Each case is analyzed in greater detail below.

<u>Case 1:</u>

As shown in Figure D.1 for a Case 1 geometry, monopole mi is entirely in Region (I) of monopole nj. The integration limits are

$$\text{Integration limits:} \quad \begin{cases} a_{mi1} = 0, & b_{mi1} = d_{mi} \\ a_{nj-} = 0, & b_{nj-} = d_{nj} \end{cases}$$

and then $P^{s}_{nj-}(a_{nj-}, b_{nj-})\, P^{r}_{mi-}(a_{mi1}, b_{mi1})$ is evaluated as required in Equation (3.26).

Case 2:

As shown in Figure D.1 for a Case 2 geometry, monopole mi is entirely in Region (III) of monopole nj. The integration limits are

$$\text{Integration limits:} \quad \begin{cases} a_{mi3} = 0, & b_{mi3} = d_{mi} \\ a_{nj+} = 0, & b_{nj+} = d_{nj} \end{cases}$$

and then $P^{e}_{nj+}(a_{nj+}, b_{nj+})\, P^{r}_{mi+}(a_{mi1}, b_{mi1})$ is evaluated as required in Equation (3.27).

Case 3:

As shown in Figure D.1 for a Case 3 geometry, monopole mi is entirely in Region (II) of monopole nj. The integration limits are

$$\text{Integration limits:} \quad \begin{cases} a_{mi2} = 0, & b_{mi2} = d_{mi} \end{cases}$$

and then $G_{mi,nj\pm}(a_{mi2}, b_{mi2})$ is evaluated as required in Equation (3.31).

Case 4:

As shown in Figure D.1 for a Case 4 geometry, monopole mi is within both Region (I) and Region (II) of monopole nj. Figure F.1 shows the four different possible ways that the Case 4 geometrical arrangement can occur. For the integration limits that follow, it is necessary to define the following terms:

$$\begin{aligned} A^{lim}_{mi} &= \frac{R_{njz} - R_{miz}}{a_{miz}} \\ B^{lim}_{mi} &= \frac{R_{njz} - R_{miz}}{a_{miz}} + \frac{a_{njz}}{a_{miz}} d_{nj}. \end{aligned} \tag{F.1}$$

The integration limits for the evaluation of $P^{e}_{nj-}(a_{nj-}, b_{nj-})$, $P^{r}_{mi-}(a_{mi1}, b_{mi1})$ and $G_{mi,nj\pm}(a_{mi2}, b_{mi2})$, as required by Equation (3.33), are given in Table F.1.

Case 5:

As shown in Figure D.1 for a Case 5 geometry, monopole mi is within both Region (III) and Region (II) of monopole nj. Figure F.2 shows the four different possible ways that the Case 5 geometrical arrangement can occur. The integration limits for the evaluation of $P^{e}_{nj+}(a_{nj+}, b_{nj+})$, $P^{r}_{mi+}(a_{mi3}, b_{mi3})$ and $G_{mi,nj\pm}(a_{mi2}, b_{mi2})$, as required by Equation (3.33), are given in Table F.2.

Case 6:

As shown in Figure D.1 for a Case 6 geometry, monopole mi is within all Regions (I),(II) and (III) of monopole nj. Figure F.3 shows the four different possible ways that the Case 6 geometrical arrangement can occur. The integration limits for the evaluation of $P^s_{nj-}(a_{nj-}, b_{nj-})$, $P^r_{mi-}(a_{mi1}, b_{mi1})$, $P^s_{nj+}(a_{nj+}, b_{nj+})$, $P^r_{mi+}(a_{mi3}, b_{mi3})$ and $G_{mi,nj\pm}(a_{mi2}, b_{mi2})$, as required by Equation (3.35), are given in Table F.3.

Case 7:

As shown in Figure D.1 for a Case 7 geometry, Region (II) of monopole nj has vanished, and monopole mi is within Region (I) and Region (III) of monopole nj. Figure F.4 shows the two different possible ways that the Case 7 geometrical arrangement can occur. The integration limits for the evaluation of $P^s_{nj-}(a_{nj-}, b_{nj-})$, $P^r_{mi-}(a_{mi1}, b_{mi1})$, $P^s_{nj+}(a_{nj+}, b_{nj+})$ and $P^r_{mi+}(a_{mi3}, b_{mi3})$, as required by Equation (3.36), are given in Table F.4.

Case 8:

As shown in Figure D.1 for a Case 8 geometry, monopole mi is entirely within Region (II) of monopole nj. However, monopole mi has no extent in the z direction, and $G_{mi,nj\pm}(a_{mi2}, b_{mi2})$ decouples, as given in Equation (3.37). Figure F.5 shows the two different possible ways that the Case 8 geometrical arrangement can occur. The following term is required for presenting the integration limits:

$$d_{nj0} = \frac{R_{miz} - R_{njz}}{a_{njz}}.$$

The integration limits for the evaluation of $P^s_{nj\pm}(a_{nj\pm}, b_{nj\pm})$ and $P^r_{mi\pm}(a_{mi2}, b_{mi2})$, as required by Equation (3.36), are given in Table F.5.

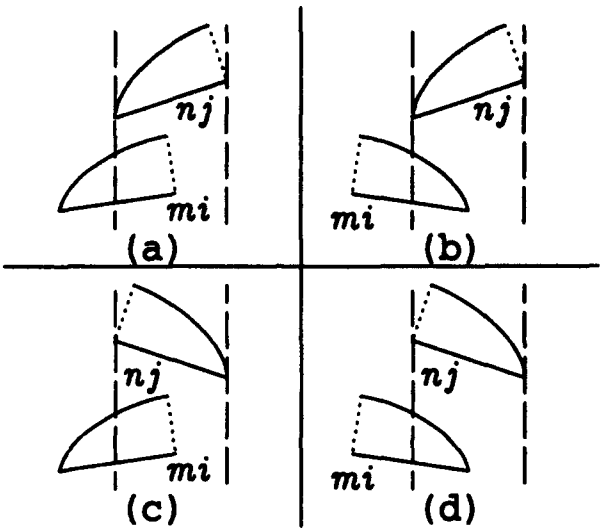

Figure F.1: The four different Case 4 impedance possibilities.

Table F.1: Integration limits for a Case 4 impedance.

	Figure F.1(a)	Figure F.1(b)	Figure F.1(c)	Figure F.1(d)
a_{nj-}	0	0	0	0
b_{nj-}	d_{nj}	d_{nj}	d_{nj}	d_{nj}
a_{mi1}	0	A_{mi}^{lim}	0	B_{mi}^{lim}
b_{mi1}	A_{mi}^{lim}	d_{mi}	B_{mi}^{lim}	d_{mi}
a_{mi2}	A_{mi}^{lim}	0	B_{mi}^{lim}	0
b_{mi2}	d_{mi}	A_{mi}^{lim}	d_{mi}	B_{mi}^{lim}

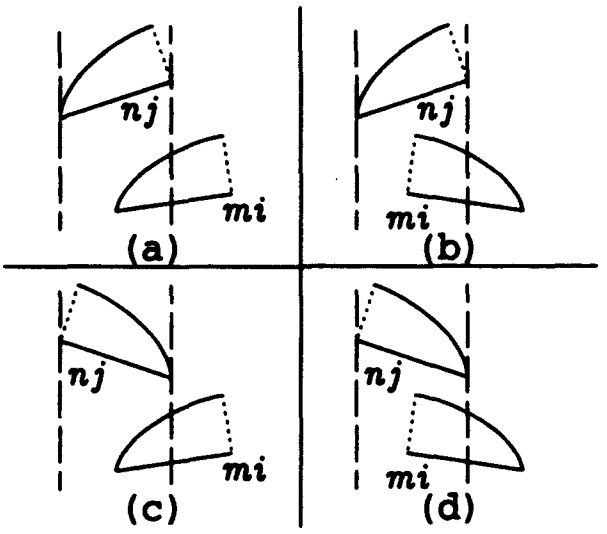

Figure F.2: The four different Case 5 impedance possibilities.

Table F.2: Integration limits for a Case 5 impedance.

	Figure F.2(a)	Figure F.2(b)	Figure F.2(c)	Figure F.2(d)
a_{nj+}	0	0	0	0
b_{nj+}	d_{nj}	d_{nj}	d_{nj}	d_{nj}
a_{mi2}	0	B_{mi}^{lim}	0	A_{mi}^{lim}
b_{mi2}	B_{mi}^{lim}	d_{mi}	A_{mi}^{lim}	d_{mi}
a_{mi3}	B_{mi}^{lim}	0	A_{mi}^{lim}	0
b_{mi3}	d_{mi}	B_{mi}^{lim}	d_{mi}	A_{mi}^{lim}

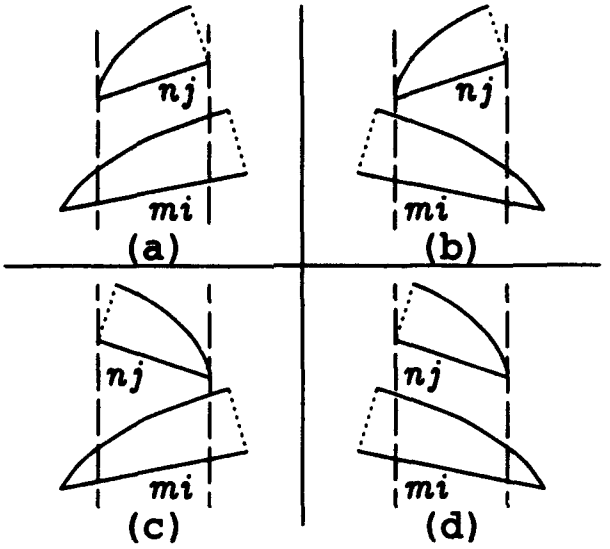

Figure F.3: The four different Case 6 impedance possibilities.

Table F.3: Integration limits for a Case 6 impedance.

	Figure F.3(a)	Figure F.3(b)	Figure F.3(c)	Figure F.3(d)
$a_{nj\pm}$	0	0	0	0
$b_{nj\pm}$	d_{nj}	d_{nj}	d_{nj}	d_{nj}
a_{mi1}	0	A_{mi}^{lim}	0	B_{mi}^{lim}
b_{mi1}	A_{mi}^{lim}	d_{mi}	B_{mi}^{lim}	d_{mi}
a_{mi2}	A_{mi}^{lim}	B_{mi}^{lim}	B_{mi}^{lim}	A_{mi}^{lim}
b_{mi2}	B_{mi}^{lim}	A_{mi}^{lim}	A_{mi}^{lim}	B_{mi}^{lim}
a_{mi3}	B_{mi}^{lim}	0	A_{mi}^{lim}	0
b_{mi3}	d_{mi}	B_{mi}^{lim}	d_{mi}	A_{mi}^{lim}

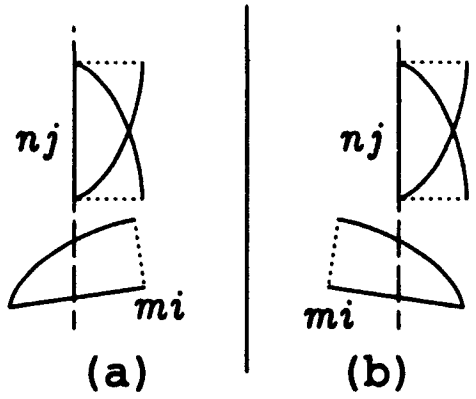

Figure F.4: The two different Case 7 impedance possibilities.

Table F.4: Integration limits for a Case 7 impedance.

	Figure F.4(a)	Figure F.4(b)
$a_{nj\pm}$	0	0
$b_{nj\pm}$	d_{nj}	d_{nj}
a_{mi1}	0	A_{mi}^{lim}
b_{mi1}	A_{mi}^{lim}	d_{mi}
a_{mi3}	A_{mi}^{lim}	0
b_{mi3}	d_{mi}	A_{mi}^{lim}

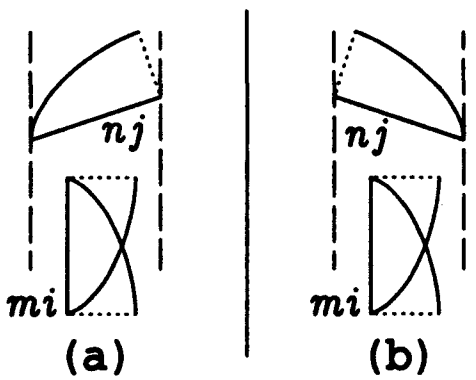

Figure F.5: The two different Case 8 impedance possibilities.

Table F.5: Integration limits for a Case 8 impedance.

	Figure F.5(a)	Figure F.5(b)
a_{nj-}	d_{nj0}	0
b_{nj-}	d_{nj}	d_{nj0}
a_{nj+}	0	d_{nj0}
b_{nj+}	d_{nj0}	d_{nj}
a_{mi2}	0	0
b_{mi2}	d_{mi}	d_{mi}

Appendix G

The Ellipsoid of Wave Normals

Consider a homogeneous real anisotropic non–magnetic medium arranged such that the coordinate axes are aligned with the three axial directions (called the *principle dielectric axes*) x, y and z. It is shown by Sommerfeld [23, Sec. 4.24] that any real anisotropic medium can be arranged in such a way. This is a uniaxial medium with permittivity tensor given by

$$\bar{\epsilon}_c = \begin{bmatrix} \epsilon_x & 0 & 0 \\ 0 & \epsilon_y & 0 \\ 0 & 0 & \epsilon_z \end{bmatrix}$$

where ϵ_x, ϵ_y and ϵ_z are called the *principle dielectric constants*. The fields $\mathbf{D}$ and $\mathbf{E}$ are related as

$$D_x = \epsilon_x E_x$$

$$D_y = \epsilon_y E_y$$

$$D_z = \epsilon_z E_z$$

The electric energy density is given by

$$w_e = \frac{1}{8\pi} \mathbf{E} \cdot \mathbf{D} = \frac{1}{8\pi} \left(\frac{D_x^2}{\epsilon_x} + \frac{D_y^2}{\epsilon_y} + \frac{D_z^2}{\epsilon_z} \right).$$

Letting $C = 8\pi w_e$, and writing x, y and z in place of $D_x/\sqrt{C}, D_y/\sqrt{C}$ and $D_z/\sqrt{C}$, and considering these as Cartesian coordinates in space, we get the equation of the *ellipsoid of wave normals*

$$\frac{x^2}{\epsilon_x} + \frac{y^2}{\epsilon_y} + \frac{z^2}{\epsilon_z} = 1. \qquad \text{(G.1)}$$

This ellipsoid can be used to predict the two phase velocities, and hence the two wavenumbers of a plane wave propagating in any direction $\hat{\mathbf{u}}_k$, as follows [24, Sec. 14.2.3]. Draw a plane normal to $\hat{\mathbf{u}}_k$ through the origin. The intersection of this plane with the ellipsoid is an ellipse. The major and minor semi-axes of this ellipse are proportional to $1/v_p$, the reciprocal of the phase velocities. Once the two phase velocities have been determined, the corresponding wavenumbers can be found as

$$k = \frac{\omega}{v_p}$$

where ω is the angular frequency in radians per second.

These results can be applied to artificial media in the following manner. Consider an anisotropic uniaxial artificial dielectric. Assume that the effective wavenumber corresponding to one of the two roots, has been determined for propagation along two of the principle dielectric axes. For example, for one of the two roots, assume $k_e = k_x$ for propagation along the x-axis and $k_e = k_y$ for propagation along the y-axis. We wish to compute the effective wavenumber for propagation in any direction in the xy-plane, i.e., $\hat{\mathbf{u}}_k = \hat{\mathbf{x}}\, u_{kx} + \hat{\mathbf{y}}\, u_{ky}$.

See Figure G.1 for the geometrical representation of the solution. The ellipse equation can be written as

$$\frac{x^2}{k_x^2} + \frac{y^2}{k_y^2} = 1. \tag{G.2}$$

Now, substituting $x = a$ and $y = b = a \tan\alpha = a(u_{ky}/u_{kx})$ into Equation (G.2), and solving, it is obtained that for the given direction of propagation at angle α,

$$k_e = \sqrt{a^2 + b^2} = k_x\, k_y \frac{\sqrt{1 + \tan^2\alpha}}{\sqrt{k_y^2 + k_x^2 \tan^2\alpha}}. \tag{G.3}$$

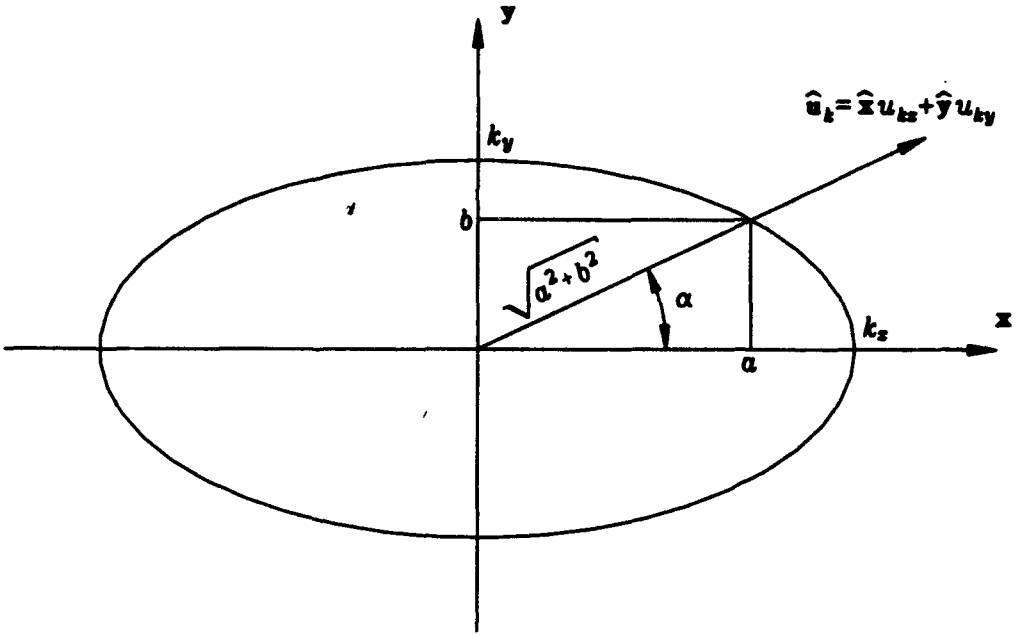

Figure G.1: The ellipse construction to solve for the effective wavenumber.

Appendix H

Material Spheres

This appendix presents an integral equation and periodic method of moments (PMM) [2, 3, 4] solution to the problem of determining the effective permittivity of an artificial dielectric composed of a 3D periodic array of small identical dielectric material spheres. Note that the material presented in this appendix is mostly self–contained, i.e., there are few references to material in this dissertation outside this appendix. However, much of the theory is similar to that presented in Chapter 2, and thus there is some repetition. The major differences are those necessary to account for the scattering objects being material spheres rather than wire objects. Also, field computations are made by employing approximations in the space domain, as opposed to the spectral domain methods presented in Sections 2.4 and 2.5.

As with the method presented in Chapter 2, this method is based upon finding the complex wavenumber for a plane wave propagating in the artificial dielectric, from which the complex effective permittivity can be deduced. As before, mutual coupling between the small spheres is included in the PMM formulation.

The scattering objects are identical dielectric spheres arranged in a 3D periodic lattice. When a plane wave propagates through an artificial dielectric, currents are induced on or in the scattering objects. These currents can be viewed as macroscopic current moments, analogous to the microscopic dipole moments induced in the molecules of an actual dielectric [1]. The effect of the macroscopic current moments is to produce a net current moment per unit volume, and thus the artificial dielectric has some complex effective permittivity.

In the present case, the complex effective permittivity of the artificial dielectric is a function of the electrical size and spacing of the dielectric spheres, and the material parameters of both the host medium and the spheres. By properly choosing these values, it may be possible to design an artificial dielectric medium of desired permittivity and loss tangent. A recent application of artificial dielectrics is in the microwave welding of polymers [11]. In this case, a lossy dielectric of desired conductivity is produced by the proper mixture of HCl doped polyaniline particles in a polyethylene host.

Section H.1 of this paper presents the integral equation of the artificial dielectric medium. This integral equation is solved by the periodic moment method using expansion functions suitable for small dielectric spheres. Details concerning the evaluating of the impedance matrix are given in Section H.2. Numerical results are presented in Section H.3, illustrating the complex effective permittivity for different artificial dielectric compositions.

H.1 Theory

H.1.1 Derivation of the Integral Equation

This section will present the integral equation and PMM solution for a plane wave propagating through an artificial dielectric medium composed of small dielectric spheres arranged on a periodic lattice. This solution will yield the complex wavenumber of the plane wave, and in turn, the complex effective permittivity of the artificial dielectric. Throughout this appendix, all fields and currents are assumed to be time harmonic with the $e^{j\omega t}$ time dependence suppressed.

As shown in Figure H.1, the geometry of the artificial dielectric consists of a 3D triple periodic array of identical dielectric spheres located in a homogeneous and isotropic host medium. The spheres have radius a, and are homogeneous with permeability and permittivity denoted by (μ_0, ϵ_1), and wavenumber $k_1 = \omega\sqrt{\mu_0\epsilon_1}$. The homogeneous host medium has permeability and permittivity denoted by (μ_0, ϵ_0), wavelength λ_0, and wavenumber $k_0 = \omega\sqrt{\mu_0\epsilon_0}$. Note that this host medium is not

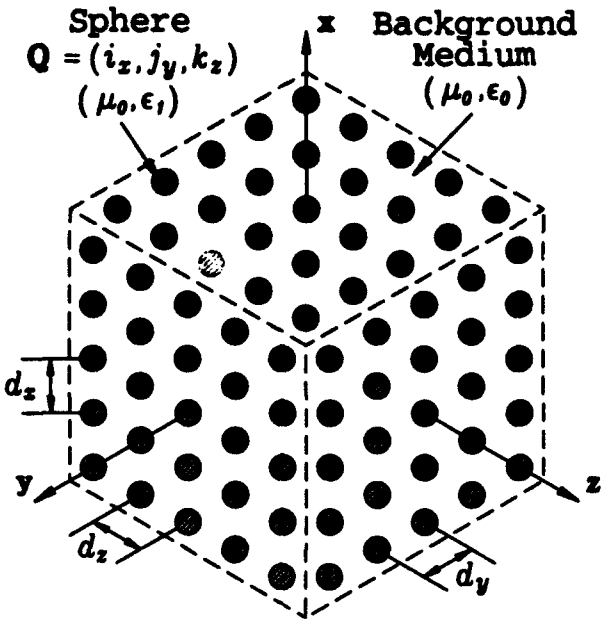

Figure H.1: Geometry of a 3D periodic artificial dielectric composed of dielectric spheres.

necessarily free space and may be lossy. The spheres are arranged in a rectangular lattice with spacings d_x, d_y and d_z in the $\hat{\mathbf{x}}, \hat{\mathbf{y}}$ and $\hat{\mathbf{z}}$ directions, respectively. They are referenced by the index $\mathbf{Q} = (i_x, j_y, k_z)$ where $-\infty \leq (i_x, j_y, k_z) \leq \infty$. The reference or center sphere is centered at the origin and is indexed by $\mathbf{Q} = \mathbf{0} = (0,0,0)$. Also, let $\Lambda\mathbf{Q} = i_x d_x \hat{\mathbf{x}} + j_y d_y \hat{\mathbf{y}} + k_z d_z \hat{\mathbf{z}}$ be the position vector from the origin to the center of sphere $\mathbf{Q}$. Typically there are a large number of electrically small spheres per cubic wavelength.

Following the general methods presented by Blanchard and Newman [21, 22], the effective permittivity of the artificial dielectric medium is determined by first assuming that a plane wave of unknown wavenumber is propagating through the medium. If the plane wave is propagating in the $\hat{\mathbf{u}}_k$ direction, then it will have spatial variation of the form

$$e^{-j\mathbf{k}_e \cdot \mathbf{R}}, \tag{H.1}$$

where $\mathbf{k}_e = k_e \hat{\mathbf{u}}_k$ is the unknown complex wave–vector, and $\dot{\mathbf{R}} = x\hat{\mathbf{x}} + y\hat{\mathbf{y}} + z\hat{\mathbf{z}}$ is a position vector from the origin to the point (x, y, z). For a given direction $\hat{\mathbf{u}}_k$, it is desired to find k_e such that this plane wave satisfies Maxwell's source free equations

and all of the boundary conditions in the artificial medium, i.e., the normal mode of propagation for the artificial dielectric medium. Once the propagation constant k_e is known, then the effective permittivity of the artificial dielectric medium is found through the relationship

$$k_e = \omega\sqrt{\mu_0\epsilon_e} \quad \text{or} \quad \epsilon_e = \frac{k_e^2}{\omega^2\mu_0}, \tag{H.2}$$

where ϵ_e is the complex effective permittivity of the artificial dielectric medium. Note that, in general, the artificial dielectric is an anisotropic medium, with different directions $\hat{\mathbf{u}}_k$ yielding different values for k_e and ϵ_e. However, since the spheres are symmetric and closely spaced, the directional variation of ϵ_e should be negligible.

In formulating the integral equation for the artificial dielectric medium, the volume equivalence theorem is used to replace the dielectric spheres by the host medium and the equivalent electric volume polarization currents [1, Sec. 7.7]

$$\mathbf{J} = j\omega(\epsilon_1 - \epsilon_0)\mathbf{E}^t, \tag{H.3}$$

where $\mathbf{E}^t$ is the total electric field inside the dielectric spheres. As illustrated in Figure H.2, the dielectric spheres are replaced by the host medium and the equivalent volume currents $\mathbf{J}$. This current $\mathbf{J}$, which exists in each and every sphere, is written as

$$\mathbf{J} = \sum_{\mathbf{Q}} \mathbf{J}^{\mathbf{Q}}, \tag{H.4}$$

where $\mathbf{J}^{\mathbf{Q}}$ is the current in the volume $V^{\mathbf{Q}}$ occupied by sphere $\mathbf{Q}$. In Equation (H.4) and others to follow, it is implicit that the summation is over all $\mathbf{Q}$, i.e., $-\infty \leq (i_x, j_y, k_z) \leq \infty$. Since we seek a solution to Maxwell's source free equations, there are no impressed currents, and thus $\mathbf{E}^t$ is the electric field of $\mathbf{J}$ radiating in the homogeneous host medium. Equation (H.3) can be rearranged as the homogeneous equation

$$-\mathbf{E}^t + \frac{\mathbf{J}}{j\omega(\epsilon_1 - \epsilon_0)} = 0 \quad \text{in each } V^{\mathbf{Q}}, \tag{H.5}$$

and is to be solved for the complex wavenumber k_e, and the current in the center $\mathbf{Q} = \mathbf{0}$ sphere, by the PMM.

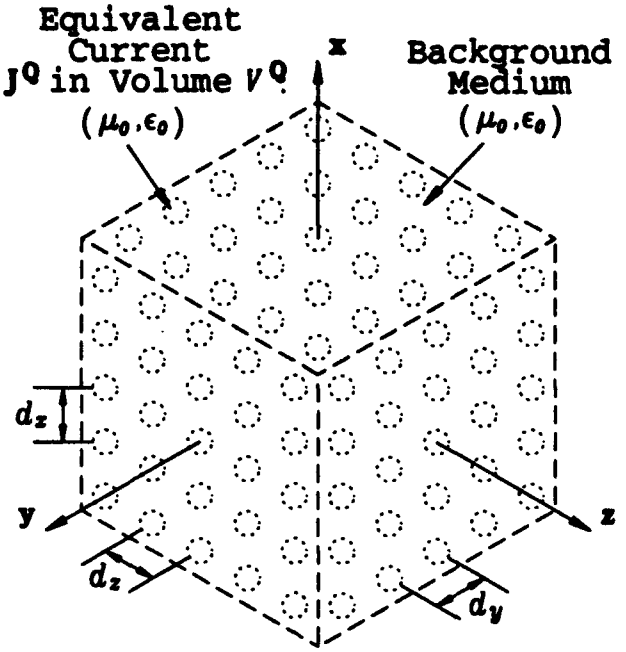

Figure H.2: Equivalent representation for the 3D artificial dielectric of spheres.

Due to the periodic nature of the array of spheres, and of the plane wave of Equation (H.1), the current is identical in each sphere except for an amplitude and phase change corresponding to the amplitude and phase of the plane wave at the center of the sphere. In other words, the current in sphere Q differs from the current in the center or reference sphere by the complex multiplier

$$C^Q = e^{-j\mathbf{k}_e \cdot \Delta \mathbf{Q}}. \tag{H.6}$$

As a result, the only unknowns are k_e and the current in the center or reference sphere.

H.1.2 PMM Solution of the Integral Equation

The first step in the PMM solution is to expand the unknown current J as

$$\mathbf{J} = \sum_{\mathbf{Q}} \mathbf{J}^{\mathbf{Q}} \approx \sum_{\mathbf{Q}} C^{\mathbf{Q}} \sum_{n=1}^{N} I_n \mathbf{J}_n^{\mathbf{Q}}, \tag{H.7}$$

where the $\mathbf{J}_n^{\mathbf{Q}}$ are N linearly independent expansion functions for the current in sphere Q, and the I_n are N unknown expansion coefficients, with $n = 1, 2, \ldots, N$. Due to

the periodic nature of the problem, it is only necessary to match Equation (H.5) over V^0, the volume of the center sphere. Next define N linearly independent weighting functions in the center sphere, denoted as $\mathbf{W}_m$ with $m = 1, 2, ..., N$. Substituting J of Equation (H.7) into Equation (H.5), and taking the inner product of the result with the N weighting functions, reduces Equation (H.5) to an order N matrix equation which can be written as

$$[Z + \Delta Z]\, I = 0. \tag{H.8}$$

Here $[Z + \Delta Z]$ is the order N impedance matrix and I is the length N solution vector containing the I_n expansion coefficients of Equation (H.7). The impedance matrix elements are given by $(m, n = 1, 2, ..., N)$

$$Z_{mn}(k_e) = \sum_{\mathbf{Q}} C^{\mathbf{Q}} Z^{\mathbf{Q}}_{mn} = -\sum_{\mathbf{Q}} C^{\mathbf{Q}} \int_{V_m} \mathbf{E}^{\mathbf{Q}}_n \cdot \mathbf{W}_m \, dv \tag{H.9}$$

$$\Delta Z_{mn} = \frac{1}{j\omega(\epsilon_1 - \epsilon_0)} \int_{V_m} \mathbf{J}^{\mathbf{0}}_n \cdot \mathbf{W}_m \, dv, \tag{H.10}$$

where $\mathbf{E}^{\mathbf{Q}}_n$ is the electric field of $\mathbf{J}^{\mathbf{Q}}_n$, the n^{th} expansion function in sphere Q, radiating in the homogeneous host medium. The integration limits V_m correspond to the region occupied by $\mathbf{W}_m$. Although the ΔZ_{mn} do not depend on k_e, the Z_{mn} do, because of their dependence upon $C^{\mathbf{Q}}$. Note that the ΔZ_{mn} terms are non-zero only when the expansion functions $\mathbf{J}^{\mathbf{Q}}_n$ are in the reference $\mathbf{Q} = \mathbf{0}$ sphere. Section H.2 discusses the numerical evaluation of the impedances in Equations (H.9) and (H.10).

The homogeneous matrix Equation (H.8) will have a non-trivial solution only if the determinant of the impedance matrix is zero. Thus, k_e is found by solving the fundamental equation

$$|Z(k_e) + \Delta Z| = 0, \tag{H.11}$$

usually on an iterative basis.

H.1.3 The MM Expansion and Weighting Functions for Small Spheres

In this section, MM expansion and weighting functions suitable for electrically small spheres are defined. For spheres of arbitrary size, the sphere eigenfunctions [37]

form a reasonable set of expansion functions. However, for electrically small spheres ($a \ll \lambda_0$), the shape of the current in a given sphere is very close to the lowest order eigenfunction current for an isolated sphere of the same radius and permittivity in the homogeneous host medium. Essentially, the higher order terms, which drop off as higher powers of $|k_0 a|$ are being ignored, and only the lowest order eigenfunction current is retained in each sphere. A Galerkin PMM solution is employed with weighting functions chosen identical to the expansion functions in the center sphere. For $N = 1$ expansion function, the fundamental equation, Equation (H.11) reduces to

$$Z_{11}(k_c) + \Delta Z_{11} = 0, \tag{H.12}$$

i.e., the self impedance of the single expansion function is zero.

The expansion function is defined by illuminating the isolated center sphere with an $\hat{\mathbf{x}}$ polarized plane wave propagating in the $+z$ direction ($\hat{\mathbf{u}}_k = \hat{\mathbf{z}}$), and with the incident electric field

$$\mathbf{E}^i = \hat{\mathbf{x}} e^{-jk_0 z}. \tag{H.13}$$

$\mathbf{J}_1^0$, the $n = 1$ expansion current in the $\mathbf{Q} = \mathbf{0}$ sphere, is the current induced by this incident field in the isolated center sphere. This current is given by [37]

$$\mathbf{J}_1^0 = C_1 \left[a_1^t \mathbf{m}_{o11}^{(1)} + j b_1^t \mathbf{n}_{e11}^{(1)} \right], \tag{H.14}$$

where a_1^t and b_1^t are the eigenfunction expansion coefficients, and $\mathbf{m}_{o11}^{(1)}$ and $\mathbf{n}_{e11}^{(1)}$ are the appropriate spherical vector wavefunctions inside the sphere. C_1 is an arbitrary normalization constant chosen here such that

$$\int_{V^0} \mathbf{J}_1^0 \, dv = C_1 \int_{V^0} \left[a_1^t \mathbf{m}_{o11}^{(1)} + j b_1^t \mathbf{n}_{e11}^{(1)} \right] dv = 1\hat{\mathbf{x}} \ \text{(Am)}. \tag{H.15}$$

The eigenfunction coefficients can be written as

$$a_1^t = \frac{j_1(\rho_0) h_0^{(2)}(\rho_0) - h_1^{(2)}(\rho_0) j_0(\rho_0)}{j_1(\rho_1) h_0^{(2)}(\rho_0) - \kappa h_1^{(2)}(\rho_0) j_0(\rho_1)} \tag{H.16}$$

$$b_1^t = \frac{h_1^{(2)}(\rho_0) j_0(\rho_0) - j_1(\rho_0) h_0^{(2)}(\rho_0)}{h_1^{(2)}(\rho_0) j_1(\rho_1) - \kappa j_1(\rho_1) h_0^{(2)}(\rho_0) + \left(\frac{\kappa^2 - 1}{\rho_1}\right) j_1(\rho_1) h_1^{(2)}(\rho_0)}, \tag{H.17}$$

where $j_n(\cdot)$ and $h_n^{(2)}(\cdot)$ are n^{th} order spherical Bessel and spherical Hankel functions of the second type, respectively, $\rho_0 = k_0 a$, $\rho_1 = k_1 a$ and $\kappa = \epsilon_1/\epsilon_0$. Denoting $\rho = k_1 r$ where r is the radial distance from the center of the sphere, the spherical vector wavefunctions inside the sphere can be written as

$$\mathbf{m}_{o11}^{(1)} = j_1(\rho) \left[\cos\phi\,\hat{\theta} - \cos\theta \sin\phi\,\hat{\phi}\right] \tag{H.18}$$

$$\mathbf{n}_{e11}^{(1)} = \frac{1}{\rho}\left[2j_1(\rho)\sin\theta\cos\phi\,\hat{\mathbf{r}} + [\rho j_1(\rho)]'\cos\theta\cos\phi\,\hat{\theta} + [\rho j_1(\rho)]'\sin\phi\,\hat{\phi}\right], \tag{H.19}$$

where the prime $'$ denotes differentiation with respect to $\rho = k_1 r$, and θ and ϕ are the usual spherical angle coordinates. Note that the expansion function $\mathbf{J}_1^{\mathbf{Q}}$ in sphere Q is identical to the expansion function $\mathbf{J}_1^{\mathbf{0}}$ in the center sphere except for the translation $\Delta\mathbf{Q}$.

H.2 Evaluation of the Impedance Matrix

This section describes the numerical evaluation of the impedance matrix element $[Z_{11} + \Delta Z_{11}]$ of Equations (H.9) and (H.10) using the expansion and weighting function given in Section H.1.3. For simplicity, the direction of propagation, $\hat{\mathbf{u}}_k$ of Equation (H.1), is assumed to be in the yz plane. Thus, the complex multiplier of Equation (H.6) does not depend on the x lattice spacing index i_x, and is written as

$$C^{\mathbf{Q}} = e^{-jk_e(j_y d_y \cos\psi + k_z d_z \sin\psi)}, \tag{H.20}$$

where ψ is the angle between $\hat{\mathbf{u}}_k$ and the y-axis.

As indicated by Equation (H.9), Z_{11} is obtained by summing $Z_{11}^{\mathbf{Q}}$, weighted by the multiplier $C^{\mathbf{Q}}$, for every expansion current, $\mathbf{J}_1^{\mathbf{Q}}$, in the infinite 3D periodic array. $Z_{11}^{\mathbf{Q}}$ is the mutual impedance between expansion function $\mathbf{J}_1^{\mathbf{Q}}$ in sphere Q and weighting function $\mathbf{W}_1 = \mathbf{J}_1^{\mathbf{0}}$ in the center sphere. In order for the triple sum of Equation (H.9) to converge absolutely, the mutual impedances, $Z_{11}^{\mathbf{Q}}$, must drop off with radial distance r more rapidly than $1/r^3$. This is not the case, since for large r the field $\mathbf{E}_1^{\mathbf{Q}}$ (and thus $Z_{11}^{\mathbf{Q}}$) drops off only as $1/r$. However, due to cancellations caused by the oscillatory behavior of $C^{\mathbf{Q}}$ and $Z_{11}^{\mathbf{Q}}$, the triple sum does converge, although its rate

of convergence is very slow. Thus, some method is desired to quickly evaluate this slowly convergent summation.

Many techniques, based upon mathematical identities such as the Poisson sum formula, have been presented to accelerate the convergence of a series [20, 38]. Here we present a method which is based more upon physical reasoning than mathematical identities. The method is based upon the assumption that the dielectric spheres are electrically very small and are on a lattice spacing which is electrically very small. The method employs increasingly crude approximations as the distance from sphere Q to the center sphere increases. As illustrated in Figure H.3, the spheres are classified as being in one of the following three regions:

Region 1: (R_1) includes only the Q = 0 or center sphere. It combines the $Z_{11}^{\bullet}$ and ΔZ_{11} terms which have the largest and most important contribution to the impedance sum, and its contribution is evaluated exactly.

Region 2: (R_2) includes the first several columns of spheres adjacent to the x–axis. As illustrated in Figure H.3, R_2 includes spheres in the rectangular cylinder:

$$-N_x \leq k_x \leq N_x, \qquad -N_y \leq j_y \leq N_y, \qquad -\infty \leq i_x \leq \infty, \tag{H.21}$$

where N_y and N_x are typically on the order of 8, and it is understood that the Q = 0 or R_1 sphere is omitted. For R_2, two approximations are made. First, the fields of $\mathbf{J}_1^{\mathbf{Q}}$ are approximated by the fields of an infinitesimal dipole of the same unit current moment. Second, the weighting function $\mathbf{W}_1$ is approximated by a Dirac delta function of the same current moment located at the center of the center sphere. Basically, the Galerkin weighting function is being replaced by point matching.

Region 3: (R_3) includes all remaining spheres external to R_2. As discussed above, it is practically impossible to directly sum the impedances associated with the R_3 spheres to convergence. This is especially true if k_x is complex, since in this case the $C^{\mathbf{Q}}$ in Equation (H.20) will *exponentially grow* as (j_y, k_x) increase in magnitude. To avoid this problem, the currents in the R_3 spheres will be

approximated by a continuous current whose field can be easily found in closed form.

As in R_2, the fields of the expansion functions $\mathbf{J}_1^{\mathbf{Q}}$ in R_3 are approximated by the fields of infinitesimal dipoles of the same unit current moment, and the Galerkin weighting is approximated by point matching. Since the separation between the spheres is electrically very small, and since the distance from a R_3 sphere to the origin (field point) is at least several lattice spacings, the infinitesimal current elements in R_3 can be approximated by a continuous volume current density, $\mathbf{J}_C$, with the same current moment per lattice cell. As described below, the fields of $\mathbf{J}_C$, which exists only in R_3, are evaluated as the fields of $\mathbf{J}_C$ in all space minus the fields of $\mathbf{J}_C$ in $R_1 + R_2$. The fields of $\mathbf{J}_C$ in all space are known in simple closed form, and the fields of $\mathbf{J}_C$ in $R_1 + R_2$ are evaluated by a relatively fast double numerical integration over $R_1 + R_2$. Essentially, the triple sum to infinity is replaced by this finite double numerical integration.

Combining the contributions from the three regions defined above, the single term impedance matrix element can be written as

$$Z_{11} + \Delta Z_{11} \approx Z_{R1} + Z_{R2} + Z_{R3} \quad \text{where}$$

$$Z_{R1} = \left(Z_{11}^{\mathbf{0}} + \Delta Z_{11}\right)$$

$$Z_{R2} = -\sum_{k_x=-N_x}^{N_x} \sum_{j_y=-N_y}^{N_y} C^{\mathbf{Q}} \sum_{i_z=-\infty}^{\infty}{}' E_{\delta x}(\Delta\mathbf{Q})$$

$$Z_{R3} = -E_{Cx}, \tag{H.22}$$

where $E_{\delta x}(\Delta\mathbf{Q})$ is the x component of the electric field of the infinitesimal dipole located at $\Delta\mathbf{Q}$ approximating $\mathbf{J}_1^{\mathbf{Q}}$, and E_{Cx} is the x component the electric field of the continuous current distribution $\mathbf{J}_C$ in R_3. In both cases, the currents are radiating in the homogeneous host medium and the field point is at the origin. The prime on the triple summation indicates that the $\mathbf{Q} = 0$ center term is omitted.

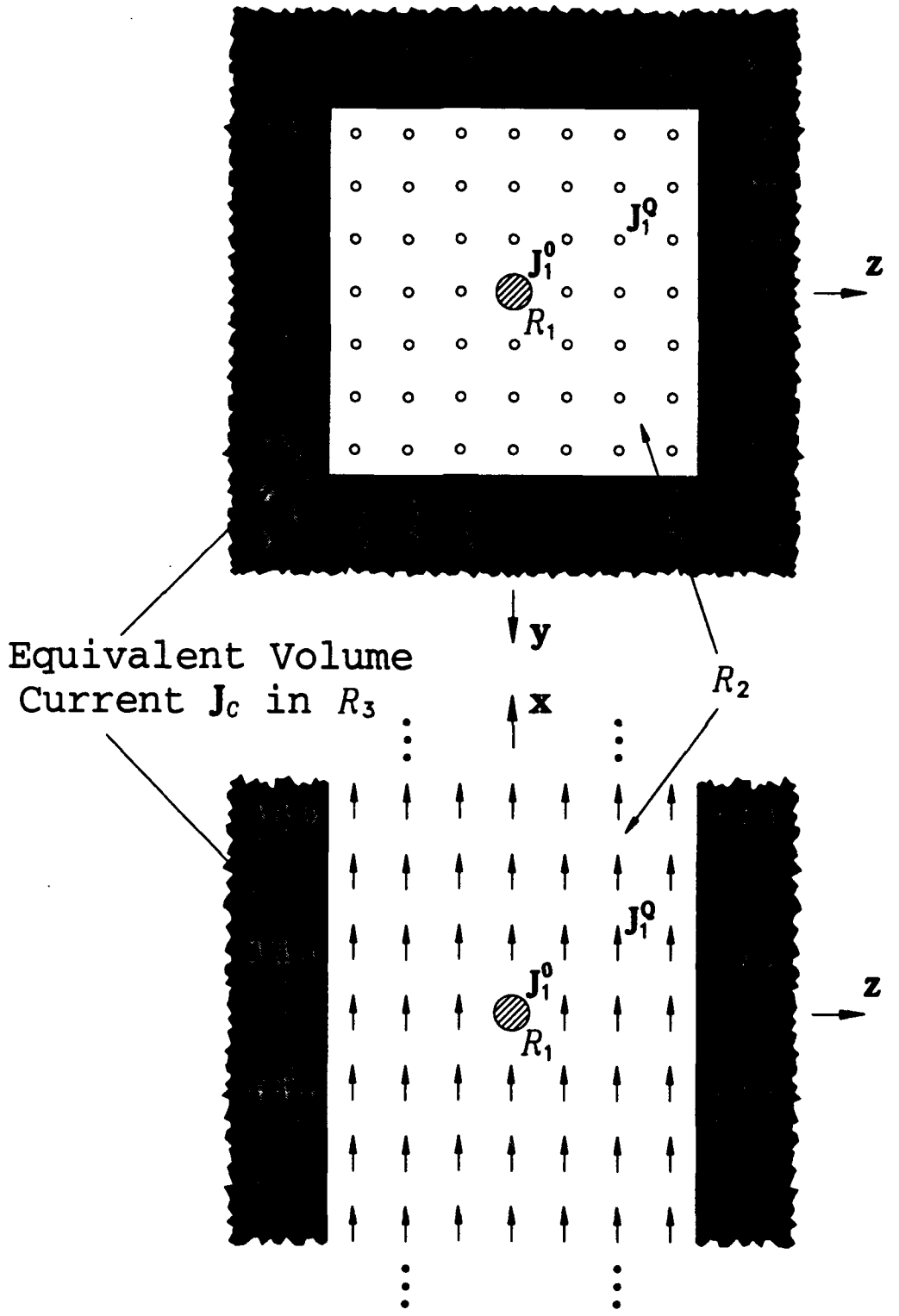

Figure H.3: Top and side views showing the different current regions and approximations.

The Region 1 Term

The self impedance contribution, Z_{R1}, is the contribution from $\mathbf{J}_1^{\mathbf{0}}$, the expansion function in the $\mathbf{Q} = \mathbf{0}$ center sphere, and includes both $Z_{11}^{\mathbf{0}}$ and ΔZ_{11}. Inside the center sphere, $\mathbf{E}_1^{\mathbf{0}}$, the field of $\mathbf{J}_1^{\mathbf{0}}$, is found by subtracting the incident field from the total field in the eigenfunction solution [37]. The total field is approximated by the lowest order eigenfunction term, but the incident field has an infinite number of terms of slowly decreasing strength. However, due to the orthogonality of the wavefunctions when integrated over the center sphere's volume $V^{\mathbf{0}}$, only the lowest order term contributes in the integration for $Z_{11}^{\mathbf{0}}$. Carrying out this operation, and also performing the integrations of Equations (H.9) and (H.10), Z_{R1} is evaluated exactly as

$$Z_{R1} = \left(Z_{11}^{\mathbf{0}} + \Delta Z_{11}\right) = \frac{C_1^2}{j\omega(\epsilon_1 - \epsilon_0)}\left[a_1^t A_{int} - b_1^t B_{int}\right]$$

$$A_{int} = \frac{8\pi}{3k_0k_1}\left[\frac{k_1 \sin\rho_1 \cos\rho_0 - k_0 \cos\rho_1 \sin\rho_0}{k_1^2 - k_0^2} - \frac{\sin\rho_1 \sin\rho_0}{k_0\rho_1}\right]$$

$$B_{int} = \frac{8\pi}{3k_0k_1}\left[\frac{k_0 \sin\rho_1 \cos\rho_0 - k_1 \cos\rho_1 \sin\rho_0}{k_1^2 - k_0^2} - \frac{\cos\rho_1 \cos\rho_0}{k_0\rho_1} + \right.$$
$$\left. \frac{k_0 \sin\rho_1 \cos\rho_0 + k_1 \cos\rho_1 \sin\rho_0}{k_0^2\rho_1^2} - \frac{\sin\rho_1 \sin\rho_0}{k_0\rho_0\rho_1^2}\right]. \qquad \text{(H.23)}$$

Region 2 Terms

For a sphere in R_2, the expansion function $\mathbf{J}_1^{\mathbf{Q}}$ is approximated as an infinitesimal dipole of the same unit current moment located at the center of sphere Q. Using the well known expressions for the electric field of an infinitesimal dipole [39], we obtain

$$Z_{R2} = -\sum_{k_x=-N_x}^{N_x}\sum_{j_y=-N_y}^{N_y} C^{\mathbf{Q}} \sum_{i_x=-\infty}^{\infty}{}' E_{\delta x}(\Lambda\mathbf{Q}), \qquad \text{(H.24)}$$

where

$$E_{\delta x}(\Lambda\mathbf{Q}) = \frac{j\omega\mu_0}{4\pi}\left[\sin^2\alpha\left(1 + \frac{1}{jk_0r} + \frac{1}{(jk_0r)^2}\right) - \right.$$
$$\left. 2\cos^2\alpha\left(\frac{1}{jk_0r} + \frac{1}{(jk_0r)^2}\right)\right]\frac{e^{-jk_0r}}{r}, \qquad \text{(H.25)}$$

where α is the angle between $\Lambda\mathbf{Q}$ and the x-axis, and $r = |\Lambda\mathbf{Q}|$.

In evaluating the innermost summation of Equation (H.24), the field $E_{\delta x}(\Lambda\mathbf{Q})$ is summed for $-\infty \leq i_x \leq \infty$. This inner sum is the contribution from the column of dipoles indexed by (j_y, k_z), and the details of this evaluation are given below.

Column of Dipoles Summation

This section evaluates the contribution to Z_{R2} from a column of infinitesimal dipole current elements indexed by (j_y, k_z), i.e., it presents the evaluation of

$$Z^{j_y k_z} = \sum_{i_x=-\infty}^{\infty}{}' E_{\delta x}(\Lambda\mathbf{Q}), \tag{H.26}$$

where $E_{\delta x}(\Lambda\mathbf{Q})$ is given by Equation (H.25) and the $'$ indicates that the $i_x = 0$ term is omitted if $j_y = k_z = 0$. Experience shows that Equation (H.26) is a slowly converging sum, and simply summing to convergence significantly increases the total CPU time. The method presented here begins by directly summing terms for which $|i_x|$ is not very large. Since the spacing d_x between dipoles is electrically small, for large $|i_x|$, the discrete array of infinitesimal dipole currents are approximated as a continuous line current distribution of the same current moment per unit length. The field of this continuous current distribution is determined by an asymptotic integration extending to infinity, which can be approximated in closed form.

From symmetry, the mutual impedances of the spheres at $x = \pm i_x d_x$ contribute equally to Equation (H.26), and thus the sum in Equation (H.26) can be reduced to only positive values of i_x. $Z^{j_y k_z}$ can now be written as

$$Z^{j_y k_z} = E_{\delta x}(\hat{\mathbf{y}} j_y d_y + \hat{\mathbf{z}} k_z d_z) + 2\sum_{i_x=1}^{N_x} E_{\delta x}(\Lambda\mathbf{Q}) + \frac{2}{d_x}\int_{x_a}^{\infty} E_{\delta x}(\Lambda\mathbf{Q})\, dx, \tag{H.27}$$

where N_x is the number of terms (dipoles) that are directly summed, and $x_a = \left(N_x + \frac{1}{2}\right) d_x$ is the x coordinate of the bottom of the line current approximating the dipoles $N_x < i_x \leq \infty$. In Equation (H.27), the first term is the $i_x = 0$ term. It is understood that this term is omitted for the $j_y = k_z = 0$ column of dipoles since it is the R_1 self impedance term that is evaluated separately.

The tail end contribution to $Z^{j_y k_z}$, given as the integral in Equation (H.27), is evaluated asymptotically. Assuming N_x is chosen large enough that $x_a \gg \rho =$

$\sqrt{(j_y d_y)^2 + (k_z d_z)^2}$, the radial distance $r = |\mathbf{AQ}|$ is approximated simply as x. Thus, $\cos\alpha \approx 1$ and $\sin\alpha \approx \rho/x$. Making these substitutions into Equation (H.25), the integral contribution becomes

$$\int_{x_a}^{\infty} E_{\delta x}(\mathbf{AQ})\,dx \approx \frac{j\omega\mu_0}{4\pi}\left[\left(\frac{-2}{jk_0}\right)I_2 + \left(\rho^2 - \frac{2}{(jk_0)^2}\right)I_3 + \left(\frac{\rho^2}{jk_0}\right)I_4 + \left(\frac{\rho^2}{(jk_0)^2}\right)I_5\right] \tag{H.28}$$

where the integrals I_p for $p = 1, 2, \ldots, 5$ are defined as

$$I_p = \int_{x_a}^{\infty} \frac{e^{-jk_0 x}}{x^p}\,dx. \tag{H.29}$$

The $p = 1$ integral can be evaluated by replacing the exponential by its Taylor series expansion and integrating term by term, yielding

$$I_1 = \frac{e^{-jk_0 x_a}}{jk_0 x_a}\left[1 - \frac{1}{jk_0 x_a} + \frac{2}{(jk_0 x_a)^2} - \frac{6}{(jk_0 x_a)^3} + \frac{24}{(jk_0 x_a)^4} - \cdots\right]. \tag{H.30}$$

The remaining integrals are evaluated through the recursion relationship

$$I_p = \frac{1}{p-1}\left[\frac{e^{-jk_0 x_a}}{x_a^{p-1}} - jk_0 I_{p-1}\right]. \tag{H.31}$$

Region 3 Terms

For R_3, the total currents in the spheres are approximated as the continuous volume current $\mathbf{J}_C$. $\mathbf{J}_C$ includes the $e^{-j\mathbf{k}_e\cdot\mathbf{R}}$ variation of the plane wave in Equation (H.1), i.e.,

$$\mathbf{J}_C = \hat{\mathbf{x}} J_C = \hat{\mathbf{x}} C_2 e^{-jk_e(y\cos\psi + z\sin\psi)} \quad \text{in } R_3, \tag{H.32}$$

where C_2 is a normalization constant such that $\mathbf{J}_C$ has unit current moment in each lattice cell.

If $\mathbf{J}_C$ existed throughout all space, instead of only in R_3, then its electric field could be found directly from Maxwell's equations as simply

$$\hat{\mathbf{x}} C_2 \frac{j\omega\mu_0}{k_0^2 - k_e^2}.$$

To find the field of J_C in R_3, it is necessary to subtract the contribution from that portion in R_1 and R_2, yielding

$$Z_{R3} = -E_{Cx} = -C_2 \frac{j\omega\mu_0}{k_0^2 - k_e^2} - \frac{k_0^2}{4\omega\epsilon_0} \int_{R_1+R_2} J_C H_0^{(2)}(k_0\rho) dy\, dz, \qquad \text{(H.33)}$$

where the integration is over the region $R_1 + R_2$ in the yz plane (where J_C is zero), $\rho = \sqrt{y^2 + z^2}$ and $H_0^{(2)}(k\rho)$ is the cylindrical Hankel function of the second type.

H.3 Numerical Results

This section presents numerical results based upon the above PMM analysis of an artificial dielectric composed of small dielectric spheres. The data will include the root of the fundamental equation, as well as the relative effective permittivity and loss tangent for different artificial dielectric compositions. In all cases, the direction of propagation is $\hat{u}_k = \hat{z}$, the polarization of the electric field is $\hat{x}$, and the host medium is free space.

The first set of data illustrates the root of the fundamental Equation (H.12) for the effective wavenumber in the complex k_e plane. The geometry of the artificial dielectric consists of spheres of radius $0.0025\lambda_0$ spaced in a cubic array where $d_x = d_y = d_z = 0.01\lambda_0$. The spheres have relative permittivity $\epsilon_{1r} = 10$ and loss tangent $\tan\delta_1 = 1$. Figure H.4 shows the magnitude of $Z_{11}(k_e) + \Delta Z_{11}$ (i.e., the magnitude of the determinant of the order $N = 1$ matrix) along several lines in the complex k_e plane parallel to the $\mathrm{Re}(k_e)$ axis, as illustrated in the insert to the figure. The root is the value of k_e such that $|Z_{11} + \Delta Z_{11}| = 0$. From Figure H.4 this occurs at $k_e/k_0 \approx 1.086 - i0.0125$. Using Equation (H.2), this corresponds to a relative effective permittivity of $\epsilon_{er} = 1.18$ with effective loss tangent $\tan\delta_e = 0.023$. Note that the effective permittivity of the artificial dielectric is between that of the host medium and the dielectric spheres.

The insert in Figure H.5 shows an artificial dielectric in which the dielectric spheres have relative permittivity $\epsilon_{1r} = 4$ with loss tangent $\tan\delta_1 = 1$. The relative effective permittivity and effective loss tangent are plotted for sphere radii of $a = 0.002$, 0.01 and $0.02\lambda_0$, as a function of cubic array lattice spacings $d_x = d_y = d_z$ varying from $2a$

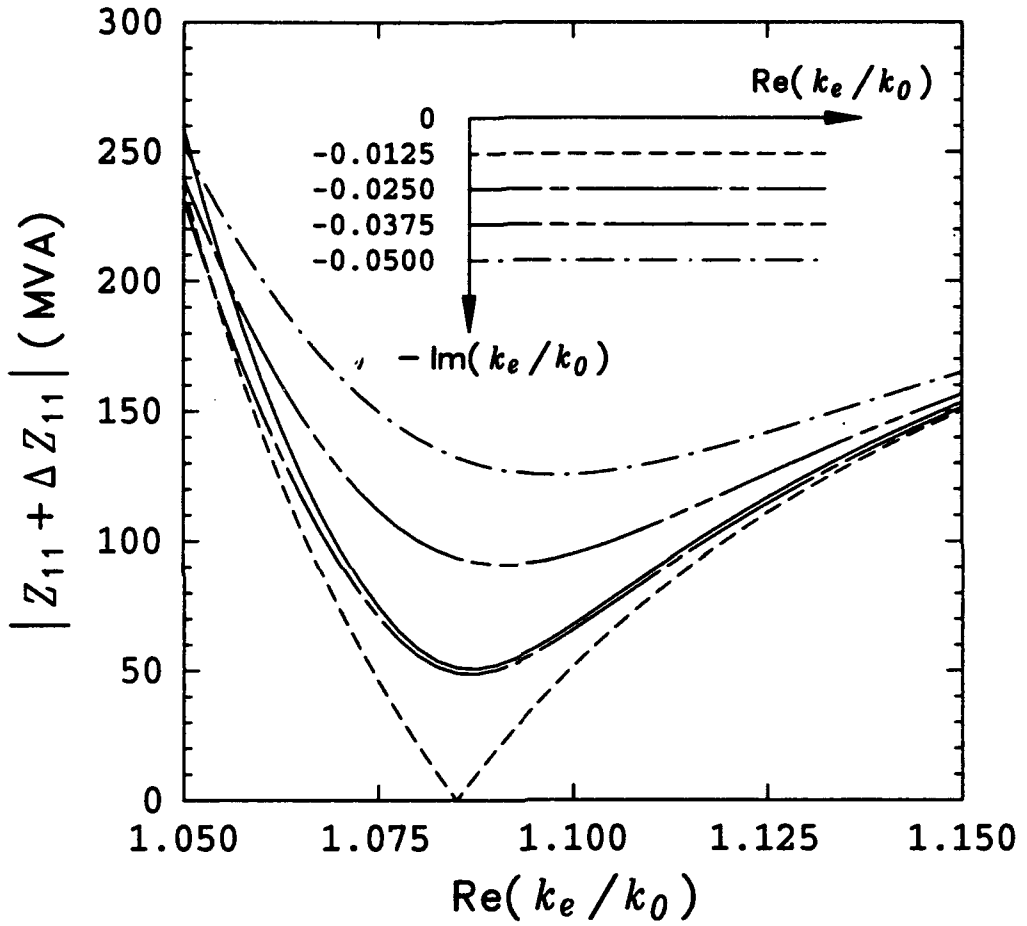

Figure H.4: Contours of $|Z_{11} + \Delta Z_{11}|$ in the complex k_e plane, for a 3D array of dielectric spheres.

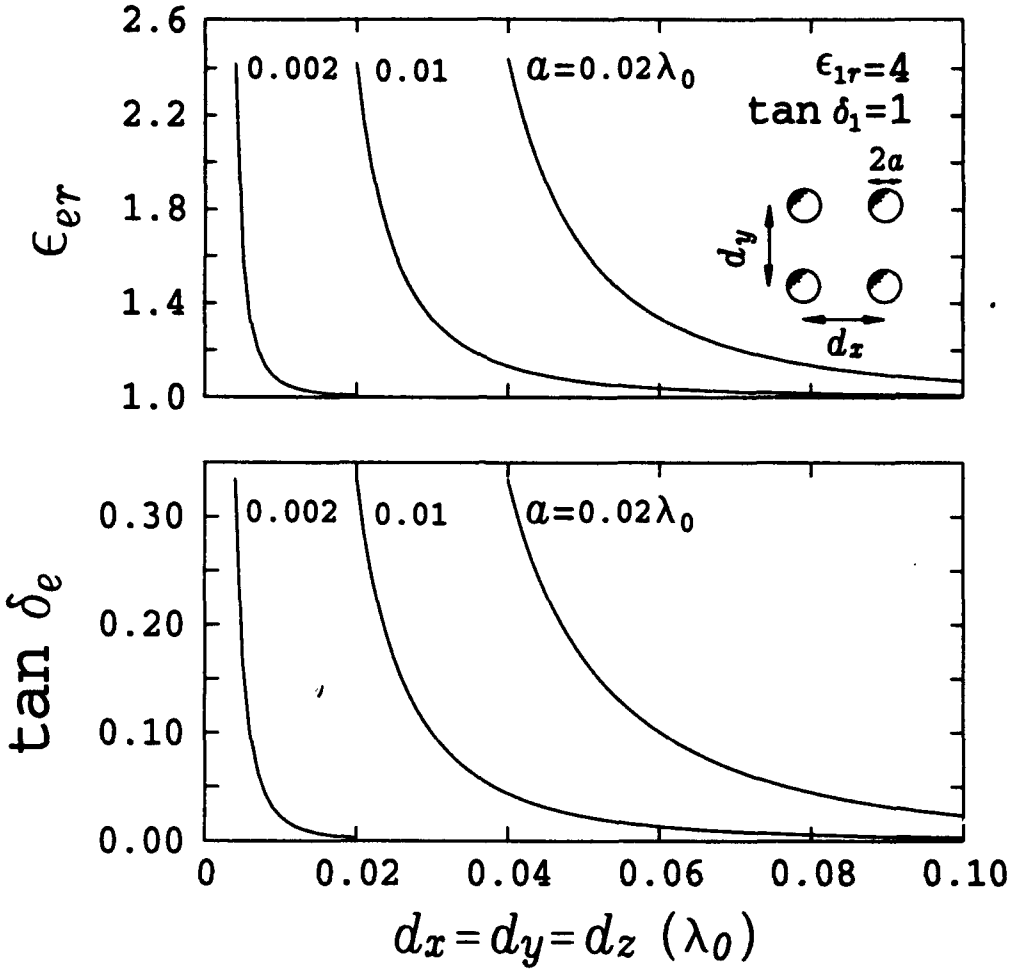

Figure H.5: Effective permittivity versus array lattice spacing, for a 3D array of dielectric spheres.

to $0.1\lambda_0$. As the lattice spacing increases, the fraction of the volume occupied by the spheres decreases, and the complex permittivity of the artificial dielectric approaches that of the host medium.

The insert in Figure H.6 shows an artificial dielectric in which the dielectric spheres have radius $a = 0.0025\lambda_0$, and are arranged in a cubic lattice of spacing $d_x = d_y = d_z = 0.01\lambda_0$. The relative effective permittivity and loss tangent are shown as a function of sphere loss tangent, $\tan\delta_1$, varying from 0 to 10, for sphere relative permittivities of $\epsilon_{1r} = 3$, 10 and 30. Note that the relative effective permittivity increases, whereas the effective loss tangent decreases, with increasing ϵ_{1r}. When $\tan\delta_1 = 0$, the spheres are lossless, and thus the artificial dielectric is also lossless

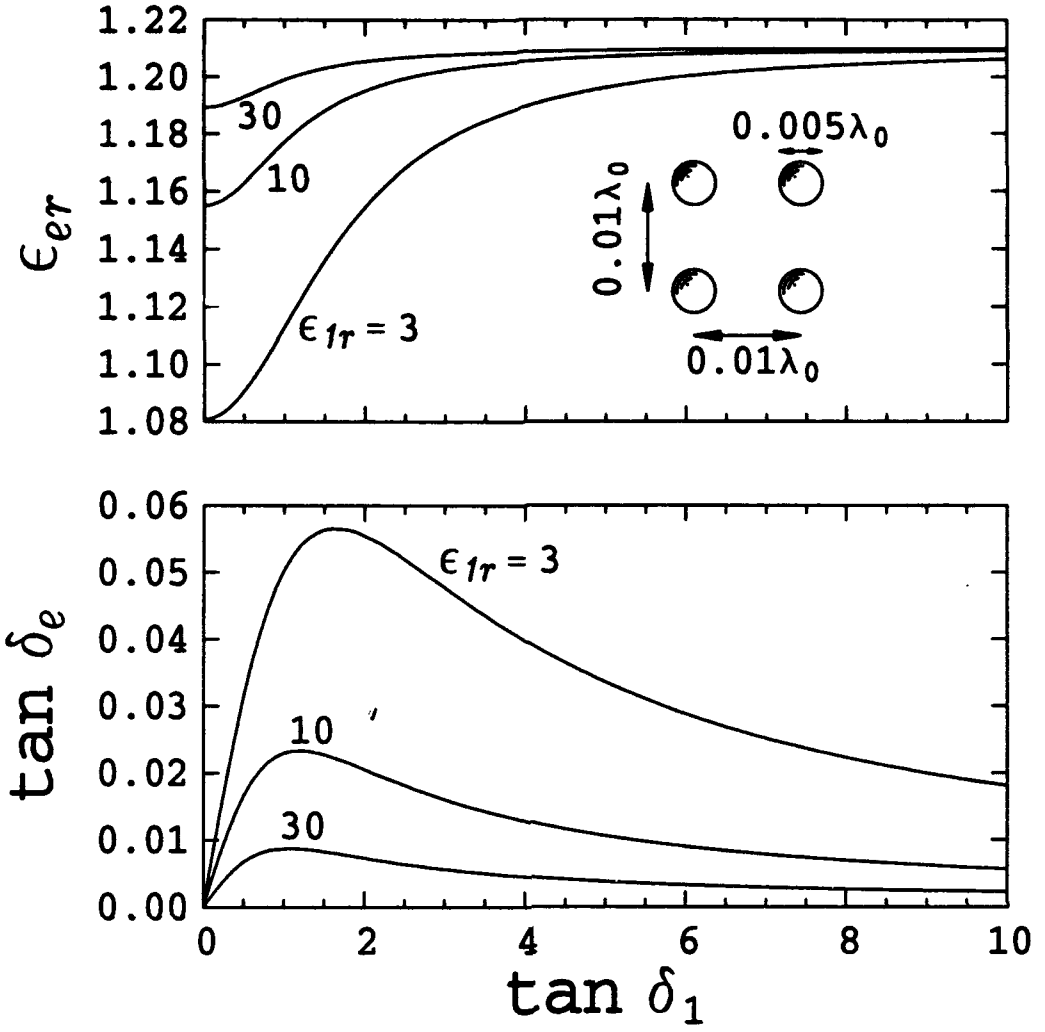

Figure H.6: Effective permittivity versus sphere loss tangent, for a 3D array of dielectric spheres.

with $\tan\delta_e = 0$. As $\tan\delta_1$ increases, $\tan\delta_e$ increases, reaches a peak, and then falls to zero as $\tan\delta_e \to \infty$.

H.4 Summary

This appendix has presented an integral equation and PMM solution to determine the effective permittivity of an artificial dielectric composed of a 3D periodic array of homogeneous dielectric spheres in a homogeneous host medium. The effective permittivity is determined by finding the complex wavenumber, k_e, for a plane wave propagating in the artificial medium. The method can compute the effective permit-

tivity of the artificial dielectric as a function of frequency, direction of propagation, and the size, material composition, and density of the dielectric spheres.

Bibliography

[1] C.A. Balanis, *Advanced Engineering Electromagnetics*, John Wiley and Sons, New York, 1989, Ch. 2.

[2] L.W. Henderson, *The Scattering of Planar Arrays of Arbitrarily Shaped Slot and/or Wire Elements in a Stratified Dielectric Medium*, Ph.D. thesis, Dept. of Elec. Engr., The Ohio State University, Columbus, 1983.

[3] L.W. Henderson, *Introduction to PMM*, Report No. 715582-5, ElectroScience Laboratory, The Ohio State University, Columbus, April, 1985.

[4] R. Mittra, C.H. Chan, and T. Cwik, "Techniques for Analysing Frequency Selective Surfaces — A Review," *Proceedings IEEE*, Vol. 76, pp. 1593–1615, Dec. 1988.

[5] W.E. Kock, "Metallic Delay Lenses," *Bell Syst. Tech. Journal*, Vol. 27, pp. 58-82, 1948.

[6] W. Rotman, "Plasma Simulation by Artificial Dielectrics and Parallel-Plate Media," *IRE Trans. Antennas Propagat.*, Vol. AP-10, pp. 82–95, Jan. 1962.

[7] I.J. Bahl and K.C. Gupta, "A Leaky-Wave Antenna Using an Artificial Dielectric Medium," *IEEE Trans. Antennas Propagat.*, Vol. AP-22, pp. 119–122, Jan. 1974.

[8] J. Brown, "Artificial Dielectrics Having Refractive Indices Less Than Unity," *Proceeding IEE*, Vol. 100, Part 4, pp. 51–62, 1953.

[9] R.J. King, D.V. Thiel and K.S. Park, "The Synthesis of Surface Reactance Using an Artificial Dielectric," *IEEE Trans. Antennas Propagat.*, Vol. AP-31, pp. 471–476, May 1983.

[10] A. Sihvola, "Macroscopic Permittivity of Dielectric Mixtures with Application to Microwave Attenuation of Rain and Hail," *Proceedings IEE*, Vol. 136, pp. 24-28, Feb. 1989.

[11] C.Y. Wu and A. Benatar, "Microwave Joining of HDPE Using Conductive Polyaniline Composites," Proceedings of the Society of Plastics Engineers 50th Annual Technical Conference (ANTEC), May 1992.

[12] L. Lewin, "The Electrical Constants of a Material Loaded With Spherical Particles," *Proceedings IEE*, Vol. 94, Part III, pp. 65–68, Jan. 1947.

[13] R.W. Corkum, "Isotropic Artificial Dielectric," *Proceedings IRE,* Vol. 40, pp.574–587, May 1952.

[14] G. Estrin, "The Effective Permeability of an Array of Thin Conducting Disks," *Journal of Applied Physics,* Vol. 21, pp.667–670, July 1950.

[15] G. Estrin, "The Effects of Anisotropy in a Three-Dimensional Array of Conducting Disks," *Proceedings IRE,* Vol. 39, pp. 821–826, July 1951.

[16] J. Brown and W. Jackson, "The Relative Permittivity of Tetragonal Arrays of Perfectly Conducting Thin Discs," *Proceedings IRE,* Vol. 102, Part B, pp. 37–42, Jan. 1955.

[17] J. Brown, "The Design of Metallic Delay Dielectrics," *Proceedings IEE,* Vol. 97, Part III, pp. 45–48, Jan. 1950.

[18] N.J. Kolettis and R.E. Collin, "Anisotropic Properties of Strip-Type Artificial Dielectrics," *IRE Trans. Microwave Theory Tech.,* Vol. MTT-9, pp. 436–441, Sept. 1961.

[19] S.B. Cohn, "Experimental Verification of the Metal-Strip Delay-Lens Theory," *Journal of Applied Physics,* Vol. 24, pp. 839–841, July 1953.

[20] R.E. Collin, *Field Theory of Guided Waves,* Second Edition, IEEE Press, New York, 1991.

[21] J.L. Blanchard, *Integral Equation Analysis of Artificial Dielectrics,* Ph.D. thesis, Dept. of Mathematics, The Ohio State University, Columbus, 1991.

[22] J.L. Blanchard, E.H. Newman and M.E. Peters "Integral Equation Analysis of Artificial Media," accepted for publication.

[23] A. Sommerfeld, *Optics, Lectures on Theoretical Physics, Vol. IV,* Academic Press, New York, 1954.

[24] M. Born and E. Wolf, *Principles of Optics,* Sixth Ed., Pergamon Press, New York, 1980.

[25] E.H. Newman, "A Unified Theory of Thin Material Wires," *IEEE Trans. Antennas Propagat.,* Vol. AP-39, pp. 1488–1496, Oct. 1991.

[26] R.F. Harrington, *Time-Harmonic Electromagnetic Fields,* McGraw-Hill, New York, 1961.

[27] J.A. Kong, *Electromagnetic Wave Theory,* John Wiley and Sons, New York, 1986.

[28] B.A. Munk, G.A. Burrell and T.W. Kornbau, *A General Theory of Periodic Surfaces in a Stratified Dielectric Medium,* Report No. AFAL-TR-77-219, ElectroScience Laboratory, The Ohio State University, Columbus, Nov. 1977.

[29] T.W. Kornbau, *Application of the Plane Wave Expansion Method to Periodic Arrays Having a Skewed Grid Geometry,* M.S. thesis, Dept. of Elec. Engr., The Ohio State University, Columbus, 1977.

[30] B.A. Munk and G.A. Burrell, "Plane-Wave Expansions for Arrays of Arbitrarily Oriented Piecewise Linear Elements and Its Application in Determining the Impedance of a Single Linear Antenna in a Lossy Half-Space," *IEEE Trans. Antennas Propagat.,* Vol. AP-27, pp. 331–343, May 1979.

[31] A. Papoulis, *The Fourier Integral and Its Applications,* McGraw-Hill, New York, 1987.

[32] R. Andre, *An Analysis Method for Double Periodic Nonplanar Antenna Arrays,* M.S. thesis, Dept. of Elec. Engr., The Ohio State University, Columbus, 1985.

[33] J.H. Richmond and E.H. Newman, "Dielectric Coated Wire Antennas," *Radio Sci.,* Vol. 11, pp. 13–20, Jan. 1976.

[34] J.H. Richmond, *Computer Program for Thin-Wire Structures in a Homogeneous Conducting Medium,* Report No. 2902-12, ElectroScience Laboratory, The Ohio State University, Columbus, August 1973.

[35] E.H. Newman, *A User's Manual for the Electromagnetic Surface Patch Code: ESP Version IV,* Report No. 716199-11, ElectroScience Laboratory, The Ohio State University, Columbus, August 1988.

[36] E.H. Newman, *A User's Manual for the Material Wire Code MATWRS,* Report No. 722767-1, ElectroScience Laboratory, The Ohio State University, Columbus, Nov. 1990.

[37] J.A. Stratton, *Electromagnetic Theory,* McGraw-Hill, New York, 1941.

[38] S. Singh, W.F. Richards, J.R. Zinecker, and D.R. Wilton, "Accelerating the Convergence of Series Representing the Free Space Periodic Green's Function," *IEEE Trans. Antennas Propagat.,* Vol. AP-38, pp. 1958–1962, Dec. 1990.

[39] C.A. Balanis, *Antenna Theory,* Harper & Row, New York, 1982.

[40] R.E. Collin, *Antennas and Microwave Propagation,* McGraw-Hill, New York, 1985.

[41] J.H. Richmond, "Radiation and Scattering by Thin-Wire Structures in a Homogeneous Conducting Medium," *IEEE Trans. Antennas Propagat.,* Vol. AP-22, p. 365, Nov. 1974.

[42] R.E. Collin, *Antennas and Microwave Propagation,* McGraw-Hill, New York, 1985.

[43] R.E. Collin and W.H. Eggimann, "Dynamic Interaction Fields in a Two-Dimensional Lattice," *IRE Trans. Microwave Thoery Tech.*, Vol. MTT-9, pp. 110–115, March 1961.

[44] L. Brillouin, *Wave Propagation in Periodic Structures*, McGraw-Hill, New York, 1946.

[45] M.M.Z. Kharadly, "Some Experiments on Artificial Dielectrics at Centimetre Wavelengths," *Proceedings IEE*, Vol. 102, Part B, pp. 17–25, Jan. 1955.

[46] S.B. Cohn, "Microwave Measurements on Metallic Delay Media," *Proceedings IRE*, Vol. 41, pp. 1177–1183, Sept. 1953.

[47] S.B. Cohn. "Electrolytic-Tank Measurements for Microwave Metallic Delay-Lens Media," *Journal of Applied Physics*, Vol. 21, pp. 674–680, July 1950.

[48] R.C. Hall, R. Mittra and J.R. Mosig, "Analysis of a Parallel Resistive Plate Medium," *IEEE Trans. Antennas Propagat.*, Vol. AP-38, pp. 299–304, March 1990.

[49] A.F. Harvey, "Optical Techniques at Microwave Frequencies," *Proceedings IEE*, Vol. 106, Part B, pp. 141–157, March 1959.

[50] Z.A. Kaprielian, "Anisotropic Effects in Geometrically Isotropic Lattices," *Journal of Applied Physics*, Vol. 29, pp. 1052–1063, July 1958.

[51] Z.A. Kaprielian, "Dielectric Properties of a Lattice of Anisotropic Particles," *Journal of Applied Physics*, Vol. 27, p. 24, Jan. 1956.

[52] J. Brown and W. Jackson, "The Properties of Artificial Dielectrics at Centimetre Wavelengths," *Proceedings IEE*, Vol. 102, Part B, pp. 11–16, Jan. 1955.

[53] M.M.Z. Kharadly and W. Jackson, "The Properties of Artificial Dielectrics Comprising Arrays of Conducting Elements," *Proceedings IEE*, Vol. 100, Part III, pp. 199–212, July 1953.

[54] H.S. Bennett, "The Electromagnetic Transmission Characteristics of the Two-Dimensional Lattice Medium," *Journal of Applied Physics*, Vol. 24, pp. 785–810, June 1953.